The Pennsylvania State University

The Graduate School

Department of Biomedical Engineering

DEVELOPMENT OF SEMI-SYNTHETIC TISSUE USING DECELLULARIZED INTESTINE AND APTAMER-FUNCTIONALIZED HYDROGEL

A Dissertation in

Biomedical Engineering

by

Xiaolong Zhang

Submitted in Partial Fulfillment
of the Requirements
for the Degree of

Doctor of Philosophy

December 2015

The dissertation of Xiaolong Zhang was reviewed and approved* by the following:

Yong Wang
Associate Professor of Biomedical Engineering
Dissertation Advisor
Chair of Committee

Nanyin Zhang
Associate Professor of Biomedical Engineering

Siyang Zheng
Assistant Professor of Biomedical Engineering

Tak-Sing Wong
Assistant Professor of Mechanical Engineering

William Hancock
Professor and Graduate Program Chair of Biomedical Engineering

*Signatures are on file in the Graduate School

ABSTRACT

Decellularized tissues, derived from native tissues by removing cellular materials, retain the inherent architectural complexity of living tissues. They provide cells with an appropriate structural support for adhesion and proliferation and have been widely studied to restore, replace, or regenerate defective tissues in the field of regenerative medicine and tissue engineering. Despite the great potential, decellularized tissues lack bioactive growth factors due to the harsh decellularization procedure and therefore cannot provide cells with appropriate microenvironment for desirable tissue regeneration.

Autograft is well accepted as the gold standard for tissue regeneration because it provides both physical (e.g., structure and mechanic) and chemical support (e.g., growth factors). To mimic autograft, a synthetic hydrogel that can sustainably release growth factors was integrated into decellularized tissue to create a semi-synthetic substitute. Because the semi-synthetic substitute can provide both physical and chemical support in tissue regeneration, it is expected to not only provide similar therapeutic outcomes as autograft, but also avoid the disadvantages of autograft, such as secondary surgery, limited material availability, and donor site morbidity.

In this study, an aptamer functionalized gelatin-PEG hydrogel was incorporated into decellularized intestine to create a semi-synthetic skin substitute as a model. Three aims were proposed to synthesize and evaluate the semi-synthetic skin substitute. Aim 1 was to prepare and characterize the decellularized small intestine tissue. Aim 2 was to engineer an aptamer functionalized gelatin-PEG hydrogel and test the capability of the hydrogel in vascular endothelial growth factor (VEGF) sequestration and release. Aim 3 was to integrate the hydrogel with the decellularized intestine and examine the functions of the semi-synthetic skin substitute. The success of this study will lead to the synthesis of a biologically functional tissue substitute for tissue regeneration.

TABLE OF CONTENTS

LIST OF FIGURES

LIST OF TABLES

ACKNOWLEDGEMENTS

Firstly, I would like to express my sincere gratitude to my advisor Prof. Yong Wang for the continuous support of my Ph.D. study and related research, for his patience, motivation, and immense knowledge.

Besides my advisor, I would like to thank the rest of my thesis committee: Prof. Nanyin Zhang, Prof. Siyang Zheng, and Prof. Tak-Sing Wong for their insightful comments and encouragement, but also for the hard questions which inspired me to widen my research from various perspectives.

I thank my fellow lab mates in for the stimulating discussions, the sleepless nights we worked together before deadlines, and all the fun we have had in the last five years. Also, I thank my friends. Without your help, I could not have finished my study here.

I would like to thank my family: my parents and my wife and my children for supporting me spiritually throughout the pursuit of this Ph.D. and exploration of my life.

Last but not the least, I thank the financial support from the U.S. NSF CAREER program under award number DMR-1332351, the National Heart, Lung, and Blood Institute of the NIH under award number R01HL122311, the Penn State Start-Up Fund, and China Scholarship

Chapter 1

Introduction

1.1 Abstract

Skin damage is a major healthcare challenge worldwide. Decellularized tissues composed of extracellular matrix (ECM) are a major branch of skin substitutes. Decellularized small intestine has been favored in skin repairs because it physically stimulates cell adhesion and proliferation by providing the appropriate architectural complexity and structure support. However, the decellularized intestine cannot chemically stimulate cells because the growth factors are denatured due to the harsh decellularization procedure. Therefore, great efforts are need to improve the chemical stimulation of decellularized intestine for skin regeneration.

Synthetic materials have been used in tissue engineering via the function of controlled growth factors delivery. By incorporating affinity ligands into synthetic materials, the functionalized synthetic materials can sustainably release growth factor. Thus, the integration of synthetic materials into decellularized tissues generates a semi-synthetic substitute, which can provide both physical and chemical support in tissue regeneration. In this study, aptamer functionalized gelatin-PEG hydrogel was chosen to be incorporated into decellularized intestine. Because the semi-synthetic skin substitute exhibits the key features of both physical (e.g., structure and mechanic) and chemical (e.g., growth factor) support. It is expected to provide a better skin regeneration than current skin substitutes.

1.2 Skin Wounds

Skin is the largest and one of most important organs in our body system.[1] It is composed of three layers known as epidermis, dermis and the subcutaneous layer (**Figure 1**).[2] The epidermis is the outer layer made mostly of keratinocytes; the dermis, near the epidermis, is a relatively thick layer of elastic and fibrous tissues; the subcutaneous layer, lying beneath the dermis, is made of fat cells. Skin tissue has many critical functions such as protection, sensation, thermoregulation, and evaporation control.[3]

Due to the location and tremendous surface area of skin tissue, skin is the most vulnerable organ in our body.[4] The most common causes of skin wounds are summarized in **Table 1-1**. The National Center for Health Statistics reported more than 31.5 million outpatient and 40 million inpatient surgeries in the United States in 2000, and the number has increased every year. [5] Another report showed that approximately 1% to 2% of the population experience chronic skin wounds in developed countries.[6] Because skin wounds are a major threat to human health, more than $25 billion is spent treating skin wounds every year. [5] Additionally, the budget rapidly increased cost due to the increase of healthcare, the incidence diabetes and obesity, and an aging population.[5] To solve these challenges, great efforts have been made to develop medical products promoting the recovery of wounded skin.[7–11] Although improvements in skin regeneration have been achieved in the past 20 years, the current skin substitutes for wound repair have been challenged by slow healing, wound contraction, scar formation, and poor integration with host tissue.[12]

Skin is an important organ for maintaining many functions including protection, sensation, thermoregulation, and evaporation control. Due to its specialties, it is the most vulnerable organ, resulting in a major threat to human health. Therefore, there is a great need to develop an effective skin substitute to improve the medication of skin wounds.

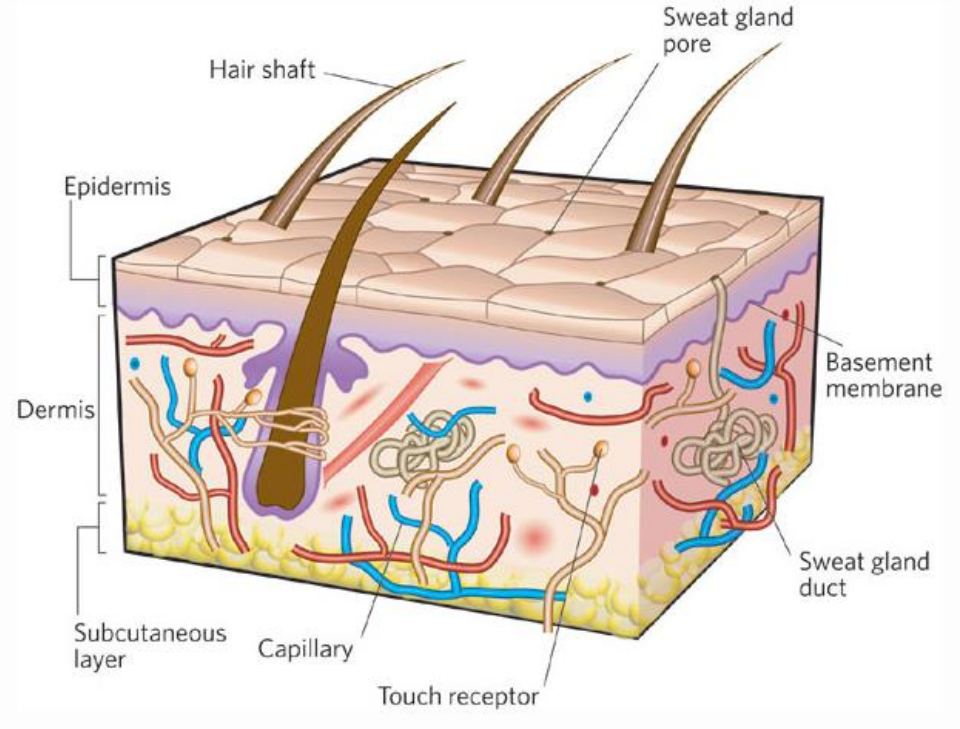

Figure 1-1 Illustration of skin structure. The epidermis is the outer layer and made mostly of keratinocytes; the dermis, near the epidermis, is a relatively thick layer of elastic and fibrous tissues; the subcutaneous layer, lying beneath the dermis, is made of fat cells. (Image adapted from Butler J.[2])

Table 1-1 Summary of skin wounds

Causes	Wound types
Skin tears	Separation of the epidermis from dermis
Burnings	Partial skin loss
Frictions	Skin surface damage
Closed intact surgical wounds	Partial loss of epidermis and dermis
Abrasions	Superficial or partial thickness skin injury
Donor sites	Partial loss of epidermis and dermis
Venous leg ulcers	Partial loss of epidermis and dermis
Lacerations	Separation of the epidermis from dermis
Open surgical wounds	Partial loss of epidermis and dermis
Neuropathic/diabetic foot ulcers	Partial loss of epidermis and dermis

1.3 Skin Substitute

Numerous skin substitutes have been studied in attempts to regenerate skin tissues in the past 100 years.[13–18] Early stage skin substitutes were focused on two aspects: 1) to prevent water, heat, protein, and electrolyte loss; 2) to exhibit antimicrobial, antioxidant, and anti-inflammatory attributes.[19] As the wound healing mechanisms were further studied in the past 20 years, the second generation of skin substitutes began to focus on the mimicking of both the physical and chemical features of native skin tissue (e.g., physical structure and signaling molecules).[20] Regardless of the types of skin substitutes available, current skin substitutes can be summarized into two categories: decellularized substitutes and synthetic substitutes.

1.3.1 Decellularized Substitutes

Decellularized substitutes are from natural tissues which have similar physical features as skin tissue such as mechanical properties, compositions, and structures.[21,22] The application of decellularized tissues is derived from autograft, which an effective technique for regenerating a variety of tissues.[23–25] Autograft is surgically removing skin tissue from one part of a patient's body and transplanting the harvested skin tissue to the defective area on the same patient.[26] As the harvested skin tissue has similarly properties to the target tissue, it can provide a desirable microenvironment for promoting skin repair. However, autograft has several limitations in clinical applications.[27,28] For example, the harvest of healthy skin can cause donor site morbidity, pain to patients, and second scars. Additionally, this method cannot be applied to the patients who have large areas of skin damage due to the limitation of available healthy skin.[27,28] To solve this problem, allogeneic and heterogenetic tissues have been studied as alternative method. In order to avoid immune rejection, these tissues were decellularized before being applied to humans.[29] **Table 1-2** lists the decellularized substitutes used for treating skin wounds. The decellularized

tissues that promote tissue regeneration are due to its major component ECM. The ECM provides a favorable physical microenvironment for cell adhesion, proliferation, migration and differentiation.[30–36], by which the decellularized tissues induce tissue recovery. However, the tissue regeneration also relies on the signaling molecules (e.g., growth factors) and growth factors are denatured in the process of decellularization.[37–39] So the decellularized skin substitutes are limited to provide a biochemical stimulation in the tissue regeneration.[40] As a result, the decellularized tissues cannot achieve the ideal skin regeneration as autograft does.

1.3.2 Synthetic Skin Substitutes

Synthetic materials are another large branch of skin substitutes. They are favored because they are able to controlled release of growth factors for promoting tissue regeneration.[41–46] A variety of growth factors have been synthesized and applied to treat skin wounds.[47–54] In the clinical tests, these growth factors activate the signaling transduction pathways and regulate cell for would healing. **Table 1-3** lists the most common growth factors in skin regeneration. Unlike decellularized tissues, synthetic materials can be tailored during or after scaffold formation. As a result, synthetic materials can be designed and fabricated to be incorporated with growth factors.[55,56] For example, Morimoto et al. developed a novel collagen/gelatin sponge, which can provide bFGF stimulation for treating skin ulcers.[57] Fujisato et al. prepared a chondrocyte-collagen composite and tested its capability to load bFGF for tissue regeneration.[58]. Although the synthetic substitutes can provide growth factor stimulation in tissue regeneration, the current synthetic substitutes cannot mimic the complex structure of native tissues.[59] As a result, the synthetic substitute cannot also achieve the ideal skin regeneration as autograft does.

Table 1-2 Decellularized skin substitutes in wound healing. [60]

Product name	Product description	Advantage	Disadvantage
Dermagraft®	Cryopreserved allogenic neonatal fibroblasts derived from neonatal foreskin	• Semitransparency allows continuous observation of underlying wound surface • Similar as allograft for graft take, wound healing time, wound exudate and infection • No adverse reactions, such as evidence of rejection	Used for temporary coverage 6 month shelf life
AlloDerm®/ Strattice®	lyophilized human acellular cadaver dermal matrix serves as a scaffold for tissue remodeling	• Immediate permanent wound coverage • Allows grafting of ultra-thin STSG as one-stage procedure • Template for dermal regeneration • Immunologically inert since the cells responsible for immune response and graft rejection are removed during the processing • Reduced scarring • Can vascularize over exposed bone and tendon • 2 year shelf life • Good aesthetic and functional outcomes (less hypertrophic scar rates, good movement) • Injectable micronized form is also available (Cymetra®)	• Risk of transmission of infectious diseases • No viral or prion screening • Collection fluid risk (seroma, hematoma, infection) • Possibility of donor rejection • Expensive
Biobrane®	acellular dermal matrix made of porcine type I collagen	• Dressing naturally separates from wound • Reserved for fresh wounds (<48 h) with low bacterial counts • Porous material allows for exudate drainage and permeability to antibiotics • Higher infection rates than other dressings • Reduces pain levels and nursing requirements when compared to traditional dressings • Shortens LOS • Biobrane-L® available for less aggressive adherence	• Does not debride dead tissue • Permanent scarring in partial-thickness scald wounds
Integra® Dermal	a porous matrix of fibers of cross-linked bovine tendon collagen and glycosaminoglycan	• Immediate permanent skin substitute • One of the most widely accepted synthetic skin substitutes • Median take of 85% • Two stage procedure requiring a minimum of 3 weeks between the application of Integra® and STSG • More aesthetic compared to autograft • Safe, effective, and widely utilized for burn reconstruction • Integra Flowable Wound Matrix® approved through 510(k) process in 2007	• Complete wound excision • High risk of infection and graft loss since it is avascular
GraftJacket®	Acellular dermal matrix from cadaver skin	• 2 year shelf life • Pre-meshed for clinical application • Single application • Utilized in both deep and superficial wound healing	Cryopreserved

Table 1-3 Growth factors in skin regeneration. [47]

Factor name	Primary activity
EGF	Attracts cells to the wound sites, promotes proliferation of mesenchymal, glial and epithelial cells
FGF	Promotes proliferation of many cell types, organizes endothelial cells into tube-like structures, promotes angiogenesis.
IGF-I	Promotes proliferation of many cell types, coordinates balanced growth among multiple tissues.
IGF-II	Promotes proliferation of many cell types (less active in the adult body)
PDGF	Promotes proliferation of connective tissue, glial and smooth muscle cells
TGF	Anti-inflammatory (suppresses cytokine production and class II MHC expression), promotes wound healing and inhibits macrophage and lymphocyte proliferation
VEGF	Regulates blood vessel formation, sustains the proliferation and differentiation of different cell types, including progenitor cells of different tissuesand the CNS, stimulates muscle regeneration, regulates endothelial cell proliferation, angiogenesis, vasculogenesis and vascular permeability

1.4 Development of a Semi-synthetic Skin Substitute

The ideal skin regeneration relies on both physical and chemical support. Physical support provides appropriate structure and achitecture for cell growth. Chemical support activates signal transduction pathways for inducing cell adhesion, proliferation, migration and differentiation. To simultaneously achieve two functions, a semi-synthetic substitute was created using decellularized intestine, gelatin-PEG hydrogel, anti-VEGF aptamer, and VEGF. Because the semi-synthetic substitute can provide both physical and chemical support in tissue regeneration, it is expected to not only provide similar therapeutic outcomes as autograft, but also avoid the disadvantages of autograft, such as secondary surgery, limited material availability, and donor site morbidity.

1.4.1 Decellularized Small Intestine

Decellularized small intestine emerged as one of naturally derived ECMs has been applied in the applications of skin regeneration for more than 20 years.[61,62] ECM of small intestine that has a natural framework is capaple of simulating the appropriate microenvironment for promoting the healing process.[63] After decellularized intestine was applied to skin wounds, it induced the body to build new tissues and replace the intestine derived materials. Additionally, the new formed tissues are same as the original tissues existed in the local area of body. The studies also showed that decellularized intestine was able to induce new blood vessel formation. The newly formed blood vessels nourish the wound sites by supplying vital molecules for rebuilding to the damaged skin tissues.

Decellularized intestine has been approved by FDA in a variety of clinical applications.[64] Matthew Parmenter, one of the first doctors to use decellularized intestine, has already treated about 150 patients successfully.[65] In addition to the skin wounds and open sores, decellularized intestines have been used to treat urinary incontinence in women, repair internal organs, and save the limbs of people suffering from deep wounds that were previously not treatable.[66] Despite the

great advantages of decellularized intestines, decellularized intestine is limited by the absence of numerous signaling proteins, such as growth factors. The growth factors are denatured in the process of decellularization, which is designed to avoid the potential for immune reactions. Decellularized intestine is a promising matrix that can be applied in skin repairs. The function of decellularized intestine in skin regeneration can be further improved if bioactive growth factors were present in decellularized intestine.

1.4.2 Aptamer Functionalized Hydrogel

Synthetic hydrogel is one of most popular synthetic materials used in skin regeneration because of its advantage in delivering growth factors. Based on mechanism of growth factor delivery, the synthetic hydrogels can be summarized into two categories: degradable and diffusible hydrogels[104,105] In degradable hydrogels, the growth factors are embedded into biodegradable polymers, which can be broken down spontaneously into harmless end products, followed by elimination via biological cycles in the body.[106] The growth factors can be sustainably released during the process of degradation. Although degradable hydrogels achieved sustainable growth factor release, their success is challenged by the denaturation of growth factors. The synthesis of polymeric hydrogels often involves harsh conditions, which can significantly denature the growth factors. Additionally, most degradable hydrogels are not porous. Thus, cells cannot penetrate into the hydrogel and achieve a three dimensional tissue regeneration. In contrast, diffusible hydrogels are permeable and the growth factor can be loaded post synthesis of polymeric hydrogels.[107] This allows the diffusible hydrogels to easily avoid the issue of protein denaturation. Therefore, diffusible hydrogels are used extensively in the applications of tissue regeneration involving growth factors. For example, Dehghani et al. modulated the porosity and microarchitecture of diffusible hydrogels as growth factor carrier for tissue regeneration.[108] Tabata et al. synthesized a collagen diffusible hydrogels to release VEGF for inducing angiogenesis *in vivo*.[109] Among these

diffusible hydrogels, gelatin based hydrogel is a promising candidate to deliver growth factors because it provides good biocompatibility. Khademhosseini et al. synthesized a gelatin-PEG hydrogel and used it to deliver growth factor. The results showed that the scaffold can not only successfully deliver growth factor, but also shows a significant improvement in cell attachment.[110] Lee et al. designed a gelatin hydrogel for delivering insulin-like growth factor (rhIGF-1). The hydrogel showed both sustained rhIGF-1 release and desirable biocompatibility to cells.[111]

As known, the skin regeneration is a time dependent medication and most skin repair needs at least weeks. To obtain a desirable skin recovery, the skin substitute is required to be able to maintain growth factors stimulation over the entire therapeutic period. To achieve the sustainable growth factor release, a variety of affinity ligands (e.g., heparin, metal ions, and peptides) have been studied to be incorporated into synthetic substitute for regulating growth factor release. [56–59] For example, Zieris et al. incorporated heparin into PEG hydrogel for sustainable growth factor delivery. [60] Lin et al. conjugated affinity peptide to the PEG hydrogel for bFGF delivery. [61] However, these affinity ligands have several limitations in regulating growth factor release. For example, heparin only relies the charge-charge interaction and has a constant binding affinity with growth factors. Metal ions also have a weak binding affinity with growth factor. Additionally, it shows low stability in vivo.[58] Although the peptide can be adjusted to obtain a different binding affinity with the growth factor and accomplish the variable growth factor release rate in various applications, the fast degradation of peptide aptamers in vivo significantly limits its applications.[61]

Nucleic acid aptamer is a new affinity ligand that has been used to control the delivery of drug molecules including growth factors.[112,113] Nucleic acid aptamers are synthetic DNA or RNA oligonucleotides that can bind to target molecules with high affinities and specificities.[114–116] The nucleic acid aptamers have been extensively applied for growth factors delivery because

of its special merits in biological applications. First, a large number of aptamers were selected and studied for growth factor delivery, which demonstrated this system works well.[117,118] Second, since the nucleic acid aptamers are small, most of them can be synthesized by chemical reactions. It means the aptamer can be easily recoded to change binding affinity to target molecule and further alter drug release profile. Third, it has been proven that nucleic acid aptamers have a strong stability with the aid of chemical modification, which ensure the long function period *in vivo*. Therefore, the nucleic acid aptamer is a good candidate to incorporate to the hydrogel system for growth factor delivery.

In summary, a diffusible based synthetic substitute was synthesized using gelatin and PEG. The nucleic acid aptamer was also incorporated into hydrogel for regulating growth factor release. Because synthetic substitute can control release of growth factors, it can provide chemical stimulations to promote cell adhesion, proliferation, migration, and differentiation in tissue regeneration.

1.4.3 Semi-synthetic Skin

In this study, semi-synthetic skin was synthesized using decellularized small intestine and aptamer functionalized gelatin-PEG hydrogel. Decellularized small intestine, derived from native tissue by removing cellular materials, leaves the inherent architectural complexity and structure, which can provide a physical support for cell growth. Aptamer functionalized gelatin-PEG hydrogel composed of synthetic polymers can achieve the controlled release of growth factors for chemically inducing cell adhesion, proliferation, migration and differentiation. VEGF was used as a model of growth factors because it has several special advantages inducing cell adhesion, proliferation, and angiogenesis. Due to the combination of two components together, the semi-synthetic skin is expected to provide both structural support and growth factor stimulation in skin repairs.

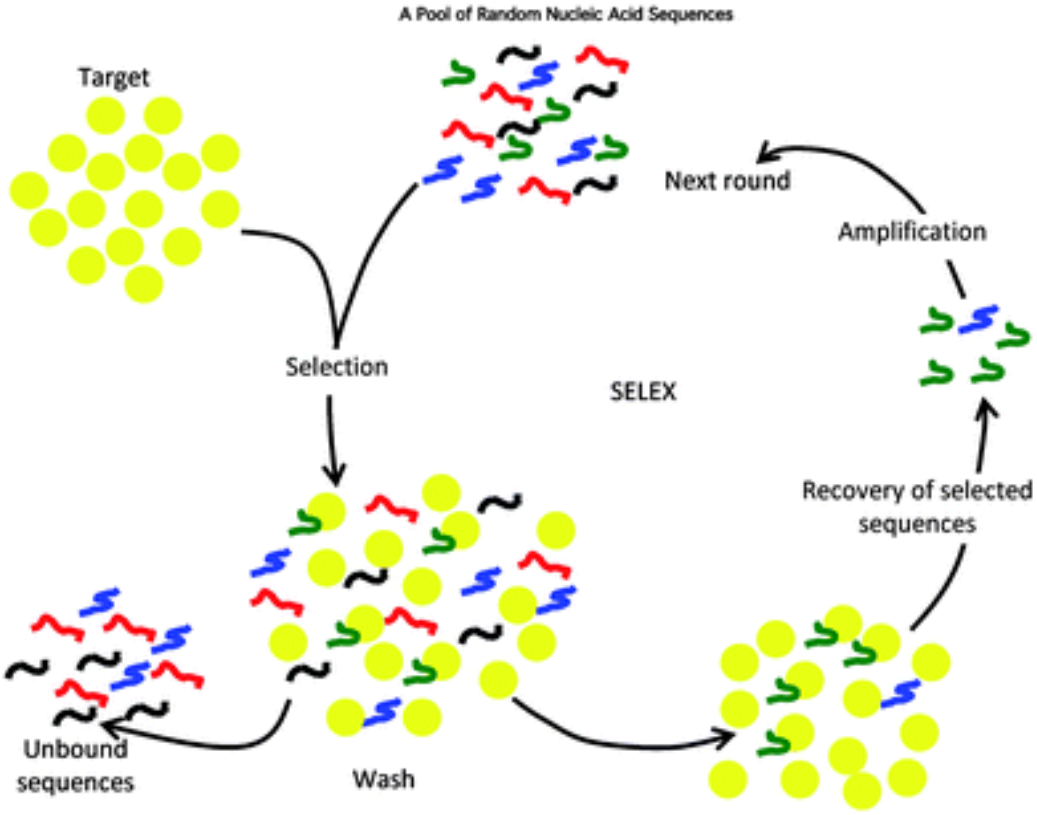

Figure 1-2 Illustration of selection of aptamers against a specific target. [67]

1.5 Conclusion

Skin damage is a major healthcare challenge worldwide. A variety of skin substitutes have been developed to regenerate skin tissues. Current skin substitutes can be summarized into two categories: decellularized tissues and synthetic materials.

Decellularized intestine, a decellularized tissue, is well accepted and extensively used to mimic the physical structure of native skin structure for inducing skin recovery while aptamer functionalized gelatin-PEG hydrogel is a promising synthetic material for controlled release of growth factors to chemically promote skin regeneration.

As known, the ideal skin regeneration relies on both physical and chemical support. However, current skin substitutes can only provide either physical or chemical support in skin repairs. In this study, a semi-synthetic skin was designed by incorporating decellularized small intestine with aptamer functionalized gelatin-PEG hydrogel. VEGF was chosen from the pool of growth factors because of its promising functionalities to promote skin recovery. Due to the fact that the semi-synthetic skin substitute inherits the advantages of both decellularized and synthetic substitutes, it is expected to opens a new avenue to provide both physical and chemical stimuli in tissue regeneration.

Chapter 2

Decellularization of small intestine

2.1 Abstract

Decellularized substitutes have been applied in tissue regeneration because the ECM extracted through the process of decellularization provides an appropriate physical microenvironment for cell adhesion, proliferation, migration, and differentiation. Among the tissues studied for skin regeneration, porcine small intestine has been favored because it can highly mimic the complex structure and architecture of native skin tissues, is relatively common, and is under moderate regulation policies.

In this chapter, different decellularization reagents were investigated for obtaining maximal removal of cellular materials and minimal damage of ECM. After the porcine small intestine was decellularized, the morphology of decellularized small intestine was studied by SEM. The cellular materials and ECM of decellularized intestine were also examined by H&E and trichrome staining. Next, the mechanical properties of small intestine before and after decellularization were evaluated. Finally, the cell adhesion of decellularized intestine was tested using HUVECs.

2.2 Introduction

Tissue decellularization is to remove all cellular material while preserving the three-dimensional organization and structure of the ECM. Unlike the synthetic materials, decellularized tissues can maximally mimic the complex architecture of target tissues. As a result, decellularized tissue can provide desirable structural support and physical microenvironment conditions for cell adhesion, proliferation and migration during tissue regeneration.

A variety of tissue resources have been used to prepare decellularized substitute for skin repairs (**Table 2-1**). Compared to other tissues, porcine small intestine is favored because it can mimic the structure of skin tissue at a low cost. For example, decellularized small intestine has been applied to a variety of clinical applications in skin regeneration.[68] Kim et al. reported that the decellularized intestine sponge presented uniform adherence to the wound surface and provide physical support for actively promoting the regeneration of dermal collagen in the wound area.[69] As a result, small intestine is a promising material as wound dressing.

Prior to the use of porcine small intestine, it was decellularized to remove the cellular materials in order to avoid immune response. Since the ECM of intestine was the major component for skin regeneration, the ECM of porcine small intestine should be minimally damaged during decellularization. During past 20 years, a variety of reagents and techniques have been developed for an ideal tissue decellularization (**Table 2-2**). For example, Wilson et al developed a detergent-enzyme extraction process involving Triton-surfactants lauryl sulfate (SDS) and other chemicals. The results showed that triton-SDS was very effective to remove nuclei and intracellular proteins, however it could damage the ECM in some degree during the process of decellularization. [70] Courtman et al tried triton only instead, which was a mild detergent. The results indicated that although the triton itself did not affect the original composition and mechanical integrity of tissue ECM, it was not effective to remove cellular materials. [71] Cartmell et al used triton-tributyl

phosphate (TNBP) to improve the outcome of decellularization. The results demonstrated that triton-TNBP not only was efficient to clean the cellular materials, but also did not significantly damage tissue ECM. [72]

In summary, porcine small intestine was studied as a decellularized skin substitute. To obtain a desirable decellularization outcome, a variety of decellularization protocols have been studied to obtain a maximal removal of cellular materials and minimal ECM denaturation. After the porcine small intestine was decellularized, the examination of decellularized intestine showed that it was a promising candidate for skin regeneration through the desirable architectural and mechanical support.

Table 2-1 Summary of clinical products for skin regeneration. [73]

Manufacture	Tissue source
AlloDerm® (Lifecell Corp.)	Human dermis
AlloPatch HD™, FlexHD® (Musculoskeletal Transplant Foundation)	Human dermis
NeoForm™ (Mentor Worldwide LLC)	Human dermis
GraftJacket® (Wright Medical Technology Inc.)	Human dermis
Strattice™ (Lifecell Corp.)	Porcine dermis
Zimmer Collagen Repair Patch™ (Zimmer Inc.)	Porcine dermis
TissueMend® (Stryker Corp.)	Bovine dermis
Oasis®, Surgisis® (Cook Biotech Inc.)	Porcine small intestine
Restore™ (DePuy Orthopaedics)	Porcine small intestine
FortaFlex® (Organogenesis Inc.)	Porcine small intestine
CorMatrix ECM™ (CorMatrix® Cardiovascular Inc.)	Porcine small intestine
AlloDerm® (Lifecell Corp.)	Human dermis
AlloPatch HD™, FlexHD® (Musculoskeletal Transplant Foundation)	Human dermis
NeoForm™ (Mentor Worldwide LLC)	Human dermis
GraftJacket® (Wright Medical Technology Inc.)	Human dermis
Strattice™ (Lifecell Corp.)	Porcine dermis

Table 2-2 Agents and techniques for decellularizing tissue. [73]

Agents/Techniques	Mode of action	Effects on ECM
Chemical Agents		
Acids and bases	Solubilizes cytoplasmic components of cells, disrupts nucleic acids, tend to denature proteins	May damage collagen, GAG, and growth factors
Hypotonic and hypertonic solutions	Cell lysis by osmotic shock, disrupt DNA-protein interactions	Effectively lyses cells, but does not effectively remove cellular residues
Triton X-100	Disrupt DNA-protein interactions, disrupt lipid-lipid and lipid-protein interactions and to a lesser degree protein-protein interactions	Mixed results with efficacy dependent on tissue, more effective cell removal from thin tissues, some disruption of ultrastructure and removal of GAG, less effective than SDS
Sodium dodecyl sulfate	Solubilize cell and nucleic membranes, tend to denature proteins	Effectively removes nuclear remnants and cytoplasmic proteins from dense tissues, tends to disrupt ultrastructure, removes GAG and growth factors and damages collagen
Triton X-200	Solubilize cell and nucleic membranes, tend to denature proteins	More effectively removes cells from thin tissues but with greater disruption of ultrastructure compared to other detergents
CHAPS	Exhibit properties of non-ionic and ionic detergents	Effectively removes cells with mild disruption of ultrastructure in thin tissues
Acetone	Cell lysis by dehydration, solubilize and remove lipids	Effectively removes cells from dense tissues and inactivates pyrogens, but crosslinks and precipitates proteins, including collagen
Tributyl phosphate	Forms stable complexes with metals, disrupts protein-protein interactions	Mixed results with efficacy dependent on tissue, dense tissues lost collagen but impact on mechanical properties was minimal
Biologic Agents		
Nucleases	Catalyze the hydrolysis of ribonucleotide and deoxyribonucleotide chains	Difficult to remove from the tissue, could invoke an immune response
Trypsin	Cleaves peptide bonds on the C-side of Arg and Lys	Prolonged exposure can disrupt ECM ultrastructure, removes ECM

		constituents such as collagen, laminin, fibronectin, elastin, and GAG, slower removal of GAG compared to detergents
Chelating Agents (EDTA, EGTA)	Chelating agents bind metallic ions, thereby disrupting cell adhesion to ECM	Typically used with enzymatic methods (e.g. trypsin) but can be used with other agents, ineffective when used alone
Physical and Miscellaneous Agents		
Temperature (freezing and thawing)	Intracellular ice crystals disrupt cell membrane	Ice crystal formation can disrupt or fracture ECM
Direct application of force	Removal of tissue eliminates cells and force can burst remaining cells	Force can directly damage ECM
Pressure	Pressure can burst cells and aid in removal of cellular material	Pressure can disrupt ECM
Electroporation	Pulsed electrical fields disrupt cell membranes	Electrical field oscillation can disrupt ECM
Techniques to Apply Agents		
Perfusion	Facilitates chemical exposure and removal of cellular material	Pressure associated with perfusion can disrupt ECM
Pressure gradient across tissue	Facilitates chemical exposure and removal of cellular material	Pressure gradient can disrupt ECM
Supercritical fluid	Pressure can burst cells, supercritical fluid facilitates chemical exposure and removal of cellular material	Pressure necessary for supercritical phase can disrupt ECM
Agitation	Can lyse cells, but more commonly used to facilitate chemical exposure and removal of cellular material	Aggressive agitation or sonication can disrupt ECM

2.3 Materials and Methods

2.3.1 Materials

Porcine small intestine was obtained from a butcher (Holland's Brothers Meats, Altoona, PA). Triton x-100, sodium dodecyl sulfate, phosphate buffered saline, haematoxylin, eosin, paraffin, Histosolve, ethanol, DPX mounting medium, Bouin's Fixative Solution, ethanol, tris base, sodium chloride, Ethylenediaminetetraacetic Acid disodium salt dihydrate, proteinase K, phenol/chloroform/isoamyl Alcohol (25:24:1 Mixture, pH 6.7/8.0, Liq.), acetic acid, sodium acetate anhydrous, Tris-EDTA solution, and penicillin were ordered from Fisher Scientific (Suwanee, GA). Biebrich scarlet-acid fuchsin solution, phosphomolybdic acid solution, Aniline Blue solution, and phosphotungstic acid solution were ordered from Sigma-Aldrich (St. Louis, MO). Human umbilical vein endothelial cells (HUVECs), Medium 200 (M200), low serum growth supplement (LSGS), and Vybrant DiD Cell-Labeling Solution were purchased from Invitrogen (Grand Island, NY).

2.3.2 Methods

2.3.2.1 Porcine Small Intestine Decellularization

The porcine small intestine was obtained from a butcher (Hollands Brothers Meats, Altoona, PA) and thoroughly washed with distilled water before use. The porcine small intestine was mixed with 3% Triton X-100 or 3% SDS with a weight ratio of 1:10. After overnight incubation with vortex, the porcine small intestine was filtered out and placed in 3% SDS for another overnight incubation with vortex. The porcine small intestine was cleaned with distilled water for 3 times to remove Triton X-100 and SDS. After that, 1% w/v penicillin was used to incubate with porcine small intestine under continuous agitation at 4 ℃ for 24 hours. The decellularized small intestine was stored at -20 ℃. When the decellularized small intestine was needed, it was thawed and washed with sterilized water to remove the penicillin.

2.3.2.2 DNA Quantification

100 mg of decellularized small intestine was weighed out and transferred to a mortar. The sample was frozen by adding liquid nitrogen and grinded with a pestle. Next, the intestine powder was digested in 1.5 mL of an extraction buffer composed of 10 mM tris (pH 8), 100 mM NaCl, 50 mM EDTA (pH 8.0), 0.5% SDS, and 5 mg/mL Proteinase K at 55 ℃ with gentle agitation overnight. The mixture was centrifuged at 2000 rpm and then the supernatant was transferred to a new tube. Equal amounts of phenol/chloroform/isoamyl alcohol (25:24:1) were added to the supernatant and centrifuged at 10000 x g for 5 minutes. The upper aqueous phase was carefully removed and transferred to another new tube. Two volumes of 100% ethanol and 0.1 volumes of 3 M sodium acetate (pH = 5.2) were added to the solution in the new tube. Next, the tube was placed at –20 ℃ for DNA precipitation from the solution. The next day, the sample was centrifuged at 4 ℃ for 30 minutes at 16,000 × g to pellet the DNA. The supernatant was carefully removed without

disturbing the DNA pellet. The DNA pellet was re-suspended in 300 µL of TE buffer by pipetting up and down 30–40 times. To assess the DNA solution, a UV measurement at 260 nm was taken using a Nanodrop 2000c. To normalize the data, the amount of DNA was divided by the dry weight of the samples.

2.3.2.3 Paraffin Embedding

Dehydration and paraffinization was done in a Leica tissue processor. The tissue samples were loaded into a Histosolve (xylene substitute) bath for storage until the embedding began. The tissues were dehydrated through 1 change each of 70% and 85% ethanol for 30 and 40 minutes, respectively. This was followed directly by 2 changes each of 95% and 100% ethanol for 40 minutes. The dehydrated samples were cleared with 3 changes of Histosolve for 40 minutes before being saturated with molten paraffin. All of the baths were gently agitated. The samples were then embedded in paraffin blocks.

2.3.2.4 Slide Preparation

Samples were sectioned at 10 µm thickness via microtome. Ribbons were stretched in a floating bath at 35 ℃ and picked up with a glass slide. Six slides of each tissue were made. Slides were dried for 2-4 hours before staining and observation.

2.3.2.5 H&E Staining

Slides underwent a combined deparaffinization and staining protocol. Slides were heated for 18 minutes followed by the removal of paraffin with 3 changes of Histosolve for 2.5 minutes. Samples were then rehydrated with 1 change each of 100% and 95% ethanol for 1.5 minutes followed by a running water wash for 1 minute. The Rehydrated samples were exposed to Hematoxylin 560 for 4.5 minutes and Define for 1 second, each followed by a-running water wash

for 1 minute. Next, the slides were placed in Bluing Buffer 8 for 30 seconds followed by a running water wash for 1.5 minutes and 1 change of 95% ethanol for 1 minute. The final stain was made with Alcoholic Eosin Y 515 for 20 second. Following the staining process, the samples were dehydrated and cleared with 2 changes of 95% ethanol for 30 seconds and 1 minute, 2 changes of 100% ethanol for 1.5 minutes and 2 changes of Histosolve for 1.5 and 2 minutes. The stained samples were mounted with DPX for observation.

2.3.2.6 Trichrome Staining

Slides underwent separate deparaffinization and staining protocols. Slides were heated for 18 minutes followed by the removal of paraffin with 3 changes of Histosolve for 10 minutes. Samples were then rehydrated with 2 changes of 100% ethanol for 3 minutes, 1 change each of 95% and 85% ethanol for 2 minutes and 1 change of 70% ethanol for 3 minutes. Rehydration was completed with 2 changes of deionized water for 2 minutes and 1 change of buffer for 5 minutes. The rehydrated samples were fixed in Bouin's solution for 1 hour at 56°C. The yellow color was removed with a running water wash for 5 minutes. The samples were stained with Weigert's hematoxylin for 10 minutes, washed with running water for 5 minutes and acidified water (pH 4.7) briefly. The second stain was made with Biebrich scarlet-acid fuchsin solution for 5 minutes, rinsed with distilled water, soaked in 1% phosphomolybdic-phosphotungstic acid solution until the red color faded, and rinsed with distilled water again. The final stain was made with aniline blue solution for 5 minutes, followed by rinsing the samples with tap water and soaking in 1% phosphomolybdic-phosphotungstic acid solution in 3 minutes. The slides were washed with 1 change distilled water for 3 minutes, and 1 change of 1% acetic acid for 2 minutes followed by running distilled water. The samples were dehydrated and cleared with 1 change each of 95% and 100% ethanol for 1 minute and 2 changes of Histosolve for 1 minute. The stained samples were mounted with DPX for observation.

2.3.2.6 SEM

Decellularized intestine was cut into 5mm x 5 mm and lyophilized for one day at -60 ℃. For SEM analysis, decellularized small intestine was mounted on an aluminum stub using carbon tape and sputter coated with a thin layer of gold for 30 seconds. Then, samples were imaged using a FEI Quanta 200 Environmental SEM at an accelerating voltage of 15kV. Images were taken at 50x, 100x, and 200x magnification.

2.3.2.7 Mechanical Stretch

The decellularized intestine was cut into rectangular strips with dimensions of 5mm x 30 mm. After the decellularized intestine was fixed by clips, the thickness of the sample was measured using a digital caliper. During the test, the samples were pulled at a rate of 500 mm/min and elongated to a failure. Values were converted to stress-strain curves and the initial modulus was calculated from the initial gradient of the resulting curves (0-10% elongation).

2.3.2.8 Decellularized Small Intestine Absorption

The decellularized small intestine was prepared according to the previously described method. The decellularized small intestine was cut into 5mm x 1 mm square and dehydrated using tissue paper. The dehydrated decellularized small intestine was weighted and then transferred into 1x PBS buffer for 12 hours of incubation. After that, the rehydrated decellularized intestine was weighted again. The absorption of decellularized intestine was calculated by the ratio of the weight difference between dehydrated intestine and rehydrated intestine to the weight of rehydrated intestine.

2.3.2.9 Cell Adhesion

Decellularized small intestine was cut into 5mm x 5 mm and washed with 2% serum supplemented M200 medium for 1 hour. After that, the decellularized tissue was transfer to a 48 well plate. HUVECs were stained with 2 μg/mL calcein AM for 30 min and harvested to a 2% serum supplemented M200 medium. The cells were washed with 2% serum supplemented M200 medium for three times and diluted to a concentration of 1.0×10^5 cells/mL. 250 μL of cell solution was added into each well for incubating with decellularized tissue overnight. The decellularized small intestine was taken out and washed with 2% serum supplemented M200 medium for another three times, followed by the imaging with a fluorescence microscopy. The cell number on decellularized small intestine was quantitated using Image J software.

2.3.2.10 Statistics

Quantitative data is presented as the mean ± one standard deviation of triplication samples. Statistical significance was evaluated using Student's *t*-test.

2.4 Results and Discussion

2.4.1 Porcine Small Intestine Decellularization

A variety of decellularization reagents have been studied to treat different tissues and organs.[74–84] Among of these reagents, Triton 100-X and SDS are two of the most popular detergents used to treat numerous types of tissues.[74–78] Triton X is a non-ionic detergent. During the decellularization, it can disrupt lipid–lipid and lipid–protein interactions while leaving protein–protein interactions intact.[85] The pretreatment of tissues with Triton 100-X can effectively improve the removal of cellular materials in the step of SDS treatment. SDS is a highly ionic and amphipathic detergent and it is an effective detergent to disrupt cellular membranes and lyse cells. Because it denatures proteins, studies are needed to verify the SDS concentration and SDS treatment time for avoiding the damage of ECM structures. According to the preliminary studies, the intestine obtained the maximal removal of cellular materials without significantly loss of ECM when it was treated by the combination of Triton 100-X and SDS.

The porcine small intestines before and after decellularizing treatment are shown in Fig. xx. Compared with native intestine, the color of Triton 100-X and SDS treated decellularized intestines transited from pink to white, which indicated a strong removal of cellular materials. The morphology of decellularized intestine was observed by SEM. As shown in **Figure 2-1A**, the native intestine showed a dense structure with epithelial cells embedded in the cross-linked ECM network of elastin and collagen fibers. In contrast, the decellularized intestine exposed the ECM networking fiber after the treatment by the combination of Triton X-100 and SDS (**Figure 2-1A**). The SEM images also showed that the decellularized intestine exposed three dimensional the porous structures (**Figure 2-1B**). These interconnected pores not only significantly improve the mass transport of nutrients, wastes, oxygen, and even cells, but also make the decellularized intestine to be an ideally biological carrier.

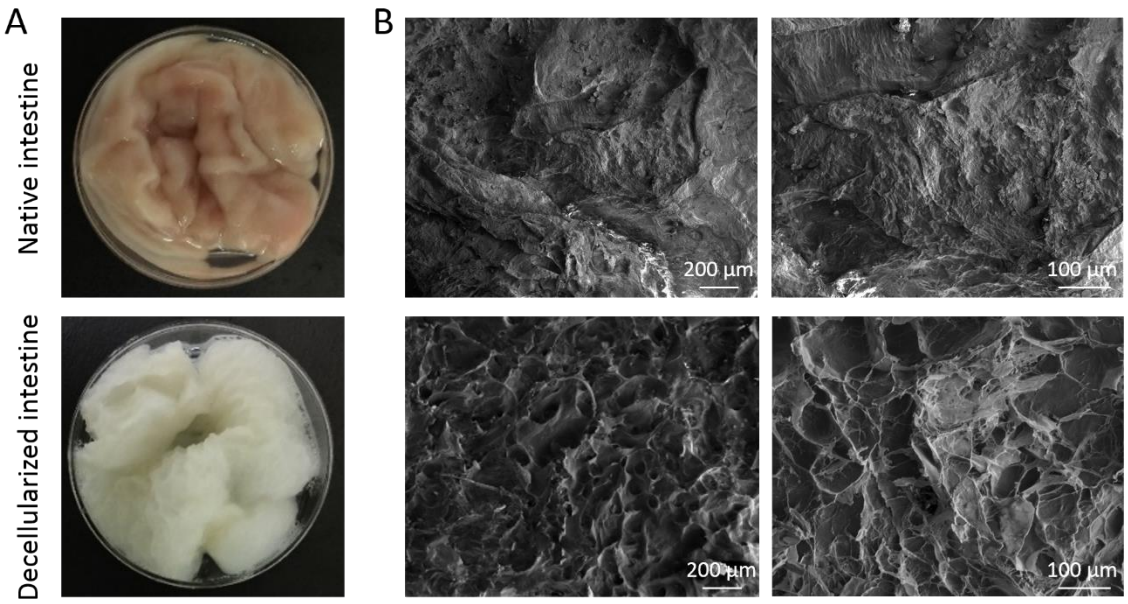

Figure 2-1 Porcine small intestine before and after decellularizing treatment. (A) Images of porcine small intestine without and with decellularization. (B) SEM images of porcine small intestine with different magnification. Native intestine (top). Decellularized intestine (bottom).

2.4.2 Examination of removal of cellular materials

The removal of cellular materials was firstly examined by Haematoxylin and Eosin (H&E) staining. Haematoxylin is a basic dye and has positive charges that can stain acidic or basophilic structures, such as nucleus, blue. In contrast, Eosin is an acidic dye and has negatively charges that can bind to the basic or acidophilic structures. Since most proteins in the ECM are basic, eosin can stain these proteins pink. The H&E staining showed that the intact intestine was stained by both pink and purple while the decellularized intestine was stained pink alone (**Figure. 2-2A**). The high magnification image of intact intestine showed that the purple color was from the dots with the diameter of 5 μm, which were cell nuclei. There were no purple dots found in decellularized intestine, which demonstrated the success of cellular materials removal (**Figure 2-2A**).

The removal of cellular materials was further quantitatively examined by the DNA content assay (**Figure 2-2B**). The results showed that DNA content of intact intestine was approximately 1,400 ng DNA/mg intestine. However, the DNA content dropped to less than 1 ng DNA/mg intestine after decellularization. Comparing to the intact intestine, the DNA content of decellularized intestine decreased 4 orders of magnitudes. The characterization of decellularization by DNA content assay showed that the decellularized intestine still contained traceable amount of DNA. Since the cells are embedded within the ECM of tissues, especially relatively dense tissues like the intestine, it is unlikely to completely remove cellular contents even with the most rigorous processing methods.

It is known that cell materials are able to elicit a host inflammatory response or stimulate an immune reaction. However, there is a threshold amount of cellular materials that is required to trigger the adverse response. Compared with other decellularized tissues, the DNA level of decellularized intestine is lower in this study. For example, Matracell® Dermis, a popular decellularized human dermis in a variety of clinic applications, contains approximately 15 ng DNA/mg intestine.[86] As a result, despite the presence of small amount of DNA in decellularized

intestine, the presence of small amounts of cellular materials is insufficient to contribute to any adverse host responses and further adversely affect biologic scaffold remodeling.

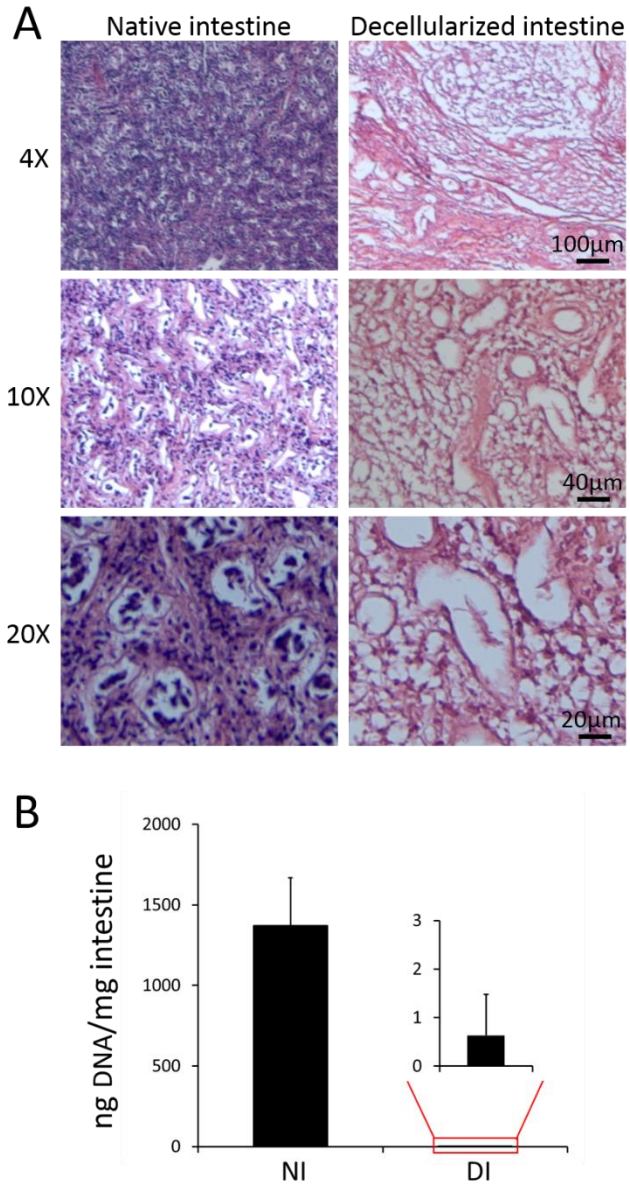

Figure 2-2 Examination of removal of cellular materials. (A) H&E staining of small intestine without and with decellularization treatment. There were blue dots showing in native intestine, which are nucleus. However, after decellularization, the cellular materials (i.e., nucleus) were effectively removal. (B) The DNA quantification of small intestines. NI: native intestine. DI: decellularized intestine.

2.4.3 Trichrome Staining

The successful decellularization is decided by not only the effective removal of cellular materials, but also the minimal damage of ECM structures. The ECM of decellularized intestine was examined by trichrome staining (**Figure 2-3**). Both intact intestine and decellularized intestine were stained blue, however, the color intensity of intact intestine was higher than that of decellularized intestine. It indicated that the ECM of intestine was observed after the decellularization treatment via Triton X and SDS (**Figure 2-3**). Compared with intact intestine, it seems that the ECM of decellularized intestine was partially damaged. During the decellularization, the detergents especially the SDS can disrupt the interaction among proteins, which results in the damage of ECM. In order to obtain the effective removal of cellular materials, the reagents are required to be able to disrupt the cell membrane and lyse cells. During this procedure, it is inevitable to break the structures of ECM. The damage of ECM has been found in a variety of tissue decellularization. For example, Weymann et al prepared decellularized aortic arch and the trichrome staining showed a portion of ECM of decellularized aortic arch was lost during the decellularization.[87] Wu et al optimized the decellularization methods and all decellularization results showed that ECM was damaged to some degree.[88] Despite the evidence of ECM damage, there is still a large amount of ECM observed in decellularized intestine, which ensures the function of supporting an appropriate microenvironment for cell adhesion, proliferation, migration and differentiation.

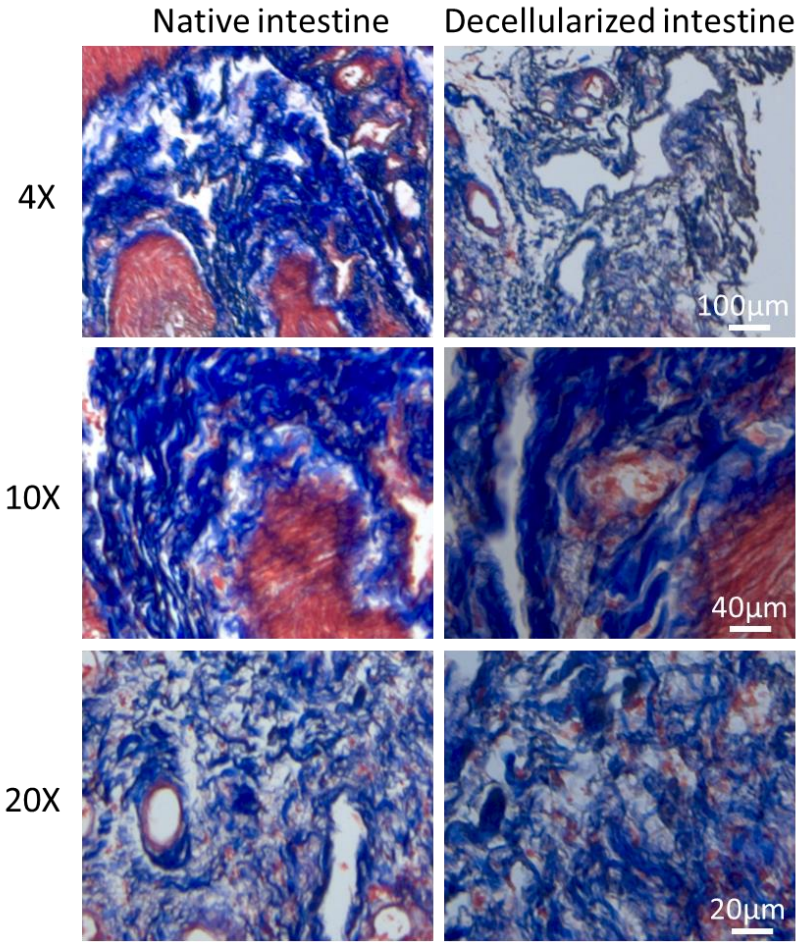

Figure 2-3 Examination of ECM in decellularization. The small intestines before and after decellularization were studied by Trichrome staining, which stains ECM to blue.

2.4.4 Physical Examination of decellularized intestine

After the cellular materials and ECM component of decellularized intestine was examined, the physical properties of decellularized intestine were studied. The mechanical properties of decellularized intestine were firstly examined by Instron 5966. The peak stress, Young's modulus, and strain at break of intestines were all measured before and after decellularization. The results showed that the intact intestine and decellularized intestine had similar peak stress, which was around 2.5 MPa (**Figure 2-4A**). However, the young's modulus of intestine was decreased from around 7 MPa to 4 MPa after decellularization (**Figure 2-4B**). After removing the cellular materials, the major components of decellularized intestine were the ECM. As a result, the decellularized intestine cannot provide as much stiffness as intact intestine. The strain at break showed that the decellularized intestine had a higher ratio between changed length and initial length after breakage than that of intact intestine (**Figure 2-4C**). The result also coincides with the data of Young's modulus because the ECM made of elastic collagens and fibronectins has high elasticity.

The swelling is another critical property of decellularized intestine because it decides loading capability of inserts including regenerative medicines, signaling proteins, and cells. During decellularization, the decellularization reagents disrupt the cell membrane and lyse cells. So the decellularization often gives rise to the swelling properties of tissues. The increased swelling allows decellularized tissue to be a good carrier for loading functional molecules or cells in tissue regeneration. The swelling of decellularized intestine was shown in **Figure 2-4D**. The intact intestine showed a swelling ratio of 182% while the decellularized intestine had 210%. Compared with intact intestine, the swelling ratio of decellularized intestine increased 28%. However, there was no significantly morphologic difference between dehydrated and rehydrated decellularized intestine, indicating the strong networking structure of ECM. The lack of change in decellularized intestine after swelling makes it a promising candidate as a transplanted scaffold.

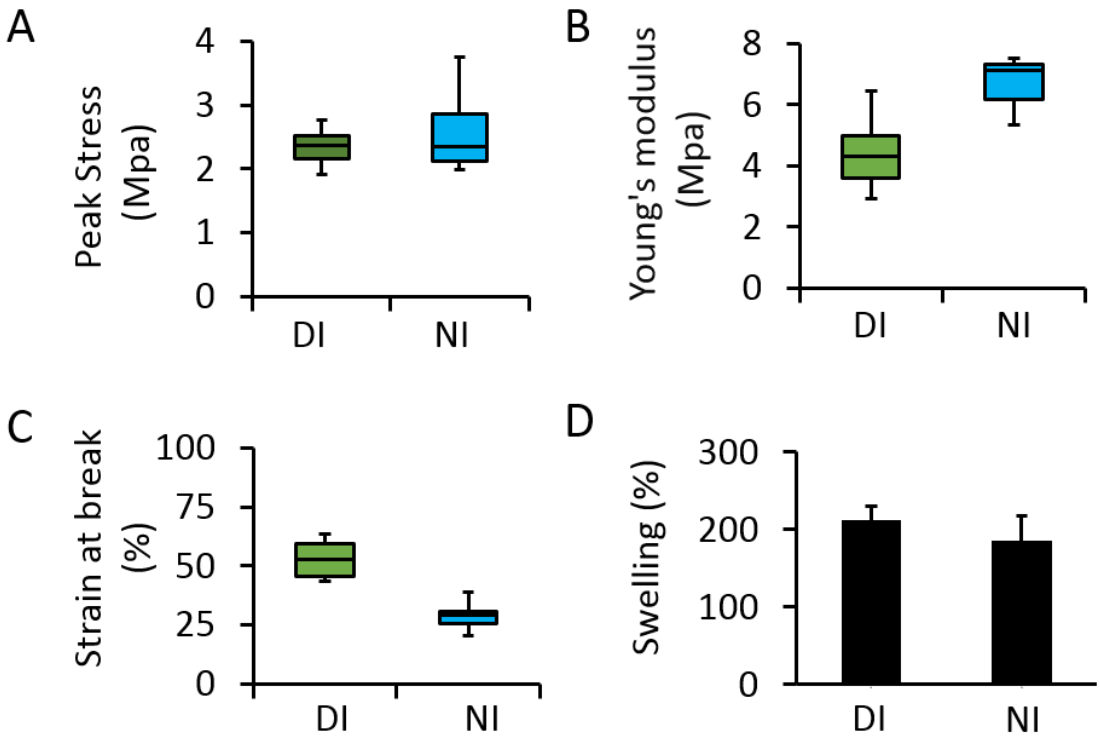

Figure 2-4 Physical Examination of decellularized intestine. (A) Peak stress. (B) Yong's modulus. (C) Strain at break. (D) Swelling property of decellularized intestine. The lyophilized decellularized intestine was soaked in 1x PBS for 1 hour. The decellularized intestine before and after incubating with PBS was scaled. The swelling ratio was determined as the increased weight over the initial weight of decellularized intestine.

2.4.5 Cell Adhesion

Cell adhesion is a critical process required in cell growth and tissue regeneration because it plays a role in regulating cell functions, contributing to cell structure, and further affecting cell survival, proliferation, and gene expression. The examination of cell adhesion by decellularized intestine was shown in **Figure 2-5**. Since the decellularized intestine has nonspecific binding to dyes, the cells was stained prior to the incubation with decellularized intestine. The results showed that the cells were able to adhere on decellularized intestine. The major component of decellularized intestine is ECM, which is made of collagen, fibronectin, and fibrin. The ECM interacts with cells for promoting cell adhesion via focal adhesion and fibrillary adhesion.[89,90]

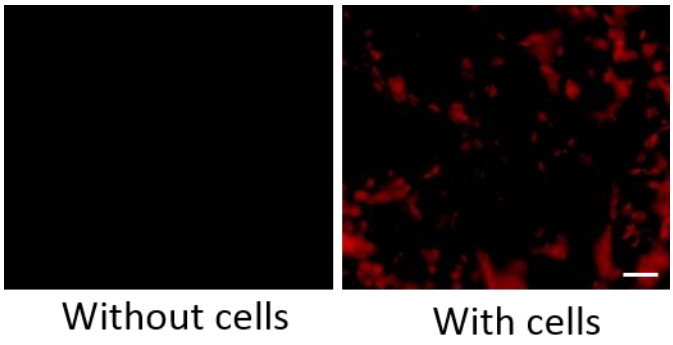

Figure 2-5 Examination of cell adhesion on decellularized intestine. The HUVEC cells were stained by Vybrant DiD following the instructions. Then the cells were harvested with the help of Trypsin. The HUVEC suspension of 250 μL with 2.5 x 10^4 cells was seeded on decellularized intestine. After 2 hours incubation, the cells seeded decellularized intestines were washed with 2% LSGS supplemented M200 for two times. The decellularized intestines were observed by fluorescence microscope. Scale bar: 100 μm.

2.5 Conclusion

Decellularized tissues have been broadly studied as tissue engineering scaffold for tissue regeneration because it has a high potential to provide an appropriate physical microenvironment for cell adhesion, proliferation, migration, and differentiation. Among the decellularized substitutes in skin regeneration, porcine small intestine has been intensively investigated because it can highly mimic the complex structure and architecture of native skin tissues, but also has plenty of sources and is under moderate regulation policies.

In this chapter, decellularized intestine was prepared based on a Triton and SDS combined decellularization method. The H&E staining and DNA quantification assay showed that the cellular materials were effectively removed while the Trichrome staining indicated a large amount of ECM still preserved after decellularization. The mechanical measurement of intact and decellularized intestines showed that the decellularized intestine had lower Young's modulus and higher strain at peak than intact intestine. It may be due to the fact that ECM is the major component of decellularized intestine. Additionally the decellularized intestine showed a good capability of swelling, which provide a way to load regenerative medicines into decellularized intestine. The cell adhesion assays also showed that decellularized intestine made of ECM supported the cell attachment.

In summary, decellularized intestine is a promising candidate as a skin substitute in tissue regeneration. Because decellularized intestine can mimic the complex structure of skin tissue, it can provide an appropriate microenvironment to support cell adhesion, proliferation, migration and differentiation. Since the decellularized intestine has plenty of pore structures and a strong swelling capability, it can also be loaded with regenerative medicines in promoting tissue recovery.

Chapter 3

Development of aptamer-functionalized hydrogel for controlled VEGF release

3.1 Abstract

Growth factors are soluble proteins participating in a variety of cellular processes during the tissue regeneration. Synthetic materials, capable of controlled growth factor delivery, have been extensively used to promote tissue recovery.

In this chapter, gelatin-PEG hydrogel was designed and fabricated for growth factor release. VEGF, the most popular growth factors for inducing cell adhesion, proliferation, and migration, was added into gelatin-PEG hydrogel to promote skin recovery. In order to obtain the ideal VEGF release curve, an anti-VEGF aptamer was incorporated into hydrogel and regulated VEGF delivery via the binding force of molecular interactions. Porous structures were also creased in gelatin-PEG hydrogel to study the interaction between cells and synthetic polymers in a 3D circumstance. The results showed that the gelatin-PEG hydrogel could be successfully synthetized with favorable property of cell adhesion. Approximately 50% of the aptamer can be conjugated into hydrogel via methacrylamide modification. The VEGF release curve showed that VEGF could be sustainably released by the aptamer functionalized hydrogel and the released VEGF was bioactive. At the end, the coculture of cells with VEGF loaded aptamer hydrogel demonstrated that controlled release of VEGF was essential to maintain cell functionalities.

3.2 Introduction

During the past twenty years, synthetic hydrogels have been studied for developing potential applicable scaffolds in tissue engineering.[91–94] Compared to the decellularized substitutes, the biggest advantage of synthetic hydrogels is that they can control the release of growth factors, which chemically stimulates cells and promotes tissue regeneration.[95–99] Growth factors are a series of signaling proteins involved in the process of tissue recovery.[100,101] They bind with cell receptors to transduce secondary signals and activate the intracellular signal transduction pathways, by which they can induce cell adhesion, proliferation, migration and differentiation.[102,103] Therefore, growth factor loaded synthetic substitutes have been extensively applied in promote tissue recovery.

As the skin regeneration is a time dependent medication, the time window of most tissue recovery is weekly based. In order to achieve the sustainable growth factor release, a variety of affinity ligands have been studied to be incorporated into hydrogel for regulating growth factor delivery. Among the affinity ligands, nucleic acid aptamer is promising because it binds to target molecules with high affinities and specificities, is stable after chemical modification, and has low immunogenicity. Therefore, aptamer functionalized hydrogel is a promising synthetic materials to control growth factor delivery for tissue regeneration.

3.3 Materials and Methods

3.3.1 Materials

Gelatin from bovine skin (type B), methacrylic acid N-hydroxysuccinimide ester, polyethylene glycol (PEG) methyl ether acrylate (Mn = 480), poly(ethylene glycol) diacrylate (Mn = 700) and Pluronic F-127 (PF127) were purchased from Sigma-Aldrich (St. Louis, MO). Dulbecco's phosphate buffered saline (DPBS), bovine serum albumin (BSA), sodium bicarbonate, glacial acetic acid, ammonium persulfate (APS), and tetramethylethylenediamine (TEMED) were obtained from Fisher Scientific (Suwanee, GA). Human umbilical vein endothelial cells (HUVEC), Medium 200 (M200), low serum growth supplement, Geltrex, Hoechst 33342, calcein AM, and ethidium homodimer-1 were purchased from Invitrogen (Grand Island, NY). Endo GRO-VEGF complete media kit was purchased from Millipore (Billerica, MA). Vascular endothelial growth factor-165 (VEGF) and VEGF enzyme-linked immunosorbent assay (ELISA) kit were obtained from Peprotech (Rocky Hill, NJ). CellTiter 96® AQueous One Solution Cell Proliferation Assay (MTS) was obtained from Promega. (Madison, WI). Anti-VEGF RNA aptamer was purchased from TriLink (San Diego, CA) and the complementary sequence of anti-VEGF aptamer was purchased from Integrated DNA Technologies (Coralville, IA), as listed in **Table 3-1**.

Table 3-1 The list of oligonucleotides

Name	Sequence (5’-3’)
VEGF aptamer	Acrydite-GAGGACGAUGCGGAAUCAGUGAAU GCUUAUACAUCCGT
C- VEGF aptamer	GATTCACTGATTCCGCATCGTCCTC
FAM/C-VEGF aptamer	FAM/GATTCACTGATTCCGCATCGTCCTC

3.3.2 Methods

3.3.2.1 Synthesis of Gelatin-methacrylamide (Gelatin-MA)

Gelatin was dissolved in 0.1 M sodium bicarbonate buffer to a final concentration of 20 mg/mL. Methacrylic acid N-hydroxysuccinimide ester (MA-NHS) was dissolved in anhydrous DMSO at a concentration of 200 mg/mL. The MA-NHS solution was added to the gelatin solution at predetermined molar ratios. The solution was incubated at 37 ℃ for 1 h with continuous stirring. The unreacted reagents and byproducts were removed using a dialysis cassette (MWCO = 10 kDa) in distilled water at 37 ℃. Following dialysis, the gelatin- methacrylamide (gelatin-MA) was concentrated using a centrifugal filter (molecular cut-off: 10 kDa, Fisher Scientific, Waltham, MA) at 4000 g for 30 min. The gelatin-MA solution was filtered through a 0.22 μm filter and stored at -20 ℃ before use.

3.3.2.2 FTIR

Gelatin and gelatin-MA were analyzed by Fourier transform infrared spectroscopy (FTIR) using a Bruker Vertex V70 Spectrometer (Bruker Optics Billerica MA) equipped with an MVP-Pro diamond single reflection ATR accessory (Harrick Scientific Pleasantville NY). 400 scans at 6 cm^{-1} resolution were averaged for each sample using a DTGS detector and scan frequency of 5 kHz. In all cases, the spectrum of the clean diamond crystal was used as the reference spectrum. All spectral manipulations were performed using OPUS 5.5 (Bruker Optics, Billerica MA).

3.3.2.3 Fluorescamine Assay

The conjugation efficiency of methacrylamide groups onto gelatin was measured according to a fluorescamine method,[119] in which the fluorescamine dye rapidly reacts with primary amines of protein and forms a complex that can produce fluorescence with a peak emission at 470 nm.

Fluorescamine was first dissolved in DMSO at a concentration of 3 mg/mL. Next, 3 μL of fluorescamine solution was mixed with 9 μL of the gelatin or gelatin-MA solution. The reaction was carried out at room temperature for 15 min and the fluorescence intensity was measured using a Nanodrop 3300 fluorospectrometer (Thermo Fisher Scientific, Waltham, MA) at an excitation wavelength of 390 nm and an emission wavelength of 475 nm. Glycine was used to generate a standard curve.

3.3.2.4 Preparation of the PEG-gelatin Hydrogel Film for Cell Adhesion

A pregel solution (12 μL) was prepared by combining 7 μL gelatin-MA (15 mg/mL), 0.6 μL PF127 (10%, w/v), 0.1 μL TEMED, 0.3 μL acetic acid, 0.4 μL APS (10%, w/v), various amount of PEG methyl ether acrylate and diH_2O. 1 μL of pregel solution was added onto a silanized glass substrate (4 mm x 4 mm), which was then covered by a cover slide.[120] After 30 min, the cover slide was gently removed. PEG diacrylate (15%, v/v) was used for synthesizing a pure PEG hydrogel film as a control. The hydrogels were washed with 1 mL sterilized diH_2O overnight to remove any unreacted monomers, PF127, ions, TEMED and APS. The hydrogels were sterilized with 70% ethanol for 1 h and subsequently washed three times with 1 mL DPBS.

3.3.2.5 Examination of Cell Adhesion on the 2D PEG-gelatin Hydrogel

HUVEC were harvested and suspended in 2% LSGS-supplemented M200 medium at a concentration of 1.0 x 10^5 cells/mL. 250 μL of the HUVEC suspension was added onto the hydrogel films coated on the glass slides and incubated at 37 ℃ overnight. Prior to cell imaging, calcein AM and Hoechst 33342 were incubated with the hydrogels for 30 min at a concentration of 2 μg/mL each. The hydrogels were washed once using 2% LSGS-supplemented M200 medium before imaging under a fluorescence microscope (Olympus IX73, Pittsburgh, PA). The number of cells on each hydrogel was quantified using the Image J software.

3.3.2.6 Examination of Cell Viability on the 2D PEG-gelatin Hydrogel

The viability of attached cells on the hydrogel was measured using a MTS assay. Briefly, hydrogels were transferred into solutions containing 160 μL of 2% serum supplemented M200 medium and 40 μL of MTS solution in a 96-well plate. After 3 h of incubation at 37 ℃, 100 μL of solutions were collected and transferred into a new 96-well plate for absorbance measurement at 490 nm using an Infinite 200 Pro microplate reader (Tecan, Morrisville, NC).

3.3.2.7 Preparation of the Macroporous Hydrogel

Macroporous hydrogels were prepared using free radical polymerization coupled with gas formation.[121] A pregel solution (120 μL) was prepared by mixing 70 μL gelatin-MA (15 mg/mL), 8 μL PEG methyl ether acrylate, 6 μL PF127 (10%, w/v), 1 μL TEMED, 3 μL acetic acid, 4 μL APS (10%, w/v), various amounts of aptamer, and diH_2O. 10 μL of the pregel solution was added into a mold containing 0.05 g of sodium bicarbonate. The pregel solution reacted with the sodium bicarbonate for the production of CO2 during the formation of the hydrogel. PEG diacrylate (15%, v/v) was used to synthesize pure PEG hydrogel in the presence of the free radical and gas forming reagents. The hydrogels were washed with 1 mL sterilized diH_2O overnight to remove any unreacted monomers, PF127, ions, TEMED and APS. The hydrogels were sterilized with 70% ethanol for 1 h and subsequently washed three washes with 1 mL DPBS.

3.3.2.8 Examination of Gelatin and Oligonucleotide Aptamer Incorporation into the Macroporous Hydrogel

To examine the gelatin incorporation, the macroporous hydrogels were incubated with Coomassie Blue G-250 staining solution. After 1h incubation, the macroporous hydrogels were washed in the destaining solution (40% methanol, 10% glacial acetic acid, and 50% diH_2O) at 37 ℃

for 2 h with the destaining solution replenished every 30 min. The macroporous hydrogels were imaged under a Maestro Imaging System (PerkinElmer, Waltham, MA). PEG diacrylate (15%, v/v) was used for synthesizing a gelatin-free hydrogel as a control. To examine the aptamer incorporation, the macroporous hydrogels (with 50 pmol of aptamer) were incubated overnight with 200 pmol of a FAM-labeled complementary oligonucleotide that binds to the anti-VEGF aptamer. The hydrogels were imaged with the Maestro Imaging System (PerkinElmer, Waltham, MA) after thoroughly washed with the DPBS buffer to remove free complementary oligonucleotides.

3.3.2.9 Morphological Examination of the Macroporous Hydrogels

Hydrogels were lyophilized for one day at -60 ℃. The hydrogels were then mounted on an aluminum stub using double-sided adhesive tape and sputter-coated with a thin layer of gold for 30 s. The coated hydrogels were imaged under an environmental scanning electron microscope (FEI Quanta 200, Hillsboro, OR) in high vacuum mode with an accelerating voltage of 15 kV.

3.3.2.10 Cell Loading into the Macroporous Hydrogels

Macroporous hydrogels were dehydrated by gently blotting the hydrogels with sterilized tissue paper. The hydrogels were placed into 96-well plates and 250 μL of HUVEC suspensions containing 2.5 x 10^4 cells (low density), 1.25 x 10^5 cells (intermediate density), and 6.25 x 10^5 cells (high density) were slowly added onto the dehydrated macroporous hydrogels. After 1h incubation, 1 mL of fresh 2% LSGS-supplemented M200 medium was added to each hydrogel, followed by overnight incubation. Cells were incubated in 2 μg/mL calcein AM for 30 min and then washed once with 2% LSGS-supplemented M200 medium. To image the cells, the hydrogels were cut into half horizontally and transferred into a chamber slide. The cross-sections of the hydrogels were observed using a scanning laser confocal microscope (Olympus FV1000, Centre Valley, PA)

equipped with an argon laser. A series of images were collected throughout the z-direction and a three-dimensional composite image was created and presented.

3.3.2.11 Examination of VEGF Sequestration

Macroporous hydrogels were prepared as previously stated. Prior to loading VEGF into the macroporous hydrogels, the hydrogels were dehydrated by gently blotting the hydrogels with sterilized tissue paper. 50 μL of the VEGF solution (200 ng and 0.1% BSA) was added to each hydrogel and the samples were incubated at 4 ℃ for 24 hours. After incubation, the VEGF-loaded hydrogel was incubated in 1 mL of DPBS with 0.1% BSA for 24 hours. The amount of VEGF in DPBS was measured by ELISA. The sequestration efficiency was determined as the amount of VEGF remaining in the hydrogel over the amount of VEGF loaded into the hydrogel.

3.3.2.12 Examination of the VEGF Release Kinetics

The VEGF-loaded macroporous hydrogels with a 5:1 molecular ratio of aptamer to VEGF were incubated in 1 mL of release medium at 37 ℃ with a shaking rate of 70 rpm. The VEGF loading amount was 200 ng. Three release media were used and compared, including DPBS, M200 and 2% LSGS-supplemented M200. The release media were totally collected every day and replaced with 1 mL of fresh release medium. The collected release media were stored at -20 ℃ until measurement with ELISA.

3.3.2.13 Tube Formation Assay

Two experiments were designed for the tube formation assay. The first experiment was used to compare the controlled release function of the macroporous hydrogels with and without the aptamer. In this experiment, the VEGF-loaded macroporous hydrogels were incubated in 1 mL of M200 medium at 37 ℃ with a shaking rate of 70 rpm. The M200 medium was changed every day.

The release media collected at day 7 and day 14 were directly used without any treatment for the tube formation assay. The second experiment was used to measure the bioactivity of VEGF in the hydrogels. In this experiment, fresh VEGF was extracted from the hydrogels that were treated and neutralized with a complementary oligonucleotide of the anti-VEGF aptamer for 1h at day 7 and day 14. The collected VEGF solutions were diluted with M200 medium to prepare two solutions containing VEGF of 10 and 20 ng/mL for the tube formation assay. The VEGF stock solution of the same concentration was used as a positive control.

The tube formation assay was performed according to the standard procedure.[122] Briefly, the Geltrex solution was first thawed at 4 ℃ overnight and 80 μL of the Geltrex solution was added into each well of a 48-well plate for 30 min incubation at 37 ˚C. 200 μL of release medium or VEGF solution were transferred onto the Geltrex-coated wells with 4.0 x 10^4 HUVECs. After incubated at 37 ℃ in 5% CO2 for 4 h, the cells were stained with calcein AM (2 μg/mL) for 30 min and then observed under a fluorescence microscope (Olympus IX73, Pittsburgh, PA). Cell participation and the total tube length were measured using Image J software. The elongated cells were counted as cells comprising the tube-like structure.

3.3.2.14 Evaluation of Cell Survival in the Macroporous Hydrogels

A solution (50 μL) containing 200 ng VEGF and 6.25 x 10^5 cells was loaded into dehydrated hydrogels. The hydrogels were incubated at 37 ℃ in a 5% CO2 environment for 1 h and then incubated in 1 mL of cell culture medium, which was EndoGRO basal medium supplemented with ascorbic acid (50 μg/mL), hydrocortisone hemisuccinate (1 μg/mL), heparin sulfate (0.75 U/mL), L-glutamine (10 mM), and 0.5% FBS. The cell culture medium was replaced every day. At predetermined time points, the hydrogels were stained with calcein AM and ethidium homodimer-1 (both at 2 μg/mL) to examine live and dead cells, respectively. The fluorescence intensity of the cells in the hydrogels was evaluated with the signals unmixed under the Maestro

Imaging System. The hydrogels were also horizontally cut into halves and examined under the confocal microscope (Olympus FV1000, Center Valley, PA).

3.3.2.15 Examination of the Effect of Macroporous Structures on Cell Viability

Hydrogels were loaded with 50 μL mixture containing VEGF (200 ng) and HUVEC (6.25 x 105 cells). To seal the macropores, 30 μL of the Geltrex solution was loaded into the macroporous hydrogels. The hydrogels were incubated in 1 mL of serum-reduced medium (EndoGRO basal medium supplemented with ascorbic acid (50 μg/mL), hydrocortisone hemisuccinate (1 μg/mL), heparin sulfate (0.75 U/mL), L-glutamine (10 mM), and 0.5% FBS). The cell culture medium was replaced every day. At different time points, hydrogels were stained with calcein AM and ethidium homodimer-1 (2 μg/mL each) for 30 min and sectioned horizontally for visualization by a scanning laser confocal microscope (Olympus FV1000, Centre Valley, PA).

3.3.2.16 Statistical Analysis

Statistical significance was evaluated via the Mann-Whitney U test. The difference was considered to be significant if $P < 0.05$. Data are reported as the mean ± one standard deviation of triplicate samples.

3.4 Results and Discussion

3.4.1 Synthesis of Gelatin-Methacrylamide

To fabricate gelatin-PEG hydrogel, gelatin methacrylamide (gelatin-MA) was synthesized using methacrylic acid N-hydroxysuccinimide ester (MA-NHS). The primary amines of gelatin reacts with the N-hydroxysuccinimide ester, by which the methacrylate groups can be conjugated on the gelatin (**Figure 3-1A**). The FTIR was used to examine the conjugation between gelatin and MA-NHS. Compared with gelatin, there was an increased peak shown in gelatin-MA at the wavelength from 1500 cm^{-1} to 1700 cm^{-1}, which results from the addition of vinyl groups (**Figure 3-1B**). In order to quantify the degree of Methacrylamide substitution, a fluorescamine based fluorescence method was used.[119] The fluorescamine is a dye that reacts rapid with primary amines to form a fluorescence complex at an emission wavelength of 470 nm. After the gelatin and gelatin-MA were incubated with fluorescamine, the fluorescence intensity of each solution was measured by Nanodrop, by which the primary amines occupied by methacrylate can be calculated in term of fluorescence intensity. To calculate the number of methacrylate conjugated on gelatin, glycine that has only one primary amine was used to make the standard curve between the number of primary amines and fluorescence intensity (**Figure 3-1C**). When the molar ratio of MA-NHS to gelatin increased from 0 to 50, the number of methacrylate groups on gelatin-MA was increased from 0 to nearly 18 (**Figure 3-1D**). However, the further increase of the molar ratio between MA-NHS and gelatin to 100 did not further increase the number of conjugated methacrylate groups on gelatin. To illustrate whether hydrogel could be synthesized, the gelatin-MA was mixed with PEG and aptamer for synthesizing hydrogel via free radical polymerization. The PEG and the aptamer were pre-labelled with acrylate and methacrylamide groups at their ends, respectively. Since each gelatin-MA had multiple methacrylamide groups, gelatin-MA could be used as a chemical linker to chemically crosslink with PEG and aptamer and form aptamer functionalized gelatin-PEG hydrogel (**Figure 3-1E**).

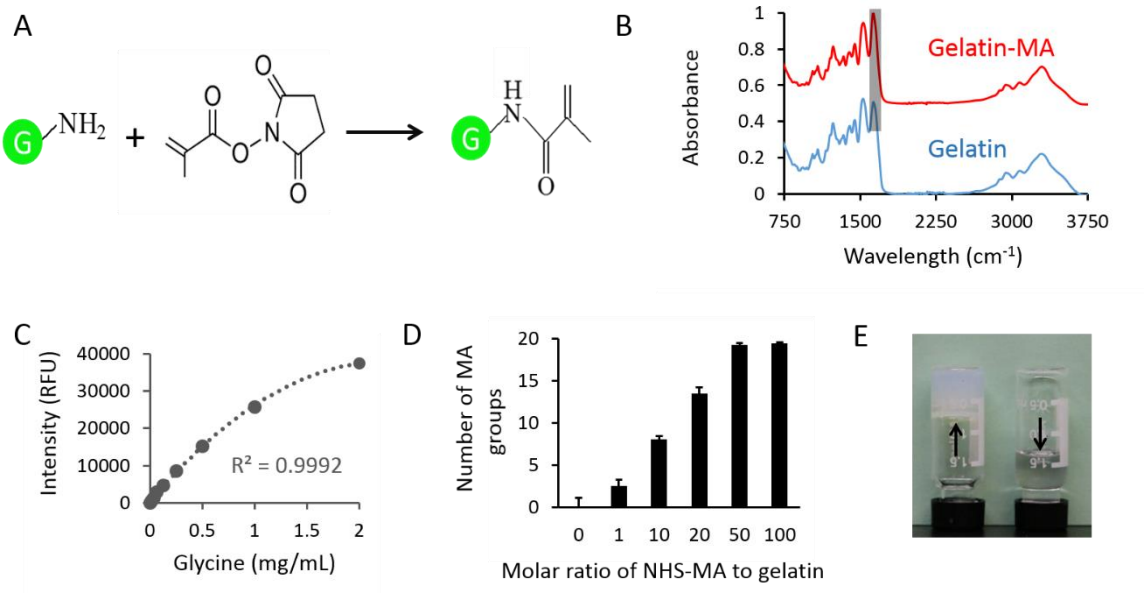

Figure 3-1 The gelatin-MA conjugation. (A) Illustration of the conjugation of the methacrylamide group to gelatin to form gelatin methacrylamide (gelatin-MA). G: gelatin. (B) FTIR characterization of gelatin-MA conjugation. (C) Standard curve of primary amine groups to fluorescence intensity in fluorescamine assay. (D) Quantification of gelatin-MA conjugation efficiency. (E) Examination of the formation of hydrogels with gelatin-MA (left) or gelatin (right). With gelatin-MA, the pregel solution formed the hydrogel (left); with gelatin, the pregel solution did not form a hydrogel (right).

3.4.2 Cell adhesion on 2D Hydrogel

Cell adhesion is a critical in designing a tissue engineering matrix because it decide the cell-cell and cell-matrix interactions, and further affect the cell proliferation, migration, and differentiation. To study the cell adhesion of gelatin-PEG hydrogel, a thin layer of gelatin-PEG hydrogel was prepared on a silanized glass slide. After washing away the hazardous chemicals involved in gel polymerization, 250 μL of HUVEC (1.0×10^5 cells/mL) was used to incubate with hydrogel layer for overnight. Hoechst and calcein AM were added into incubation medium to stain cells, followed by the fluorescence imaging. The different molar ratio of gelatin-MA to PEG acrylate (1:400, 1:800, 1:1600, 1:3200) was used to form hydrogel for testing cell adhesion. Pure gelatin and PEG were used as positive and negative control. The result showed that there were a large amount of HUVEC attached on both gelatin and gelatin-PEG hydrogels, however few of HUVEC attached on the PEG hydrogel (**Figure 3-2A**). Calcein AM, a cell-permeant dye converted to a green-fluorescent calcein after acetoxymethyl ester hydrolysis by intracellular esterases, can only stain live cells while Hoechst bound to dsDNA can stain both live and dead cells. Therefore, most cells attached on the gelatin-PEG hydrogel remained high bioactive because the cell images of Calcein AM and Hoechst merged with each other well (**Figure 3-2A**). The number of attached cells on hydrogels were further quantified and shown in **Figure 3-2B**. The results indicated that the cell adhesion of gelatin-PEG hydrogel still remained more than 70% when compared with pure gelatin hydrogel. The pure gelatin hydrogel was not used because its mechanical properties were weak resulting in the failure of forming porous structures in the hydrogel.

After the cell adhesion was studied, the viability of attached cells on gelatin-PEG hydrogel was also measured by MTS assay. The MTS result was correlated with the number of cells on hydrogel, which demonstrated the attached cells were bioactive (**Figure 3-2C**).

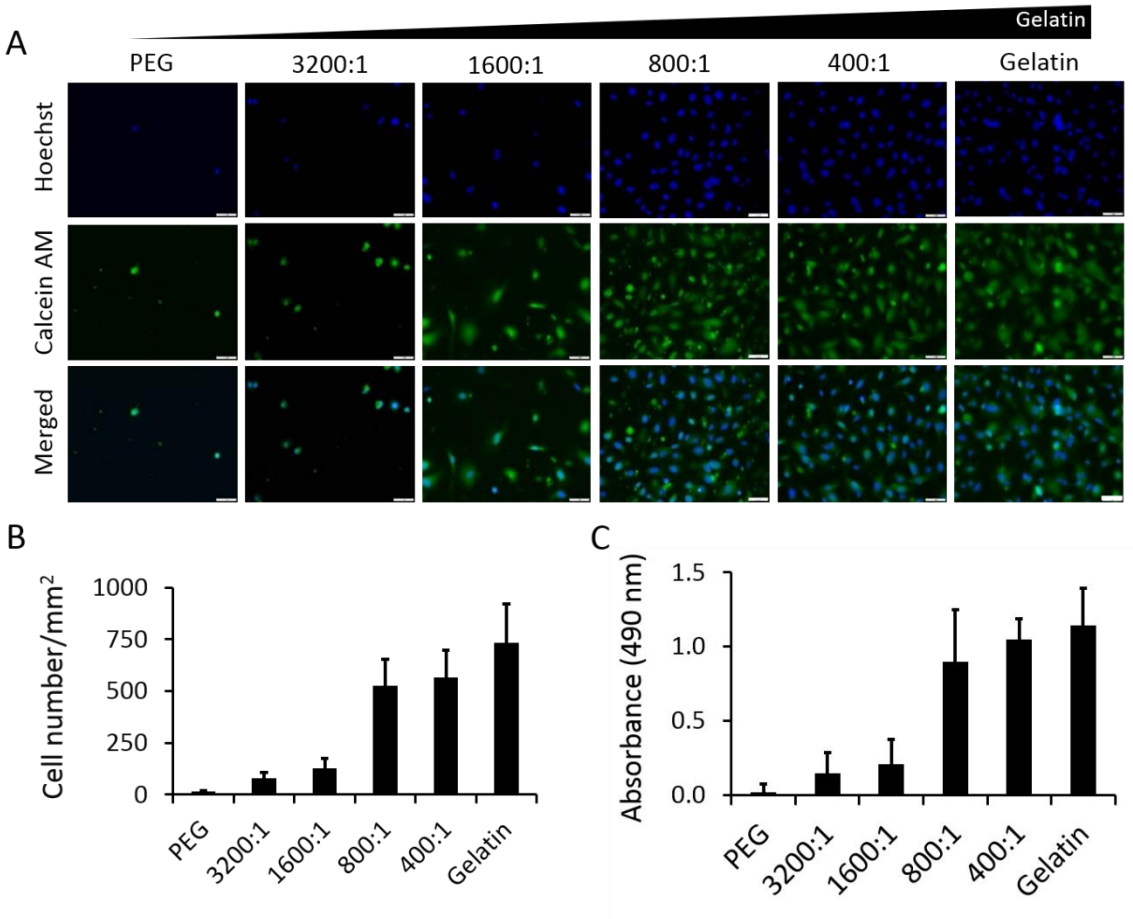

Figure 3-2 Examination of cell adhesion on the PEG-gelatin hydrogel. (A) Micrographs of cell adhesion. The HUVEC suspension of 250 µL with 2.5 x 10^4 cells was seeded on the hydrogel. After overnight incubation, the cells were stained with Hoechst 33342 and calcein AM. The numbers indicate the different molar ratios of PEG acrylate to gelatin-MA. The pure PEG hydrogel was synthesized with PEG diacrylate. Scale bar: 100 µm. (B) Quantification of HUVECs on the hydrogels using Image J. (C) Examination of HUVECs on the hydrogel using the MTS assay.

3.4.3 Synthesis of Porous Hydrogel

To generate the macroporous structure in aptamer-gelatin hydrogel, a gas forming reaction was coupled with free radical polymerization to produce carbon dioxide bubbles during the formation of the hydrogel (**Figure 3-3A**). The pore structure was examined with scanning electron microscopy (SEM). The SEM images showed that PEG could form a macroporous hydrogel via the coupled reactions (**Figure 3-3B**). In contrast, when the same reaction conditions were used, gelatin-MA itself could not form a macroporous hydrogel (**Figure 3-3B**). This difference suggests that PEG would promote the formation of macroporous structures through mechanical stabilization when mixed with gelatin-MA. Indeed, the solution of gelatin and PEG could form a macroporous hydrogel via free radical polymerization coupled with gas formation (Figure 3.3B). When the molar ratio of gelatin to PEG reached 1:1600, the pore density was decrease, resulting from the high concentration of PEG. Since the molar ratio of 1:400 had very low mechanical strength, the molar ratio of 1:800 was used to synthesize hydrogels for next experiments.

After demonstrating the formation of the macroporous hydrogel, we further characterized the chemical incorporation of gelatin and oligonucleotide aptamers into the macroporous hydrogel. The result of the Coomassie Blue staining showed that the gelatin-PEG hydrogel showed a much more dye absorption than PEG hydrogel. Since the Coomassie dye specifically binds to proteins, the increased blue intensity indicated that successful conjugation of gelatin into hydrogel (**Figure 3-3C**). One FAM labeled complementary sequence that specifically binds to anti-VEGF aptamer was designed and used to stain hydrogel. The aptamer incorporated hydrogel showed strong fluorescence while the control hydrogel without aptamer did not. It demonstrated that the aptamer was chemically conjugated to the hydrogel during the hydrogel formation (**Figure 3-3D**). To quantify the aptamer incorporation efficiency, the new formed aptamer hydrogel was washed by PBS for three times. The washing buffer was concentrated by centrifugal filter with cutoff size of 3,000 Da, followed by the measurement of nucleic acid aptamer via UV Vis at a wavelength of 260

nm. The aptamer conjugation efficiency was calculated by the amount of aptamer remaining in hydrogel over initial amount of aptamer. The result showed that that around 50% acrydite-aptamer could be conjugated into hydrogel (data not shown).

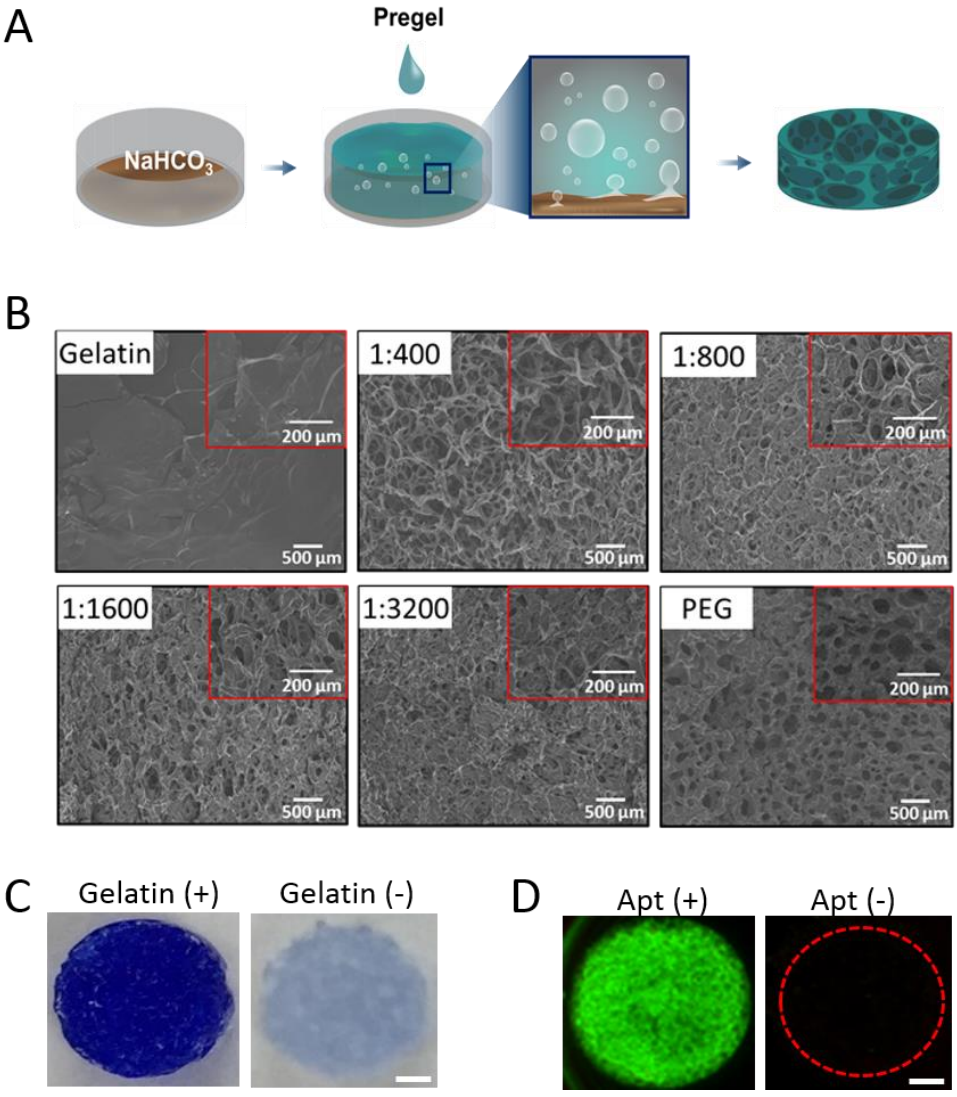

Figure 3-3 Synthesis of porous hydrogel. (A) Illustration of porous hydrogel synthesis. (B) Morphological examination of porous hydrogels. The inserted number is the molar ratio of gelatin-MA to PEG. The molar ratio of 1 to 800 was used for the next experiments. (C) Examination of gelatin incorporation into the hydrogels with Coomassie Blue staining. Scale bars: 2 mm. (D) Examination of aptamer incorporation into the hydrogels with a FAM-labelled complementary oligonucleotide. Apt: aptamer; +/-: with/without. Scale bars: 2 mm.

3.4.4 Hydrogel degradation

To verify the degradation property of gelatin-PEG hydrogel, the synthetized hydrogels were incubated with digestion solution supplemented by collagenase I. The results showed that the hydrogel degraded fast in collagenase I supplemented PBS buffer while no hydrogel degradation was observed in PBS buffer alone. The results also showed that almost all hydrogel was degraded within 3 days with 0.001% collagenase I (**Figure 3-4A and 3-4B**). The morphological examination of hydrogels by SEM showed that the hydrogel surface was smooth before the hydrogel was incubated with collagenase I buffer. After 1 day incubation, the hydrogel surface was rough, indicating the hydrogel degradation. As the increase of incubation time, the roughness of hydrogels was increased (**Figure 3-4A**). Additionally, the porous structure was observed after hydrogel was incubated with collagenase I buffer for 3 days, which demonstrated the strong degradation of hydrogel (**Figure 3-4A**).

After the gelatin-PEG hydrogel was demonstrated to be degradable, the degradation rate in growth factor release medium was studied because the degradation can significantly affect the growth factor release rate. **Figure 3-4C** showed that only around 10% gelatin-PEG degradation was found in serum supplemented medium in first two weeks. The slow degradation of gelatin-PEG hydrogel indicated that the hydrogel degradation barely affected the growth factor release in first two weeks.

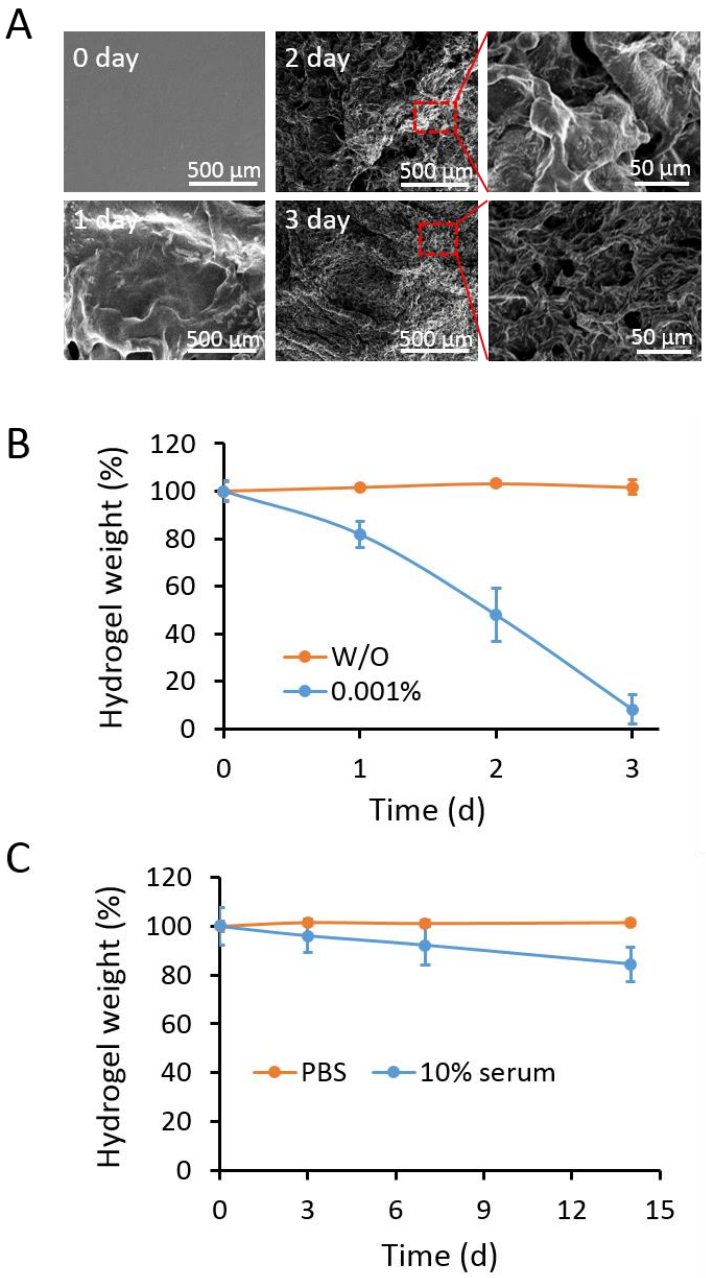

Figure 3-4 Gelatin-PEG hydrogel degradation. (A) SEM images of hydrogel degradation. The gelatin-PEG hydrogels were incubated in 0.001% collagenase I supplemented PBS solution. At predetermined time, the hydrogels were taken out, lyophilized, and observed by SEM. (B) Quantification of the degradation of gelatin-PEG hydrogel in collagenase I supplemented PBS. (C) Examination of the degradation of gelatin-PEG hydrogel in 10% serum supplemented M200.

3.4.5 Cell Loading in 3D Hydrogel

The cell behaviors in response to the 2D and 3D scaffold are different due to the different physical properties, such as the spatial patterns of scaffold presentation, topography of cellular environment, and mechanical stiffness. As a result, a 3D model generated by porous gelatin-PEG hydrogel was used to simulate the interaction between cells and scaffold *in vitro*.

Currently two strategies including one-step and two-step loading methods have been studied for loading cells into polymeric systems.[123] In the one-step method, cells are mixed with a polymer solution before the formation of the polymeric system. While the overall procedure is simple and straightforward, the synthesis of many polymeric systems often involves harsh conditions. For instance, free radicals produced during free radical polymerization may lead to the decrease or loss of cell bioactivity.[124] Thus, the two-step method has also been studied for cell loading. In this method, polymeric systems with porous structures are generated, which is followed by cell loading. [123] The two-step method was used in the current work. The macroporous hydrogel after the synthesis was thoroughly washed to remove free monomers, initiators, catalysts and byproducts and then dehydrated before loaded with HUVECs. After the gentle washing of unbound cells, the hydrogel was cut into two halves to expose the cross-section of the central hydrogel region for confocal microscopy imaging. Consistent with the observation of cell attachment on the two-dimensional PEG hydrogel surface, few cells were observed to stably bind to the macroporous PEG hydrogel when the initial cell loading was 6.25×10^5 cells (**Figure 3-5**). In contrast, in the same loading condition, approximately 9,500 cells/mm^3 were observed in G-PEG hydrogel. This corresponds to a cell loading efficiency of 76%. It was also observed that the cell density in the hydrogel increased with the cell loading amount (**Figure 3-5**). Moreover, the cells could be loaded into the central regions of the macroporous hydrogel with the thickness of ~2.5 mm. Thus, these data show that the macroporous hydrogel with gelatin can provide cells with binding sites for effective cell loading.

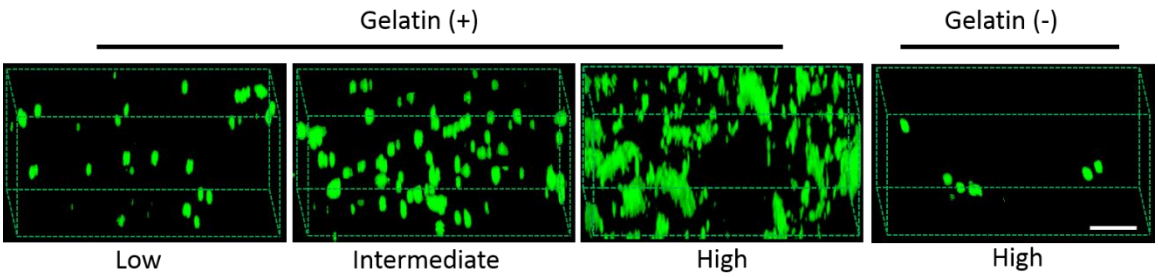

Figure 3-5 Confocal microscopy images of the HUVEC-loaded PEG hydrogels with (+) and without (-) gelatin. Low: 2.5×10^4 cells; intermediate: 1.25×10^5 cells; high: 6.25×10^5 cells. These numbers mean the initial cell loading amount. Before the confocal microscopy imaging, hydrogels were treated with calcein AM for cell staining and washed to remove unbound cells. Scale bar: 100 μm.

3.4.6 VEGF Sequestration and Release

After the demonstration of the cell binding and loading function, the macroporous chimeric hydrogel was evaluated to examine the function of VEGF sequestration and release. The aptamer is a chemically modified RNA oligonucleotide with 20 nucleotides modified with 2'-Ome and 15 nucleotides modified with 2'-F (**Figure 3-6A**). The results showed that the Apt (+) hydrogel could effectively sequester VEGF (**Figure 3-6B**). The sequestration efficiency increased with the density of the aptamer, reaching 91.6% at the density of 2.5 nmol/cm3 (**Figure 3-6B**). In contrast, Apt (-) hydrogel had the poor capability in sequestering soluble signaling molecules, with a VEGF sequestration efficiency of only 5% (**Figure 3-6B**). The poor VEGF retention in Apt (-) hydrogel, on the other hand, demonstrates that the macroporous hydrogel indeed has high permeability, which is critical to free transport of nutrients and wastes for normal cell metabolism.

The VEGF release results showed that approximately 89.6% and 94.7% of VEGF was released from the macroporous Apt (-) hydrogel in the M200 medium by day 1 and day 2, respectively (**Figure 3-6C**). By contrast, approximately 4.2% and 7.7% of VEGF was released from the macroporous Apt (+) hydrogel by day 1 and day 2, respectively. These data clearly demonstrate that the initial burst VEGF release was significantly reduced in the presence of the aptamer. Moreover, VEGF was released from the macroporous Apt (+) hydrogel in a sustained manner afterwards. The cumulative VEGF release was 20.3 and 28.1% by days 7 and 14, respectively (**Figure 3-6C**). To further demonstrate the capability of the aptamer in controlling VEGF release, the macroporous Apt (+) hydrogels were incubated in three different release media. The results showed that VEGF was released with the same trend. The rate of VEGF release in LSGS-supplemented M200 was slightly higher than that in DPBS and M200. Since LSGS-supplemented M200 contains serum, it suggests that the chemically modified RNA aptamer had sufficient stability in prolonging VEGF release in biological fluids (**Figure 3-6D**).

Macroporous materials have been studied for controlled release of signaling molecules. The typical example is collagen sponge that has been approved by Food and Drug Administration (FDA) for controlled release of bone morphogenetic proteins in the clinic.[125] However, the results showed that more than 50% and 90% of protein drugs were released from collagen sponge by days 7 and 14, respectively.[126] Presumably because of this fast release profile, to induce therapeutic effects, a very high amount of protein drugs were loaded into collagen sponge for implantation.[127] Clinical results have indicated that the use of a large amount of protein drugs and the fast release could cause severe side effects and even increase cancer risk.[128] In contrast, our data clearly show that a highly permeable macroporous hydrogel could strongly sequester soluble signaling molecules

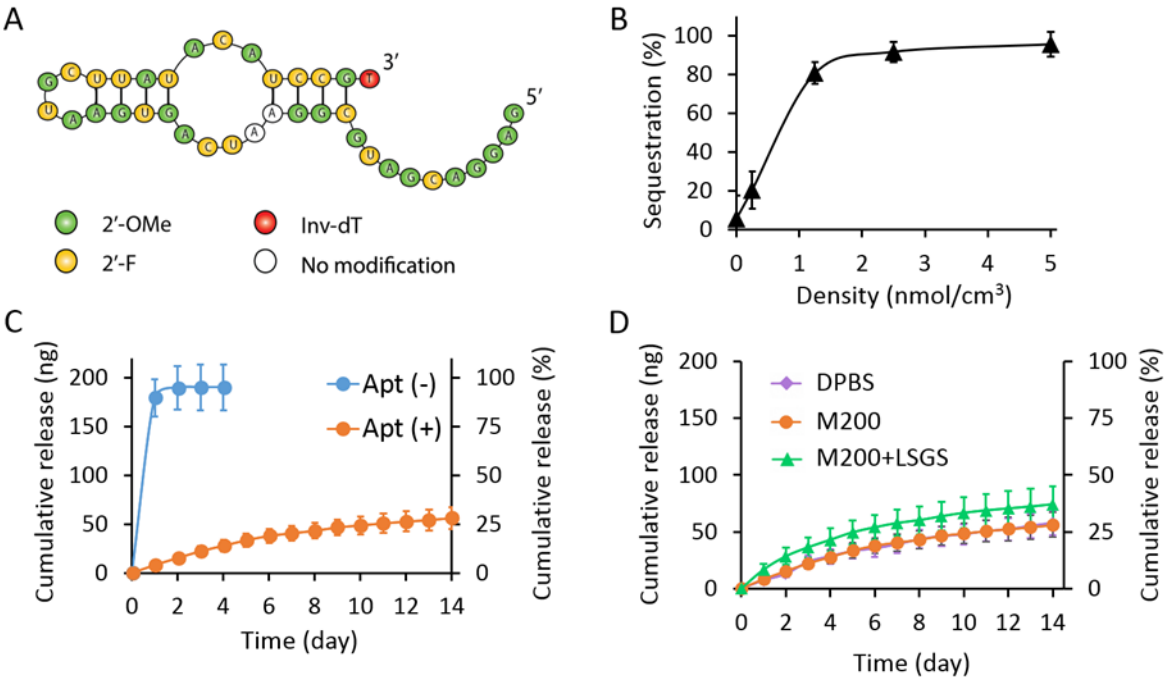

Figure 3-6 Examination of VEGF sequestration and release. (A) Composition and structure of the anti-VEGF RNA aptamer. The secondary structure was generated by using the RNAstructure software (Version 5.3, from Mathews Lab). 2'-OMe: 2'O-methyl modification; 2'-F: 2' fluorine modification; Inv-dT: 3' inverted dT. (B) VEGF sequestration. 50 µL of the solution with 200 ng VEGF was added to each hydrogel and the samples were incubated at 4℃ for 24 hours. The sequestration efficiency was determined by the ratio of the amount VEGF remaining in the hydrogel after 24 hour release to that originally loaded into the hydrogel. (C) Comparison of VEGF release from the hydrogels with (+) and without (-) the aptamer in the M200 medium. (D) Comparison of VEGF release from the Apt (+) hydrogels in three different media including DPBS, M200, and LSGS-supplemented M200. The density of the aptamer was 2.5 nmol/cm3; the initial VEGF loading amount was 200 ng. In both C and D experiments, the hydrogels were directly incubated in the release media without any prewashing treatment.

3.4.7 Examination of VEGF Bioactivity

Two experiments were performed to evaluate and compare the potential of the Apt (-) and Apt (+) hydrogels in supporting normal cell metabolism using the tube formation assay. In the first one, the daily release media without any dilution were directly used for treatment of HUVECs. In the second one, VEGF remaining in the hydrogels was extracted and diluted to the same concentration as the stock solution.

The results showed that the release media collected at day 7 and day 14 in the Apt (-) group could not stimulate cell alignment and tube formation (**Figure 3-7A**), suggesting that these release media had little VEGF bioactivity in stimulating the cells. However, those collected at day 7 and day 14 in the Apt (+) group stimulated 73% and 43% of the cells to self-assemble and form tubes with the length of 1,088 and 550 μm/mm2, respectively (**Figure 3-7A**). This difference between the Apt (-) and Apt (+) groups is consistent with the VEGF release data showing that more than 95% of VEGF was released from the Apt (-) hydrogel during the first two days with little amount left for release during the following days whereas VEGF was released from the Apt (+) hydrogel in a sustained manner (**Figure 3-6C**). These data further suggest that the aptamer plays an important role of prolonging the release of soluble signaling molecules to local microenvironment of the macroporous hydrogel.

Since it is important for signaling molecules in a polymeric system to maintain high bioactivity during the release period, we further examined the bioactivity of VEGF retained inside the chimeric hydrogel. VEGF was extracted from the hydrogels at day 7 and day 14 by the inactivation of the aptamer, and diluted to 10 and 20 ng/mL, respectively. HUVECs treated with the VEGF solutions were self-assembled to form tubes (**Figure 3-7B and 3-7C**). When 10 ng/mL of VEGF was used to treat HUVECs, the percentages of HUVECs participating into the formation of tubes were 98.9%, 96.7%, and 83.7% in the stock, day 7 and day 14 groups, respectively (**Figure 3-7B**). These differences are not statistically significant. The total lengths of the tubes in these three

groups were 4,693, 4,027 and 2,389 μm/mm2, respectively (**Figure 3-7B**). The lengths of the tubes induced by the stock VEGF solution and the VEGF extracted from the hydrogel at day 14 were statistically different (**Figure 3-7B**). When 20 ng/mL of VEGF was used to treat HUVECs, there was no statistically significant difference among these three VEGF samples in either cell participation into the tube formation or the total tube length (**Figure 3-7B**).

Since the formation of tubes indicates the VEGF bioactivity, these results suggest that VEGF inside the macroporous hydrogel could at least maintain ~ 50% bioactivity by day 14. In contrast, the literature shows that it is challenging to maintain the high bioactivity of therapeutic proteins (e.g., VEGF) owing to their fragile structures.[129] For instance, Gu and coworkers found that the bioactivity of VEGF in photocrosslinked elastomers decreased to ~15% after 10 days of in vitro release;[130] Ekaputra and coworkers showed that the bioactivity of VEGF in a hydrogel composite decreased to 5% after 7 days of in vitro release.[131] The difference between the previous studies and ours are most likely due to the facts that the synthesis of the chimeric hydrogel was decoupled from VEGF loading and that the aptamers strongly bound VEGF in the chimeric hydrogel. Thus, our data demonstrate that the aptamer functionalized macroporous hydrogel can not only sequester growth factors for sustained release but also maintain their high bioactivity of stimulating cells.

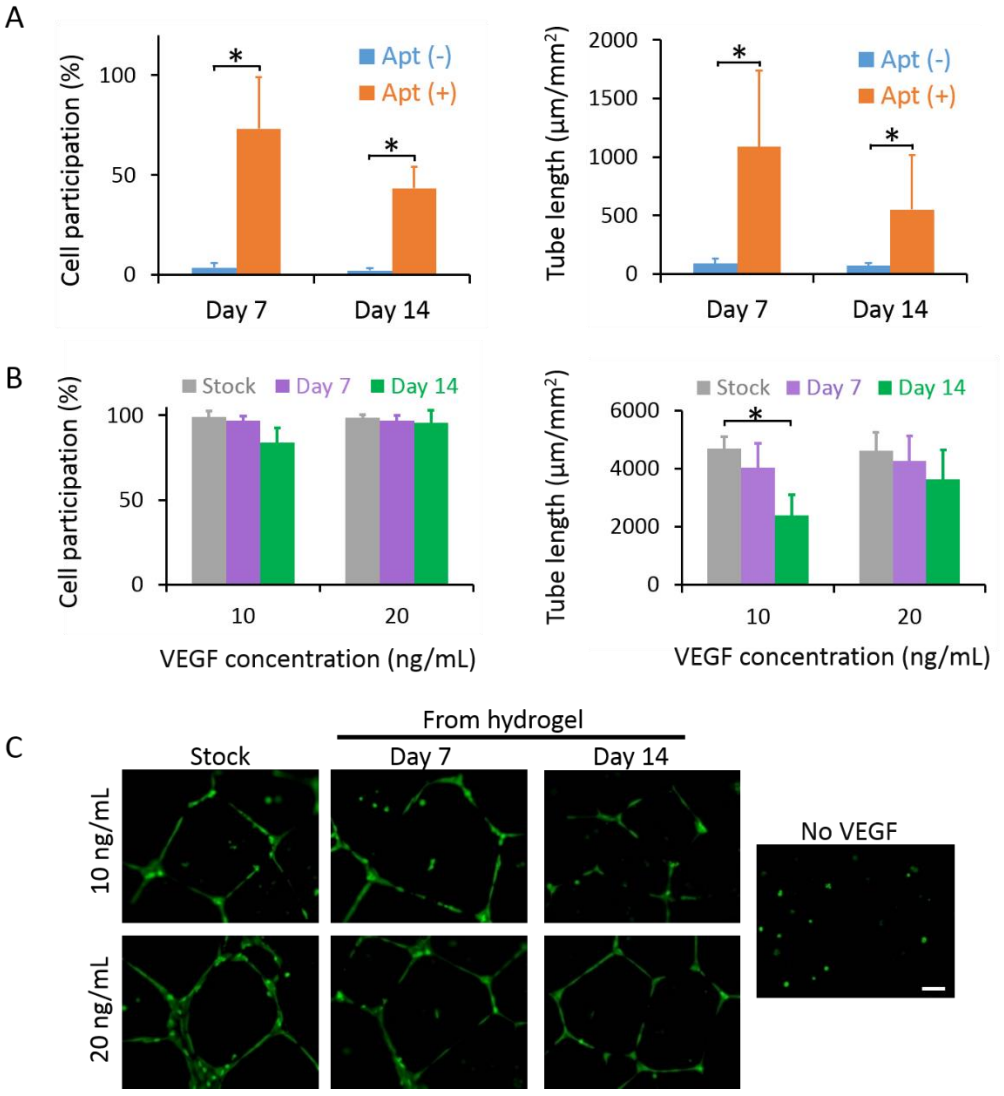

Figure 3-7 Examination of VEGF bioactivity. (A) Comparison of the VEGF release media collected at day 7 and day 14 in stimulating the tube formation. The release media from Apt (+) and Apt (-) hydrogels were collected and used to incubate with HUVECs in stimulating the tube formation. Quantification of cell participation into the formation of tubes (left) and the total length of tubes (right). * $P < 0.05$. (B) Comparison of activity between stock and released VEGF. To obtain high VEGF concentration, one complementary sequence of aptamer was used to actively trigger a large amount VEGF release at different period of time. During the test, HUVEC were mixed with different VEGF solution, followed by the transfer of mixture into geltrex coated 48 well plates. After 4 hours incubation, cells were stained by calcein AM and imaged by 10x fluorescence microscopy. Scale bar: 100 μm. Quantification of cell participation into the formation of tubes (left) and the total length of tubes (right). * $P < 0.05$. (C) The representative images of cell tube stimulated by stock and released VEGF. Scale bar: 100 μm.

3.4.8 Evaluation of Cell Activity

After separately demonstrating the two functions of the chimeric hydrogel in loading cells and controlling growth factor release, we simultaneously loaded HUVECs and VEGF into the chimeric hydrogel. In each hydrogel, 6.25 x 10^5 cells and 200 ng VEGF were loaded. Since cells often experience harsh microenvironment (e.g., lack of dynamic molecular transport) in real applications, the hydrogels were incubated in a serum-reduced medium for static cell culture. The cells in the hydrogels were evaluated after calcein AM staining.

At 12 hours, the cells in both Apt (-) and Apt (+) hydrogels exhibited a strong fluorescence intensity (**Figure 3-8A and 3-8B**), which indicates that the cells had a high activity in these hydrogels. However, the fluorescence intensity of the cells in the Apt (-) hydrogel quickly decreased with time (**Figure 3-8A and 3-8B**). It decreased by 70% from day 0.5 to day 3. In contrast, the fluorescence intensity of the cells in the Apt (+) hydrogel virtually maintained the same during the first 3 days (Figure 5A and 5B). Moreover, except day 0.5, the fluorescence intensity of the cells in the Apt (+) hydrogel was much stronger than that of the Apt (-) hydrogel (**Figure 3-8A and 3-8B**). On day 14, the cell intensity of the Apt (+) hydrogel was ~8 times as much as that of the Apt (-) hydrogel.

VEGF has been used for functionalization of hydrogels in two ways.[132] One is to physically entrap soluble VEGF for sustained release;[109] the other is to chemically conjugate VEGF as the cell binding sites.[133] Both soluble and conjugated VEGF are able to support cell survival.[109,133] In this work, VEGF was non-covalently entrapped in the hydrogel through physical binding to the anti-VEGF aptamer. It is important to note that this aptamer is a VEGF inhibitor, which has been shown in both preclinical and clinical studies.[134,113] Since this aptamer is able to inhibit VEGF bioactivity, it was approved by FDA as an anti-angiogenic agent for treatment of age-related macular degeneration.[62] In another word, once VEGF binds to this aptamer, VEGF loses its bioactivity of binding to and stimulating VEGF receptors.[134,113] Thus,

the difference between the Apt (-) and Apt (+) hydrogels demonstrates that the Apt (+) hydrogel could release soluble VEGF in a sustained manner and the released VEGF could enhance the survival of HUVECs whereas the Apt (-) hydrogel could not.

The HUVECs in the macroporous hydrogel were further examined under the confocal microscope. Consistent with the macroscopic imaging analysis (**Figure 3-8A**), the microscopy images show that more living cells were observed in the Apt (+) hydrogel than in the Apt (-) hydrogel (**Figure 3-8C**). Notably, some HUVECs in the Apt (+) hydrogels could connect together to form tube-like structures (**Figure 3-8D**). The effect of the macroporous structure on cell activity was also studied. The macroporous Apt (+) hydrogel was treated with the Geltrex solution that was gelated to block the macroporous structure (**Figure 3-8E**). The imaging data show that fewer cells survived in the pore (-) hydrogel than in the pore (+) hydrogel (**Figure 3-8F**). This difference clearly demonstrates that the macroporous structure is essential to maintain the activity of the cells in a hydrogel.

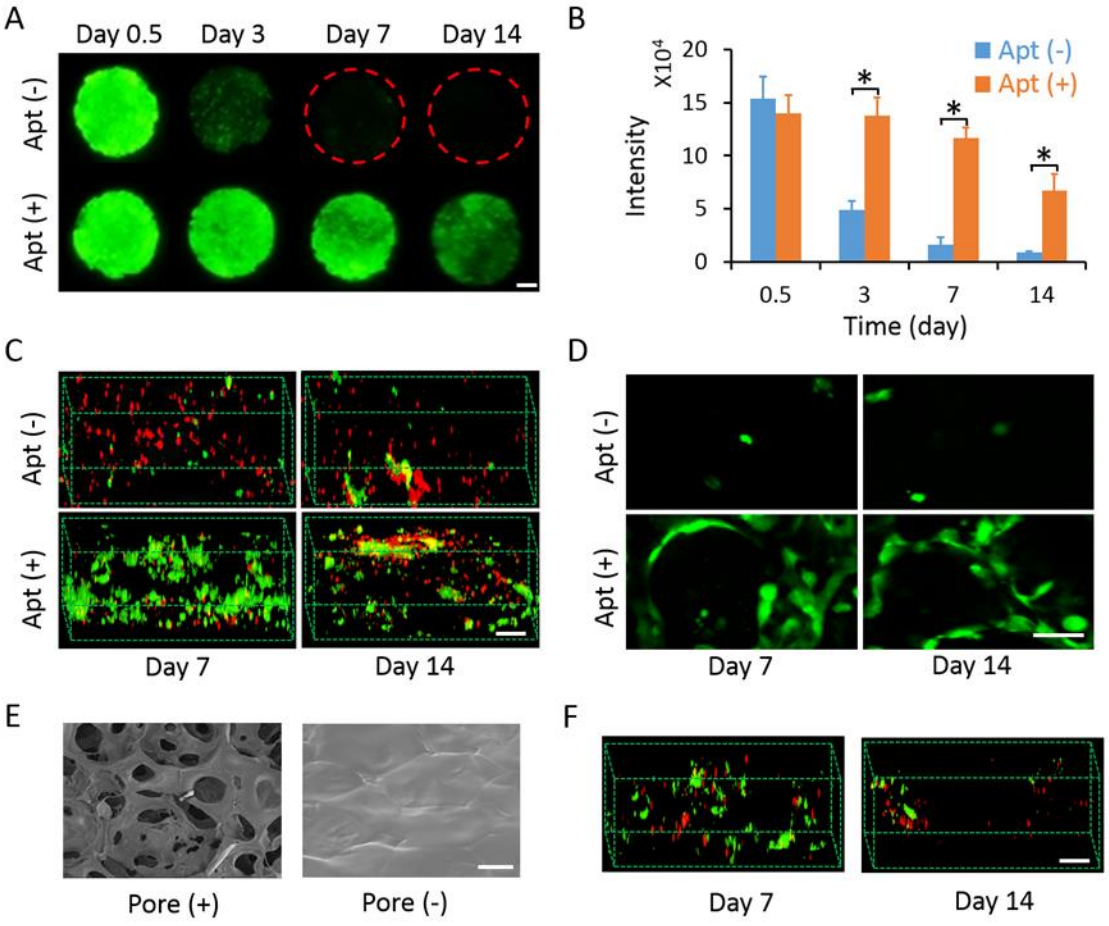

Figure 3-8 Evaluation of the chimeric hydrogel loaded with VEGF and HUVECs cultured at a static serum-reduced condition. (A) Representative fluorescence images of the macroporous hydrogels. The cells were stained with calcein AM and the hydrogels were imaged using the Maestro Imaging System. Scale bar: 2 mm. (B) Quantification of cell fluorescence intensity of the macroporous hydrogels. * $P < 0.05$. (C) Confocal microscopy images of live and dead cells in the macroporous hydrogels. Calcein AM and ethidium homodimer-1 were used to stain live (green) and dead (red) cells, respectively. Dead cells were often washed away during the sample treatment. Scale bars: 200 μm. (D) Examination of cell-cell connection in the macroporous hydrogels. The images show that the surviving cells in the Apt (+) hydrogels could connect together to form tube-like structures. Scale bar: 30 μm. (E) SEM images of the hydrogels. Pore (+): macroporous hydrogels without Geltrex treatment. Pore (-): macroporous hydrogels with Geltrex treatment. Scale bar: 100 μm. (F) Confocal microscopy images of live and dead cells in the pore (-) hydrogels. Scale bar: 200 μm.

3.5 Conclusion

Synthetic materials have been applied as skin substitutes due to its advantage of controlling growth factor release. In this chapter, we synthesized a macroporous aptamer functionalized gelatin-PEG hydrogel using three macromonomers including PEG, gelatin, and an anti-VEGF aptamer via free radical polymerization coupled with carbon dioxide formation. PEG can stabilize the macroporous structure of the macroporous hydrogel that is highly permeable to molecular transport; gelatin can provide cells with binding sites for cell loading; and the aptamer can strongly sequester VEGF for its sustained release with high bioactivity. The synthesized hydrogel achieved a sustainable VEGF release for two weeks. The released VEGF remained more than 50% bioactivity after two weeks. The coculture of cells with the VEGF loaded hydrogel indicated that cells can not only easily adhere on the hydrogel, but also maintain a high viability with the continuous stimulation of VEGF. Therefore, aptamer functionalized gelatin-PEG hydrogel is a promising synthetic materials that can control the growth factor release for regulating cell behaviors.

Chapter 4

Synthesis and Characterization of Semi-synthetic Skin

4.1 Abstract

In this chapter, a semi-synthetic skin was designed through the integration of aptamer functionalized gelatin-PEG hydrogel and decellularized intestine. To study the effect of hydrogel loading on the original physical properties of decellularized intestine, decellularized intestines were tested to load different amounts of hydrogel. The results showed that the porous structure was sealed as increasing the hydrogel loading. To maintain the original porous structure of decellularized intestine, the hydrogel loading was kept 25% of maximum loading of decellularized intestine. Next, the functions of semi-synthetic skin including cell adhesion, cell proliferation, and controlled VEGF release were individually examined *in vitro*. The results showed that the semi-synthetic skin not only supported cell adhesion and proliferation, but also achieved sustainable VEGF release.

4.2 Introduction

Skin wound healing is an important lifesaving issue for massive lesions. The use of biologically responsive graft is one of most common skin regenerative treatments. To develop highly efficient skin graft, natural and synthetic materials have been extensively studied in skin tissue regeneration. For example, Wu et al. studied the decellularized pig peritoneum as a natural materials for promoting the recovery of skin wounds.[135] Bannasch et al used decellularized human dermis as skin scaffold for dermal substitution to the patients with severe burns.[136] Mohammad et al synthesized an EGF encapsulated nanofibrous scaffold using poly (lactic-co-glycolic acid) and gelatin for regenerating skin tissue.[137] Wang et al used collagen/chitosan to mimic the sophisticated bilayer structure of natural dermis.[138] Although both natural and synthetic skin grafts are able to promote the skin recovery, each of them has drawbacks in promoting skin regenerations. For example, natural materials (e.g., decellularized tissues) derived from tissues by removing cellular materials remains the inherent architectural complexity and structure, which, however, cannot provide chemical stimulations via signaling molecules (e.g., growth factors).[139] Synthetic materials, composed by polymers can offer chemical stimulation in skin regeneration via the control release of growth factors, which, however, have difficulty to mimic the complex structure of tissues.

In this chapter, a semi-synthetic skin graft was created by incorporating natural and synthetic skin grafts together. Because the semi-synthetic skin graft inherits the advantages of both natural and synthetic skin grafts, it is expected to provide not only the appropriate physical microenvironment via structural support, but also the chemical stimulations to cells and tissues via the controlled release of growth factors for skin would healing and repair.

4.3 Materials and Methods

4.3.1 Materials

Gelatin from bovine skin (type B), methacrylic acid N-hydroxysuccinimide ester, polyethylene glycol (PEG) methyl ether acrylate (Mn = 480), poly(ethylene glycol) diacrylate (Mn = 700), Pluronic F-127 (PF127), and dimethylphenylphosphine (DMPP) were purchased from Sigma-Aldrich (St. Louis, MO). Dulbecco's phosphate buffered saline (DPBS), bovine serum albumin (BSA), sodium bicarbonate, glacial acetic acid, ammonium persulfate (APS), and tetramethylethylenediamine (TEMED) were obtained from Fisher Scientific (Suwanee, GA). Human umbilical vein endothelial cells (HUVEC), Medium 200 (M200), low serum growth supplement, Geltrex, Hoechst 33342, calcein AM, and ethidium homodimer-1 were purchased from Invitrogen (Grand Island, NY). Endo GRO-VEGF complete media kit was purchased from Millipore (Billerica, MA). Vascular endothelial growth factor-165 (VEGF) and VEGF enzyme-linked immunosorbent assay (ELISA) kit were obtained from Peprotech (Rocky Hill, NJ). CellTiter 96® AQueous One Solution Cell Proliferation Assay (MTS) was obtained from Promega. (Madison, WI). Anti-VEGF RNA aptamer was purchased from TriLink (San Diego, CA) and the complementary sequence of anti-VEGF aptamer was purchased from Integrated DNA Technologies (Coralville, IA).

4.3.2 Methods

4.3.2.1 Gelatin-Methacrylate Synthesis

Gelatin was dissolved in 0.1 M sodium bicarbonate buffer to reach a final concentration of 20 mg/mL at 37 ℃. Methacrylic acid *N*-hydroxysuccinimide ester was first dissolved in anhydrous DMSO at a concentration of 200 mg/mL. Next, the methacrylic acid *N*-hydroxysuccinimide ester solution was added to the gelatin solution at a molar ratio of 50:1 (methacrylic acid *N*-hydroxysuccinimide ester: gelatin). The solution was incubated at 37 ℃ for 1 hour with continuous stirring. The unreacted reductants were removed using a 10,000 Da MWCO dialysis cassette three times using distilled water (2 h, 2 h, and overnight) at 37 ℃, followed by concentrating with 10,000 Da cutoff spin column at 4000 g. The final concentration of gelatin-methacrylate (gelatin-MA) was diluted into 15 mg/mL. The gelatin-MA solution was sterilized by passing the solution through a 0.22 μm filter. The solution was stored at -20 ℃, and heated at 37 ℃ and mixed well before use.

4.3.2.2 Gelling Kinetics

Rheological tests were undertaken using an AR-G2 rheometer (TA Instruments, UK) in a parallel plate configuration, employing sandblasted stainless steel 40 mm diameter plates throughout and a Peltier plate for temperature control. In a typical rheological test for gelling kinetics, 1.5 mL of precursor solution (10 mg/mL of gelatin-MA, 666 mg/mL of PEG methyl ether acrylate, 1% APS, and 0.25% TEMED was loaded to the lower plate, which was preheated to 25 ℃. The upper plate was immediately brought down to a plate separation of 0.5 mm and the measurement was started. A low frequency of 1 Hz and 1% strain was applied to minimize interference with the gelation process and keep the measurement within the linear viscoelastic region. The gelling kinetics was measured in a time sweep by the monitoring of the change of storage (G′) and loss (G″) moduli as a function of time.

4.3.2.3 Aptamer Incorporated Gelatin-PEG Hydrogel

Precursor solution was prepared by combining 8 μL of gelatin-MA (15 mg/mL), 0.8 μL of PEG methyl ether acrylate (100%), and 50 pmol of anti-VEGF aptamer. Next, 0.1 μL of APS (10%), and 0.1 μL of TEMED (25%) were added into precursor solution for polymerizing hydrogel. Then the hydrogels were washed by dH_2O to remove unreacted monomers, APS, and TEMED. After that, the hydrogels were sterilized by 70% ethanol for 1 hour, followed by another washing with sterilized 1 x PBS for 1 day before use.

4.3.2.4 Degradation

Gelatin-PEG hydrogels were prepared as previously described method. The hydrogels were washed by dH_2O for 1 day to remove unreacted monomers, APS, and TEMED. Then the hydrogels were weighted and transferred into digestion buffer (0.001% collagenase I in 1xPBS). At different time point, the hydrogels were taken out from digestion buffer and weighted. The hydrogel morphology at different time point was also examined by SEM.

4.3.2.5 Porcine Small Intestine Decellularization

The intestine was obtained from a butcher (Hollands Brothers Meats, Altoona, PA) and thoroughly washed by distilled water before use. The porcine small intestine was mixed with 3% Triton X-100 or 3% SDS with a weight ratio of 1:10. After overnight incubation with vortex, the porcine small intestine was filtered out then placed in 3% SDS for another overnight incubation with vortex. The porcine small intestine was cleaned with distilled for three 3 times to remove Triton X-100 and SDS. After that, 1% w/v penicillin was used to incubate with porcine small intestine under continuous agitation at 4℃ for 24 hours. The decellularized small intestine was stored at -20℃. When the decellularized small intestine was needed, it was thawed and washed with sterilized water to remove the penicillin.

4.3.2.6 Incorporation of Decellularized Intestine with Gelatin-PEG-aptamer Hydrogel

Different amount of precursor solutions was added to 20 mg of dehydrated decellularized intestine. The precursor solution loaded intestine was incubated at room temperature for 30 min for hydrogel formation. The hydrogel-intestine mixture was incubated in 10 mL distilled water to wash away unreacted monomers, APS, and TEMED. Then the hydrogel-intestine mixture was sterilized by incubating with 1% penicillin for 1 day. After that, the hydrogel-intestine mixture was incubated with sterilized 1x PBS for 1 day to remove penicillin.

4.3.2.7 Optical Profilometer

The hydrogel incorporated decellularized intestine was examined by optical profilometer. In brief, the decellularized intestine with different amount of hydrogel loading was lyophilized for overnight. After that, the hydrogel loaded intestines were loaded on the platform of optical profilometer. The samples were measured using 20x magnification with a vertical scanning of 800 μm. Three different zones were selected and measured for each surface.

4.3.2.8 Confocal Microscopy

One FAM labelled complementary sequence that specifically binds to anti-VEGF aptamer was add into precursor solution before the hydrogel was incorporated into decellularized intestine. The hydrogel incorporated decellularized intestine was thoroughly washed in 1x PBS buffer and cut in half in horizontal direction. The top, middle, and bottom layers of hydrogel incorporated decellularized intestine were observed by Confocal Microscopy.

4.3.2.9 SEM

For morphological analysis, 10 μL of pregel solutions were used to form macroporous hydrogels according to the above method. Hydrogels were lyophilized for one day at -60 ℃. For

SEM analysis, hydrogels were mounted on an aluminum stub using double sided conductive adhesive tape and sputter coated with a thin layer of gold for 30 seconds. Then, samples were imaged using a FEI Quanta 200 Environmental SEM at an accelerating voltage of 15 kV.

4.3.2.10 Mechanical Stretch

The decellularized intestine was cut into rectangular strips to dimensions of 5mm x 30 mm. After the decellularized intestine was fixed by clips of Instron, the thickness of the sample was measured using a digital caliper. During the test, the samples were pulled at a rate of 500 mm/min and elongated to a failure. Values were converted to stress-strain curves and the initial modulus was calculated from the initial gradient of the resulting curves (0-10% elongation).

4.3.2.11 Cell Adhesion

HUVECs were cultured in 2% serum supplemented M200 until it reached 80% confluence. Calcein AM with final concentration of 1 μg/mL was used to stain the HUVECs for 30 min. The Calcein AM supplemented cell culture medium was withdraw and replace with fresh 2% serum supplemented M200 medium for washing away the dyes. With the help of trypsin, HUVEC were harvested and suspended in 2% serum supplemented M200 medium at a concentration of 1.0×10^6 cells/mL. Fifty microliters of the HUVEC suspension was added onto decellularized intestine with and without hydrogel incorporation. The decellularized intestines were cultured with the HUVEC solution overnight. Prior to cell imaging, the decellularized intestines were washed once before imaging via fluorescence microscopy. The number of cells on each hydrogel was calculated using the software Image J.

4.3.2.12 VEGF Retention

Macroporous hydrogels with different aptamer density were prepared according to the above method. Prior to loading VEGF (200 ng) into the macroporous hydrogels, the hydrogels were dehydrated by gently blotting with sterilized tissue paper. Lyophilized VEGF powder was dissolved in DPBS with 0.1% BSA. Next, 50 μL of the VEGF solution (4 μg/mL) was added to each hydrogel and the samples were incubated at 4 ℃ for 24 hours. The VEGF loaded hydrogel was incubated by 1 mL of DPBS with 0.1% BSA for 24 hours. The VEGF concentration of incubation buffer was measured by ELISA. The sequestration efficiency was determined by the ratio of the amount of VEGF remaining in the hydrogel to the amount of VEGF originally loaded into the hydrogel.

4.3.2.13 VEGF Release

The 200 ng of VEGF loaded hydrogels (Apt: VEGF=5:1) were incubated in 1 mL of release medium (M200 or 2% serum supplemented M200) at 37 ℃. At predetermined time points, the release medium was collected and replaced with 1 mL of fresh release medium. The collected release medium was stored at -20 ℃ until VEGF concentration was measured with a VEGF ELISA kit. To obtain high VEGF concentration for tube formation assay, the complementary sequence (CS) of the anti-VEGF aptamer was added to the release medium at a molar ratio of 10:1 (CS: aptamer) to trigger the massive VEGF release.

4.3.2.14 Cell Migration

HUVECs were seeded on 24 well plates and grown to 80% confluence. A gap was created by scraping with a pipette tip. Next, 1 mL of M200 medium was added into each well plate to wash the cells. The M200 medium was withdraw and replaced with M200 medium supplemented with either fresh or released VEGF. After overnight incubation, the cells were imaged and wound closure was measured with the help of Image J software.

4.3.2.15 Cell Tube Formation

Geltrex solution was thawed at 4 ℃ overnight before use. A volume of 80 µL geltrex was added to each well of a 48-well plate and incubated at 37 ˚C for 30 minutes. The HUVEC were trypsinized and suspended in serum-free medium. A volume of 190 µL VEGF release medium (M200 medium) was mixed with 10 µL stock cell solution to reach a final cell concentration of 2.0 x 10^5 cells/mL. The cell suspension was then transferred onto the matrigel-coated wells. After incubating at 37 ℃ and 5% CO_2 for 4 hours, cells were stained with calcein AM (2 µg/mL) for 30 min, followed by fluorescence imaging. Using Image J, tube lengths were measured and the number of cells comprising a tube was counted.

4.4 Results and Discussion

3.4.1 Synthesis of Aptamer Functionalized Hydrogel

Due to the complex composition, decellularized tissues have been found to non-specifically bind to a variety of small molecules. In this research, the aptamer and VEGF were pre-examined by non-specific binding test (data not shown). The results showed that the decellularized intestine had strong non-specific binding to the aptamer, which may be due to charge-charge interaction. The non-specific binding of aptamer to the decellularized intestine could significantly affect the aptamer incorporation into the synthetic hydrogel, which further obstructs the controlled VEGF release.

To solve this issue, the aptamer was pre-conjugated into gelatin. As the charge density of gelatin-aptamer conjugates decreased, the conjugated aptamer can avoid non-specifically binding to the decellularized intestine. The conjugation of aptamer into gelatin was shown in **Figure 4-1A.** The thiol modified aptamer reacted with the methacrylate groups of gelatin with the help of DMPP via Michael addition reaction. After the aptamer and gelatin conjugation, the conjugates were washed to remove free aptamer and examined by electrophoresis (**Figure 4-1B**). One FAM labeled complementary sequence that specifically binds with aptamer was used for detecting the aptamer. The electrophoresis results showed that the conjugate with DMPP had an obvious band shift. It indicated that aptamer could be successfully conjugated to the gelatin. However, the successful conjugation relied on the help of DMPP as catalyst.

After the aptamer was successfully conjugated into gelatin, the hydrogel formation and gelatin time were studied by rheometer. The results showed that aptamer-conjugated gelatin could crosslink the PEG acrylate to form gelatin-PEG hydrogel (**Figure 4-1C**). Additionally the gelation time of hydrogel was around 5 min, which is good for the incorporation of hydrogel into decellularized intestine.

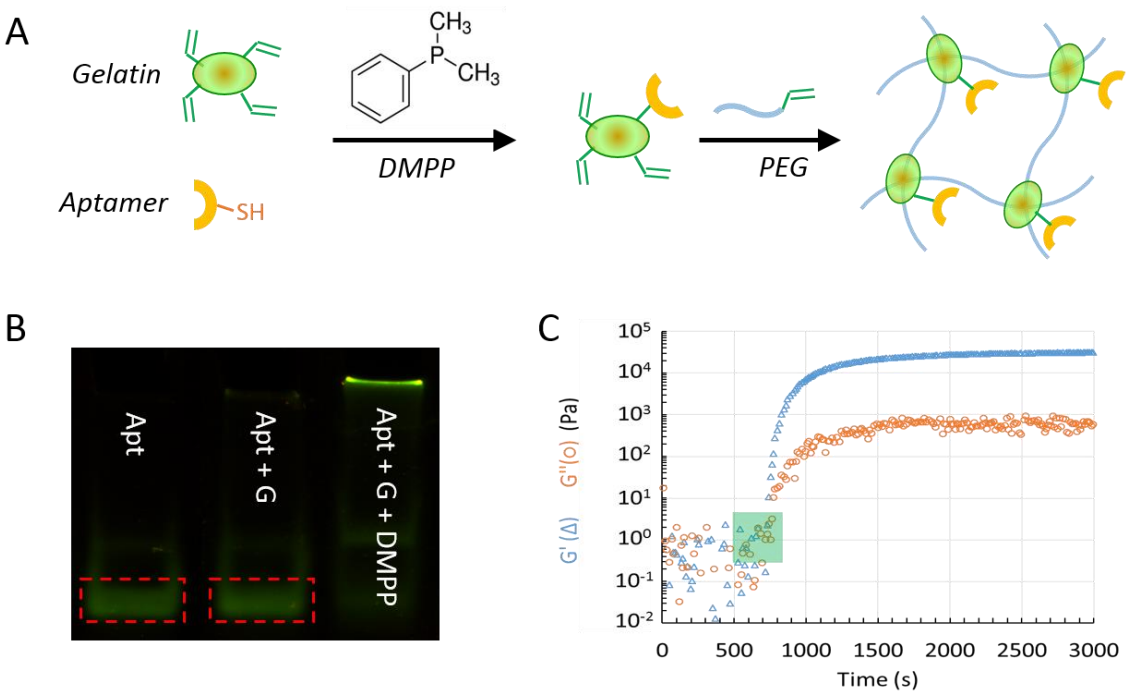

Figure 4-1 The synthesis of aptamer functionalized gelatin-PEG hydrogel. (A) Schemetic illustration of the formation of aptamer functionalized gelatin-PEG hydrogel. (B) the examination of the conjugation between gelatin and aptamer by electrophoresis. Apt: aptamer. G: gelatin. DMPP: dimethylphenylphosphine. (C) the study of hydrogel formation using rheometer. G': storage modulus. G'': loss modulus.

3.4.2 Incorporation of Hydrogel into Decellularized Intestine

In the previous chapter, it was shown that 1) the decellularized intestine can mimic the complex structure of human skin and provide physical support to maintain an appropriate microenvironment for cell adhesion, proliferation, migration, and differentiation; 2) the synthetic materials can be programed to control the release of growth factors, which are signaling proteins and can activate signal transaction pathways for regulating cell functions in tissue regeneration. In this chapter, the decellularized intestine and VEGF-aptamer loaded synthetic hydrogel were integrated together for synthesizing a semi-synthetic skin substitute that provides both physical and chemical stimuli to cells during tissue regeneration.

The incorporation of decellularized intestine with synthetic hydrogel was shown in **Figure 4-2.** The precursor solution was loaded into the decellularized intestine, which was pretreated by lyophilization. It showed that a large amount of porous structures were shown in the decellularized intestine before the addition of precursor solution. However, after the precursor solution was added into the lyophilized decellularized intestine, the porous structures of synthetic hydrogel incorporated decellularized intestine were decreased. Additionally, when the hydrogel loading reached 50% of loading capability of decellularized intestine, most of porous structures were blocked by hydrogel polymerized by precursor solution. When the hydrogel loading reached 100% of loading capability of decellularized intestine, few pore structures were observed in decellularized intestine.

Porous structure is critical for biological substitute in tissue regeneration. The interconnected pores increase the growth factor transport after they dissociate from the state of binding with aptamer. Additionally the pores provide endothelial cells an appropriate structure to adhesion, proliferate, and migration for achieving a three dimensional skin recovery. For these purposes, the 25% hydrogel loading was chosen in the next experiments for preserving porous structures.

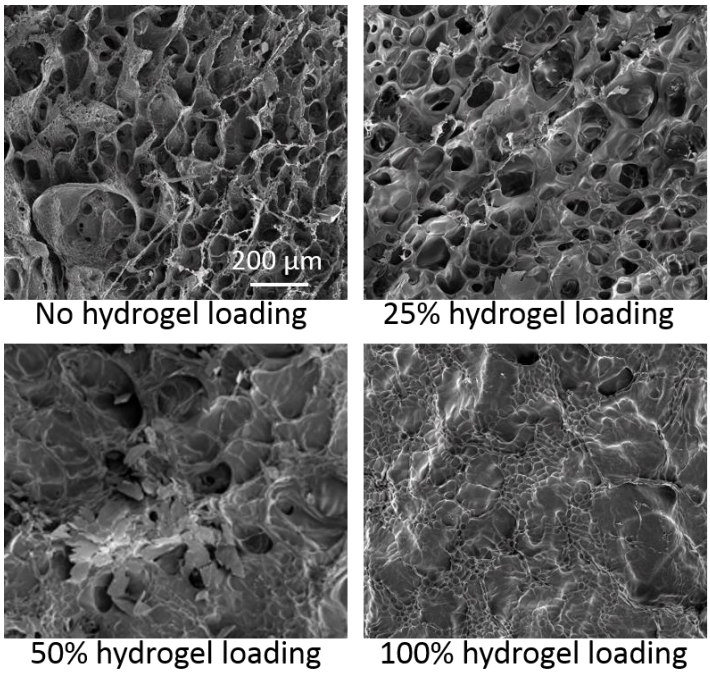

Figure 4-2 Examination of hydrogel loading into decellularized intestine. The precursor solution was uniformly added into pre-lyophilized decellularized intestine. After 30 min incubating for gel polymerization, the hydrogels incorporated decellularized intestine was washed by PBS to remove unreacted monomers, APS, and TEMED. The hydrogel loaded decellularized intestines were lyophilized, sputter coated and observed by SEM.

3.4.3 Examination of Hydrogel Loading into Decellularized Intestine

The incorporation of synthetic hydrogel with decellularized intestine was examined by optical profilometer (**Figure 4-3A, B, C, and D**). The results showed that the decellularized intestine had a rough surface and pore like structure without hydrogel loading. However, the roughness of decellularized intestine was decreased when synthetic hydrogel was loaded. When hydrogel loading reached 25% of loading capability of decellularized intestine, the total roughness of decellularized intestine was decreased from 9.3 mm to 7.4 mm (**Figure 4-3E**). The roughness of decellularized intestine was further decreased to 4.6 mm when hydrogel loading reached to 50% loading capability of decellularized intestine (**Figure 4-3E**). Additionally, the most of pore like structures disappeared. The further increase the hydrogel loading to 100% of loading capability of decellularized intestine resulted in a relatively smooth surface of decellularized intestine (**Figure 4-3E**). These results were consistent with SEM data.

To further examine the hydrogel distribution, the hydrogel incorporated decellularized intestine was imaged by Confocal Microscopy (**Figure 4-3F**). Before hydrogel loading into decellularized intestine, one FAM labeled complementary sequence of aptamer was added to precursor solution as hydrogel indicator. The fluorescence imaging showed that the top, middle and bottom sections of decellularized intestine all showed fluorescence, indicating the successfully incorporation of hydrogel with decellularized intestine. Additionally the homogenous fluorescence intensity of the sections of decellularized intestine demonstrated uniform hydrogel incorporation with decellularized intestine.

Cells can sense and respond to the mechanical property of scaffold in tissue engineering. So the peak stress, Young's modulus, and strain at break of intestines were all measured before and after hydrogel incorporation (**Figure 4-3G**). The peak stress, Young's modulus, and stain at break of decellularized intestine with and without hydrogel incorporation were similar, indicating the little influence of hydrogel on the mechanical properties of decellularized intestine.

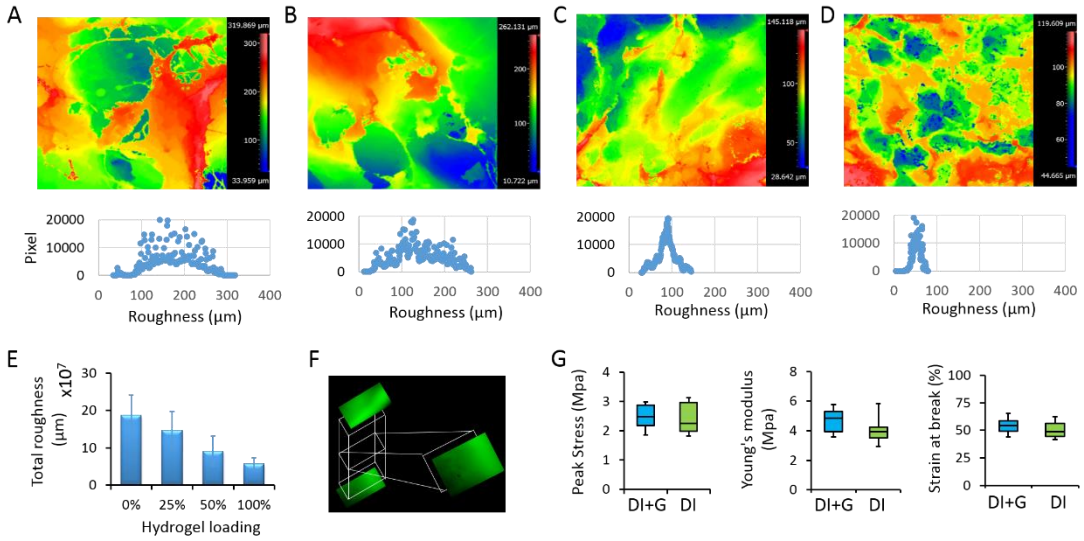

Figure 4-3 Characterization of hydrogel loaded decellularized intestine. The study of surface roughness of hydrogel incorporated decellularized intestine using optical profilometer. (A) No hydrogel loading. (B) 25% hydrogel loading. (C) 50% hydrogel loading. (D) 100% hydrogel loading. (E) Quantification of total roughness of decellularized intestines with different hydrogel loadings. (F) Examination of hydrogel distribution in decellularized intestine. A FAM labeled DNA was conjugated into hydrogel as indicator. After the hydrogel was loaded into decellularized intestine, the decellularized intestine was cut in horizontal direction. The top, middle, and bottom layers were imaged by fluorescence microscope. (G) Physical examination of decellularized intestine with hydrogel loading.

3.4.4 VEGF Loading and Release

After the synthetic hydrogel was successfully incorporated into decellularized intestine, the functionality of the semi-synthetic substitute to capture the VEGF was examined. The semi-synthetic substitute was dehydrated and loaded with 200 ng of VEGF, followed by the incubation with 1x DPBS for 24 hours. After quantifying the VEGF concentration of incubation buffer, the VEGF sequestration by the semi-synthetic substitute can be calculated. As the sequestration of VEGF by the semi-synthetic substitute was obtained via the molecular interaction between aptamer and VEGF, the VEGF sequestration increased with increasing aptamer density in the semi-synthetic substitute (**Figure 4-4A**). When there was no aptamer existing in the semi-synthetic substitute, the VEGF sequestration only reached around 10%. However, the VEGF sequestration significantly increased after the addition of aptamer into the semi-synthetic substitute. The VEGF sequestration reached nearly 31%, 70%, and 93% when the molar ratio of aptamer to VEGF was 1:1, 1:5, and 1:10. However, after that, the VEGF sequestration reached plateau and cannot significantly increased with further increasing the ratio of aptamer to VEGF.

After the VEGF sequestration was examined, the VEGF release by the semi-synthetic substitute was studied (**Figure 4-4B**). Compared to the semi-synthetic substitute without aptamer, the aptamer functionalized semi-synthetic substitute showed a significantly different VEGF release profile. The non-aptamer functionalized semi-synthetic substitute released more than 90% VEGF in the first day and showed almost no VEGF release in the following days. However, with the help of aptamer, the semi-synthetic substitute could prevent the VEGF burst release and achieved a sustained VEGF release. There was less than 10 % VEGF release in the first day with 2-5% VEGF release in the following days.

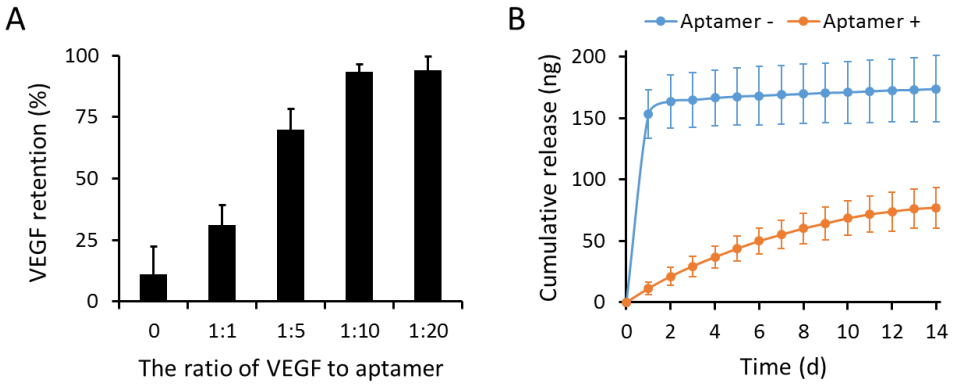

Figure 4-4 Examination of VEGF retention and release. (A) VEGF sequestration. 50 μL of the solution with 200 ng VEGF was added to each semi-synthetic skin and the samples were incubated at 4 ℃ for 24 hours. The sequestration efficiency was determined by the ratio of the amount VEGF remaining in the semi-synthetic skin after 24 hour release to that originally loaded into the semi-synthetic skin. (B) Comparison of VEGF release from the semi-synthetic skin with (+) and without (-) the aptamer in the 10% LSGS supplemented M200 medium. The molar ratio of the aptamer to VEGF was 10:1. The initial VEGF loading amount was 200 ng.

3.4.5 Bioactivity of Released VEGF

HUVECs were grown on a Geltrex-coated cell culture plate in the cell culture basal medium with the released VEGF for 4 hours and then stained with calcein AM. The tubes were examined under a fluorescence microscope. Without VEGF, HUVECs on the Geltrex barely participated into the formation of tubes (**Figure 4-5A**). With VEGF, HUVECs were self-assembled to form tubes. When the concentration of VEGF was 10 ng/mL, the total length of the tubes was 7,249 $\mu m/mm^2$ in the stock VEGF group. When the VEGF samples of the same concentration collected from the chimeric hydrogels at day 7 and day 14 were used to treat HUVECs, the total lengths of the formed tubes were 6,158 and 3,725 $\mu m/mm^2$, respectively (**Figure 4-5B**). Statistically, there is a significant difference in stimulating tube formation between the stock VEGF solution and the VEGF sample collected at day 14. Since the formation of tubes indicates VEGF bioactivity, the results demonstrate that VEGF in the macroporous hydrogel could maintain ~ 50% bioactivity by day 14. By contrast, the literature shows that it is challenging to maintain the high bioactivity of therapeutic proteins (e.g., VEGF) owing to their fragile structures.[129,140]

Another biofunction of VEGF is to induce cell migration in tissue regeneration. The gap model of cell migration was used to test the VEGF in promoting cell migration. The results showed that the cell gap was fully refilled with fresh VEGF while released VEGF at day 7 and day 14 only partially filled the cell gap (**Figure 4-5C and 4-5D**). It indicated that VEGF denaturation happened with increasing incubation time. The measured VEGF stability by cell migration assay was also similar with the results from cell tube assay.

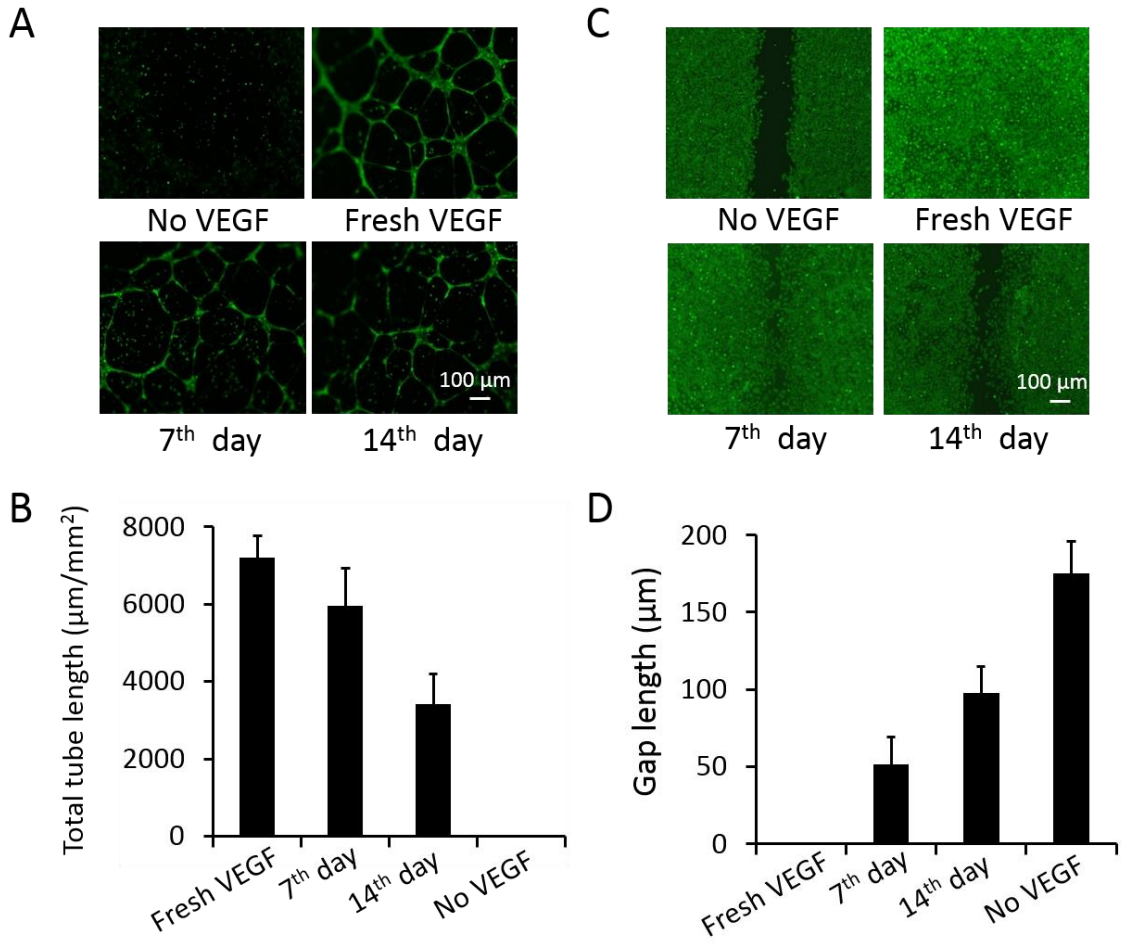

Figure 4-5 Examination of VEGF bioactivity. (A) Comparison of the VEGF release media collected at day 7 and day 14 in stimulating the tube formation. The release media from Apt (+) and Apt (-) semi-synthetic skin were collected and used to incubate with HUVECs in stimulating the tube formation. (B) Quantification of the total length of tubes. (C) Examination of the activity of released VEGF in cell migration assay. (D) Quantification of the gap length.

4.5 Conclusions

Current biological substitutes for tissue regeneration have been challenged not be able to simulate autograft in providing both physical and chemical support. This study creates a semi-synthetic skin substitute composed of decellularized small intestine and aptamer functionalized hydrogel. The decellularized small intestine derived from tissue by removing cellular materials remains the inherent architectural complexity and ultrastructure, which can provide an appropriate physical microenvironment for cell growth. Aptamer functionalized hydrogel can achieve the sustainable release of growth factors, which bind with receptors and activate signal transduction pathways for inducing cell adhesion, proliferation, migration and differentiation. Because of the combination of two components together, the hybrid scaffold is expected to provide both structural supports and growth factor stimulation in skin regeneration.

Chapter 5

Conclusions and future work

5.1. Conclusions

Tissue substitute is a significant research topic in tissue engineering. Decellularized tissues with the ability to physically stimulate cell behavior such as cell adhesion and proliferation hold great potential for tissue regeneration or repair. However, tissue regeneration relies on both physical (e.g., structure and mechanic) and chemical (e.g., growth factors) stimuli. The growth factors in decellularized tissues were denatured owing to the harsh conditions used during the decellularization procedure and cannot provide chemical stimulation in tissue repairs. Therefore, the decellularized tissues cannot provide desirable tissue regeneration due to the long therapy period, scar formation, and tissue malfunctions. Synthetic hydrogel is a well-studied platform that can achieve the controlled growth factor delivery. Synthetic hydrogel has been used in tissue regeneration by providing sustainable growth factor stimulation.

To mimic the autografts relying on both physical (e.g., structure and mechanic) and chemical support (e.g., growth factors), synthetic hydrogel was incorporated into decellularized tissue for creating a semi-synthetic substitute. Because the semi-synthetic substitute can provide both physical and chemical support in tissue regeneration, it is expected to not only provide similar therapeutic outcomes as autografts, but also avoid the disadvantages of autografts such as secondary surgery, limited availability, and donor site morbidity.

In this study, a semi-synthetic skin substitute composed of aptamer functionalized gelatin-PEG hydrogel, VEGF, and decellularized small intestine was created and tested as a model. The semi-synthetic skin substitute presents not only the similar physical properties (e.g., structure, pore, and mechanic), but also the controlled VEGF release for weeks. The semi-synthetic skin substitute also showed strong capability to stimulate the angiogenesis in *ex ovo* CAM assay. The results

demonstrated that the hydrogel incorporation could endow decellularized tissue with chemical stimulations. The succeed of this work will provide a new avenue in the development of tissue substitutes

5.2. Future Work

The work presented herein has demonstrated the advantages of semi-synthetic substitute in promoting cell adhesion and proliferation and in controlled VEGF release *in vitro*. However, much work remains to evaluate the capability of semi-synthetic substitute in promoting skin tissue regeneration *in vivo*.

In this study, VEGF could be sustainably released from semi-synthetic substitute and the released VEGF remained bioactive *in vitro*. The semi-synthetic substitute also proved the capability to induce angiogenesis in *ex ovo* CAM assay. However, it is unclear how the semi-synthetic substitute will react in an animal model. For this assay, a skin defect mice model is suggested. To test the both physical and chemical stimulations of semi-synthetic substitute, four groups will be implanted including 1) VEGF loaded aptamer hydrogel, 2) decellularized intestine, and 3) VEGF loaded semi-synthetic substitute. The first group will test the chemical support to promote tissue regeneration while the second group will examine the physical support. The third group will evaluate the tissue regeneration under both physical and chemical support. Although the first and second groups will promote tissue recovery to some degree, the third group is expected to be much better than first and second groups in terms of recovery time and therapy outcome.

Appendix A

Applying aptamer Hydrogel for Controlled Release of Small Molecule

A.1. Experimental Procedure

A.1.1. Materials

Two DNA oligonucleotides (oligo-1 and oligo-2) were purchased from Integrated DNA Technologies (Coralville, IA). These two oligonucleotides have the same nucleotide composition but have different sequences. The sequences of oligo-1 and oligo-2 are 5′-CGTACGGAATTCG CTAGCCCCCCGGCAGGCCACGGCTTGGGTTGGTCCCACTGCGCGTGGATCCGAGCTC CACGTG-3′ and 5′-TGTTAGCTTGTCACGGCCTGTGTCCAGGCCCGGGCGCGGTCCGAA GGCCCCTCGGCGGCAACTCTCAGGCACGTCA-3′, respectively. Acrydite was conjugated to their 5′ ends with a six-carbon linker. PEG diacrylate (Mn: ~700 Da) and tetracycline hydrochloride were purchased from Sigma-Aldrich (St. Louis, MO). Ammonium persulfate (APS) and N,N,N′,N′-tetramethylenediamine (TEMED) were purchased from Fisher Scientific (Suwanee, GA).

A.1.2. Methods

A.1.2.1. Synthesis of Oligonucleotide-Functionalized Hydrogels

The hydrogels were synthesized with 20 μL of 20% PEG in a cylindrical mold in the presence of APS (1% w/v) and TEMED (1% w/v) using free radical polymerization. PEG diacrylate

solution was sterilized by filtration with a 0.2 μm filter unit (Fisher Scientific, GA) before polymerization. Hydrogels were allowed to cure at room temperature for 3 h, followed by thorough washing to remove unreacted molecules.

A.1.2.2. Gel Electrophoresis

Gel electrophoresis was used to characterize qualitatively the incorporation of oligonucleotides to the PEG hydrogel. The PEG solutions were carefully loaded into the wells of a preformed polyacrylamide gel. After 3 h, electrophoresis was run at 160 V using a Bio-Rad Mini-PROTEAN tetra cell electrophoresis system. The polyacrylamide gel was stained with ethidium bromide and imaged with the Bio-Rad GelDoc XR system (Hercules, CA).

A.1.2.3. Swelling Quantification

The swelling of the hydrogels was examined by measuring water uptake of the hydrogels. The hydrogels were dehydrated in a Labconco DNA concentrator (Kansas City, MO). The dehydrated hydrogels were sequentially incubated in the release buffer at 4 and 37 ℃, each for 12 h. At predetermined time points, the hydrogel samples were taken out of the buffer, blotted with tissue paper, and weighed. The swelling of the hydrogels was calculated by the increased weight divided by their initial weight. The swelling was determined by using the following equation: Swelling ratio (%) = $[(Ws - Wi)/Wi] \times 100$, where Ws is the wet weight of the rehydrated hydrogel and Wi is the initial weight of the dehydrated hydrogel. The hydrogels before and after swelling were also imaged using a digital camera (Nikon D60).

A.1.2.4. Rheological Characterization

The storage (G′) and loss (G″) moduli of the hydrogels were measured with an AR-G2 rheometer (TA Instruments, New Castle, DE). Hydrogels were carefully loaded into the central

region of the chamber. The gap (20 mm) was adjusted until the normal force reached 0.2 N. To obtain a steady condition for the measurement, a stress sweep was performed by varying the oscillation stress from 0.01 to 1000 Pa at a fixed frequency of 6 rad/s. Afterward, frequency sweep experiments were performed at a fixed oscillation stress of 1 Pa with the frequency varied from 0.5 to 100 rad/s.

A.1.2.5. Tetracycline Loading and Release

Dehydrated hydrogels were immersed in 1 mL of tetracycline solution (100 μg/mL) overnight at 4 ℃. For the test of tetracycline release, the hydrogels loaded with tetracycline were incubated in the release buffer of 100 μL at 37 °C and at a shaking rate of 50 rpm. The release buffer contained NaCl (100 mM), Tris–HCl (20 mM, pH 7.6), MgCl2 (2 mM), KCl (5 mM), and CaCl2 (1 mM). At predetermined time points, the release buffer was completely collected and replenished with a fresh release buffer. The amount of tetracycline in the release buffer was quantified by fluorescence measurement at an excitation wavelength of 395 nm and an emission wavelength of 522 nm (Nanodrop 3300, Thermo Scientific, DE). The hydrogels were also imaged with the Bio-Rad GelDoc XR system (Hercules, CA) to illustrate tetracycline release qualitatively. All experiments were performed in duplicate.

A.1.2.6. Determination of Partition Coefficient

The partition coefficient of tetracycline between the hydrogel and the loading buffer was calculated using the tetracycline concentration in the hydrogel divided by that in the loading buffer. The amount of loaded tetracycline was determined by the total amount of released tetracycline.

A.1.2.7. Antimicrobial Assays

Two assays were carried out to determine the antimicrobial activity of the released tetracycline using E. coli DH5α as a model (Life Technologies, NY). E. coli was grown in a Lysogeny broth (LB) medium, collected in the mid-log phase, and diluted with PBS buffer before use for antimicrobial assays.

The first assay was based on a "hole-plate diffusion method". In this assay, LB agar plates were inoculated with 200 μL of E. coli suspension (~10^4 cells/mL). After inoculation, three holes with a radius of 3 mm were punched in the same LB agar plate. The released tetracycline solution of 50 μL was carefully transferred to each hole. The agar plates were incubated at 37 °C overnight. The images of agar plates were captured using a digital camera (Nikon D60).

The second assay was based on the culture of bacteria in the release medium. The E. coli suspension of 5 μL (~10^4 cells/mL) was mixed with 45 μL of released tetracycline solution. After incubation at 37 °C overnight, 150 μL of PBS buffer was added to the E. coli suspension. The diluted suspension was inoculated on a LB-agar plate and incubated at 37 ℃ overnight. All experiments were performed in duplicate. The images of agar plates were captured using a digital camera (Nikon D60). The images were analyzed to calculate the number of E. coli colonies using Image J software. The antimicrobial efficiency was determined by the following equation: antimicrobial efficiency (%) = [C0 – C)/C0] × 100, where C is the number of E. coli colonies after tetracycline treatment and C0 is the number of E. coli colonies in the control group that was treated only by PBS buffer.

A.1.2.8. Examination of the Functionality of Refilled Hydrogels

To test the feasibility of refilling hydrogels with tetracycline, we collected hydrogels after the first-time drug release experiment. The hydrogels were washed with 1.5 mL of pure water overnight, dehydrated by DNA concentrator, and immersed in 1 mL of tetracycline solution (100

μg/mL) at 4 °C overnight. The experiments of tetracycline release and bacterial inhibition were run using the same procedure as previously described.

A.2. Results

A.2.1. Chemical Incorporation of DNA Oligonucleotides into the Hydrogel

The DNA oligonucleotides were functionalized with acrydite at their 5′ ends to incorporate them chemically to the polymer backbone. To demonstrate the success of chemical incorporation, we used gel electrophoresis to characterize the reaction mixture because free oligonucleotides would be driven to flow out of the hydrogel in an electric field. The result showed that the majority of DNA oligonucleotides were conjugated to the hydrogel through free radical polymerization (**Figure A1.A**). The qualitative analysis of band intensity indicated that the efficiency of oligonucleotide incorporation was ~80%.

A.2.2. Characterization of Hydrogel Properties

A swelling test and a rheology test were applied to characterize the properties of the hydrogels with and without DNA oligonucleotides. The results showed that the swelling of dehydrated hydrogels was very fast and virtually reached equilibrium within 1 h (**Figure A1.B**). The swelling ratio was close to 300% at 4 ℃ and decreased by ~50% when the temperature was shifted from 4 to 37 ℃. In addition to the swelling test, the dynamic moduli of the hydrogels were also characterized (**Figure A1.C**). There was no significant difference between the loss moduli of the hydrogels with and without DNA oligonucleotides. The storage moduli of the native hydrogel at both 4 and 37 ℃ were slightly higher than those of the hydrogels functionalized with DNA oligonucleotides.

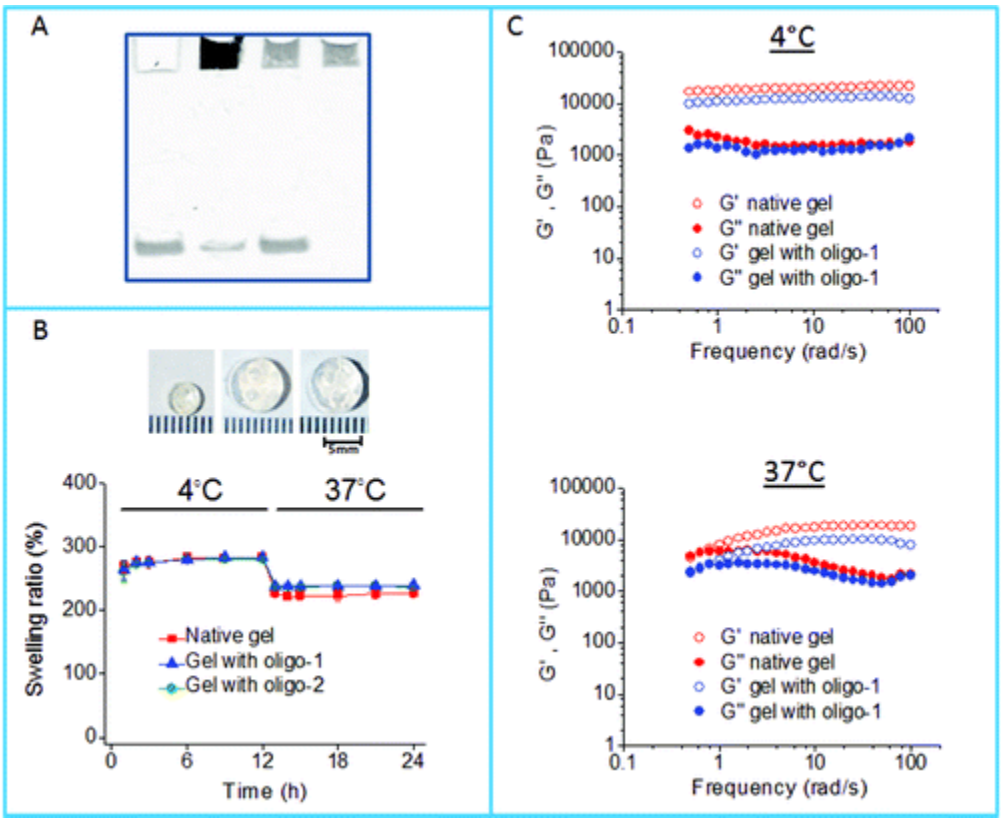

Figure A1. Characterization of oligonucleotide incorporation and hydrogel properties. (A) Gel electrophoresis image. From left to right: oligonucleotides, PEG, PEG with unmodified oligonucleotides, and PEG functionalized with acrydite-modified oligonucleotides. (B) Swelling test. The dehydrated hydrogels were sequentially incubated in PBS for 12 h at 4 and 27 ℃, respectively. The inset image shows the morphology of an oligonucleotide-functionalized hydrogel under different conditions. From left to right: dehydrated hydrogel, rehydrated hydrogel at 4 ℃, and rehydrated hydrogel at 37 ℃. (C) Rheology test. *G′*: storage modulus; *G″*: loss modulus. The frequency sweep experiments were performed from 0.5 to 100 rad/s at a 1 Pa oscillation stress.

A.2.3. Effects of Oligonucleotide Incorporation on Enhancing Tetracycline Loading and Prolonging Its Release

The hydrogels were incubated in the tetracycline solution overnight before the release test. A further increase in the incubation time did not increase the total amount of tetracycline loading or change the release profile (data not shown), demonstrating that overnight incubation was sufficient to load tetracycline into the hydrogels. Therefore, all experiments of tetracycline loading were performed using overnight incubation. The total amount of tetracycline released from the hydrogel functionalized with oligo-1 was similar to that from the hydrogel functionalized with oligo-2 (**Figure A2.A**). It was ~13 μg, three times as high as that released from the native hydrogel. These results demonstrate that the existence of the DNA oligonucleotides in the hydrogels enhanced tetracycline loading.

Although the concentration of tetracycline in the oligonucleotide-functionalized hydrogels was much higher than that in the native hydrogel, the rate of tetracycline release from the oligonucleotide-functionalized hydrogels was slower than that from the native hydrogel. For instance, ~60% tetracycline was released from the native hydrogel in the first hour. In contrast, <30% tetracycline was released from the oligonucleotide-functionalized hydrogels during the same period of time (Figure A2.B). It is also important to note that there was no difference between oligo-1 and oligo-2 (i.e., the scrambled sequence of oligo-1) in enhancing tetracycline loading and prolonging the sustained release of tetracycline. The tetracycline release and the images of the hydrogels at representative time points are also shown in **Figure A2.C and Figure A2.D**. On the basis of calculations, the incorporation of DNA oligonucleotides led to a two-time increase in the partition coefficient (**Figure 2A.E**). The overall data showed that the DNA oligonucleotides could enhance tetracycline loading and prolong the sustained release of tetracycline.

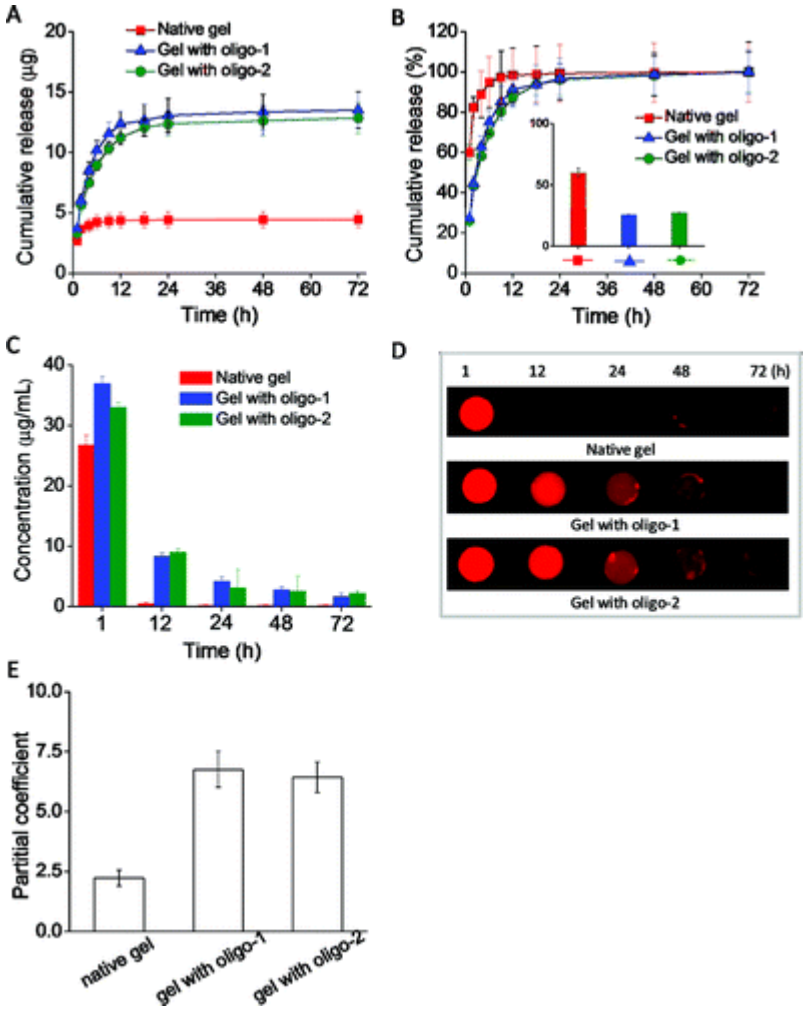

Figure A2. Comparison of different hydrogels in loading and releasing tetracycline. (A) Absolute quantity of released tetracycline. Hydrogels were incubated in the tetracycline solution (100 μg/mL) for 12 h before the release test. The concentrations of oligo-1 and oligo-2 were 0.75 mM. (B) Cumulative percentage of tetracycline release. The inset figure shows 1 h tetracycline release. (C) Concentrations of released tetracycline at representative time points. (D) Fluorescence images of hydrogels at different release time points. (E) Comparison of partition coefficients of tetracycline in different hydrogels.

A.2.4. Effects of Concentrations of DNA on Tetracycline Loading and Release

To understand further the effect of DNA oligonucleotides on tetracycline loading and release, a series of hydrogels were prepared with oligo-1. The increase in oligo-1 concentration led to an increase in tetracycline loading that was indicated by the total amount of released tetracycline (**Figure A3.A**). Importantly, the partition coefficient exhibited a linear relationship to the oligo-1 concentration ranging from 0 to 1 mM (**Figure A3.B**). Although the linear trend weakened with the concentration further increased from 1 to 3 mM, the partition coefficient was still increased to ~10 at 3 mM.

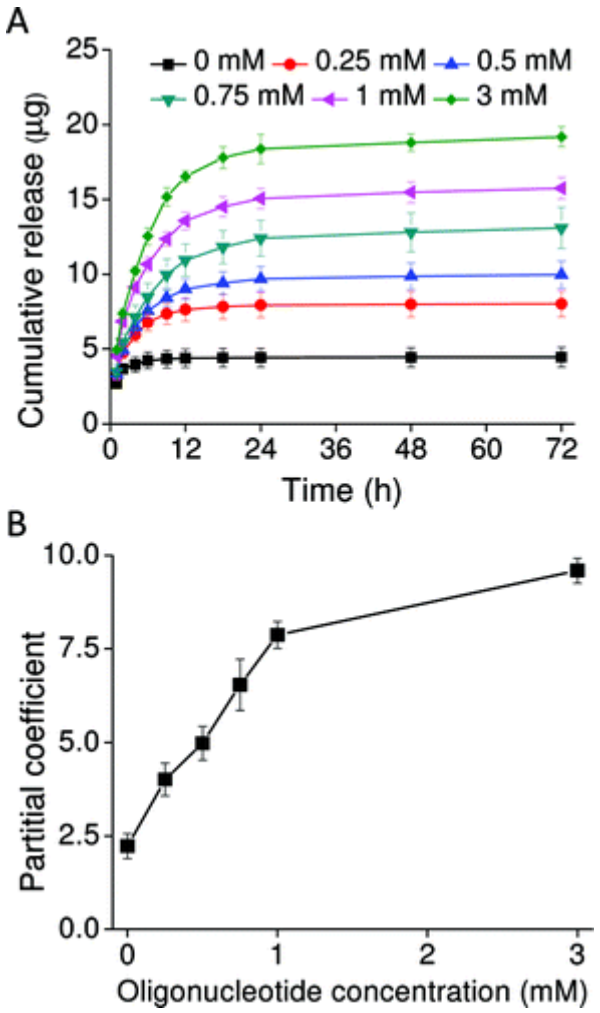

Figure A3. Effect of oligonucleotide concentration on tetracycline enrichment and release. (A) Cumulative tetracycline release. The numbers indicate the initial concentration of oligonucleotides for hydrogel synthesis. The concentration of tetracycline in the loading buffer was fixed at 100 μg/mL. (B) Relationship of partition coefficient to oligonucleotide concentration.

A.2.5. Effects of Concentrations of Tetracycline on Tetracycline Loading and Release

Because the concentration gradient of a drug is critical to drug loading and release, the effects of the tetracycline concentration on tetracycline loading and release were also studied (**Figure A4.A**). The total amount of released tetracycline in the hydrogel increased with the increase in tetracycline concentration in the loading buffer (**Figure A4.B**). This result confirms that the incorporation of oligonucleotides leads to more drug loading.

For the native hydrogel, the partition coefficient of tetracycline did not change with the tetracycline concentration (**Figure A4.C**). However, for the oligonucleotide-functionalized hydrogel, the relationship between the partition coefficient and the tetracycline concentration exhibits a bow-like profile (**Figure A4.C**). When the concentration of tetracycline was increased from 25 to 75 μg/mL, the partition coefficient increased from 5.3 to 7.7. When the concentration was further increased to 100 μg/mL, the partition coefficient decreased to 6.7.

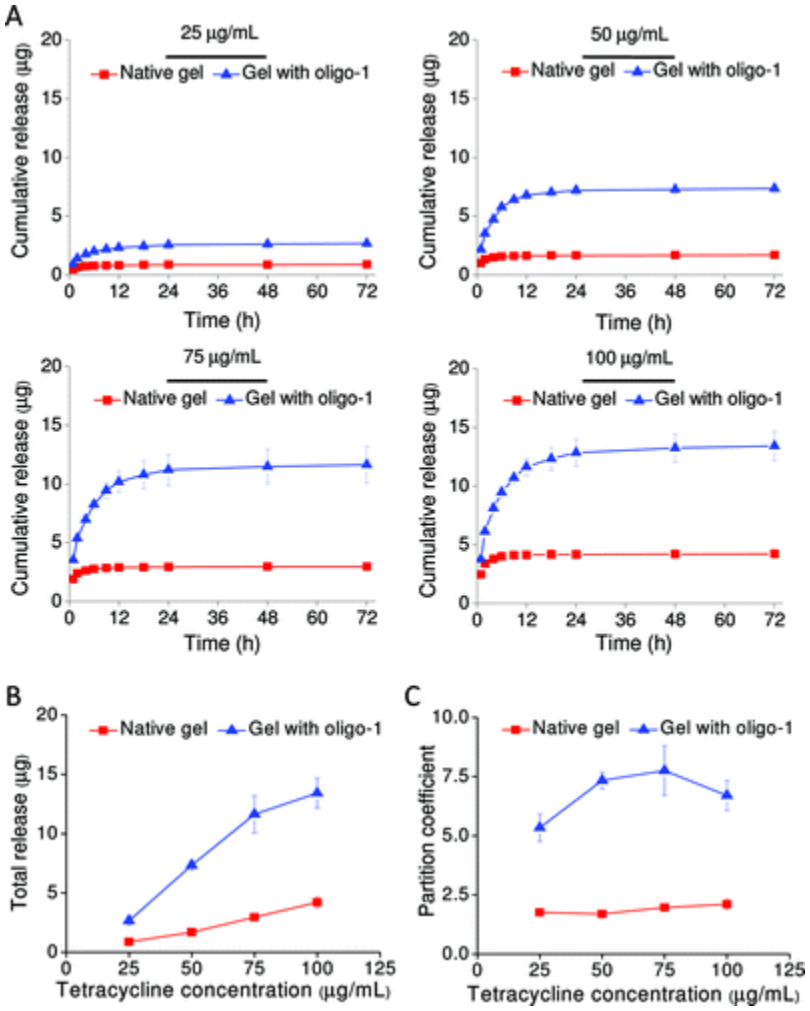

Figure A4. Effect of tetracycline concentration on tetracycline loading and release. (A) Cumulative tetracycline release. The concentration of oligo-1 was 0.75 mM for the synthesis of all hydrogels. (B) Relationship of total tetracycline release to tetracycline concentration in the loading buffer. (C) Relationship of partition coefficient to tetracycline concentration in the loading buffer.

A.2.6 Tetracycline Release for Bacterial Inhibition

Antimicrobial experiments were performed to evaluate the antimicrobial activity of released tetracycline against *E. coli* DH5α. One antimicrobial experiment was based on the formation of zones of bacterial inhibition. The release media were collected at five representative time points and loaded into the holes in the agar plate. As shown in **Figure A5.A**, few bacteria can be observed in the circled areas surrounding the small holes that were loaded with the tetracycline solution collected at 1 h. These areas become smaller with the increase in the release time. In addition, the areas of O1 and O2 are larger than that of *n* (**Figure A5.A**). These results show that the released tetracycline could inhibit bacterial growth within 48 h and induce the formation of zones of inhibition on the agar plate. Moreover, the oligonucleotide-functionalized hydrogels could induce more effective bacterial inhibition than the native hydrogel.

In another set of antimicrobial experiments, bacteria were first suspended in the release media. After the treatment with the release media, the bacterial suspension was spread on the agar plate for the examination of bacterial growth. As shown in **Figure A5.B**, the agar plates in the 1 h release column have few bacterial colonies. However, the bacteria treated with the release media collected at 12 h in the native gel group virtually reached confluence on the agar plate. In contrast, only a few bacterial colonies could be observed on the agar plates in the oligonucleotide-functionalized hydrogel groups. The quantitative analysis indicated that the antibacterial efficiency of the oligonucleotide-functionalized hydrogels maintained above 97% within 24 h. These data demonstrate that the oligonucleotide-functionalized hydrogels were more effective in bacterial inhibition than the native hydrogel.

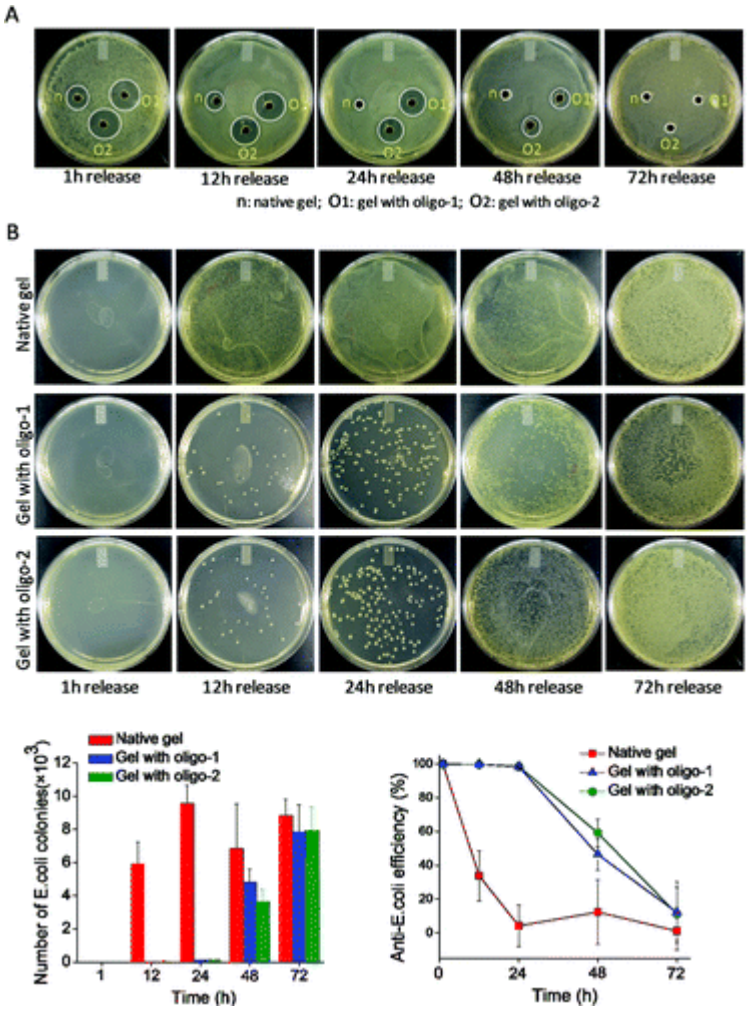

Figure A5. Characterization of antibacterial activity. (A) Zones of bacterial inhibition in the hole-plate diffusion assay. (B) Bacterial growth after the treatment of bacterial suspension with the released tetracycline. The concentration of oligonucleotides was 0.75 mM. The concentration of tetracycline was 100 μg/mL. Images were captured to demonstrate the formation of bacterial colonies. The images were analyzed using Image J software to count the number of bacterial colonies and calculate antibacterial efficiency.

A.2.7 Examination of Tetracycline Reloading for Bacterial Inhibition

The hydrogels after the initial tetracycline release were further incubated in a fresh tetracycline solution to reload tetracycline. As shown in **Figure A6.A and Figure A6.B**, the fresh and reloaded hydrogels exhibited virtually no difference in both tetracycline loading and partition coefficients. In addition, the oligonucleotide-functionalized hydrogels still held more tetracycline for a slower tetracycline release than the native hydrogel (**Figure A6.C and Figure A6.D**). The antimicrobial activity was also studied to examine tetracycline reloading for bacterial inhibition. Consistent with the results shown in **Figure A5.A**, tetracycline released from the oligonucleotide-functionalized hydrogels inhibited bacterial growth more effectively than that released from the native hydrogel (**Figure A6.E**). These data demonstrate that DNA oligonucleotides can be applied to develop a refillable drug delivery system for antibiotic loading and release.

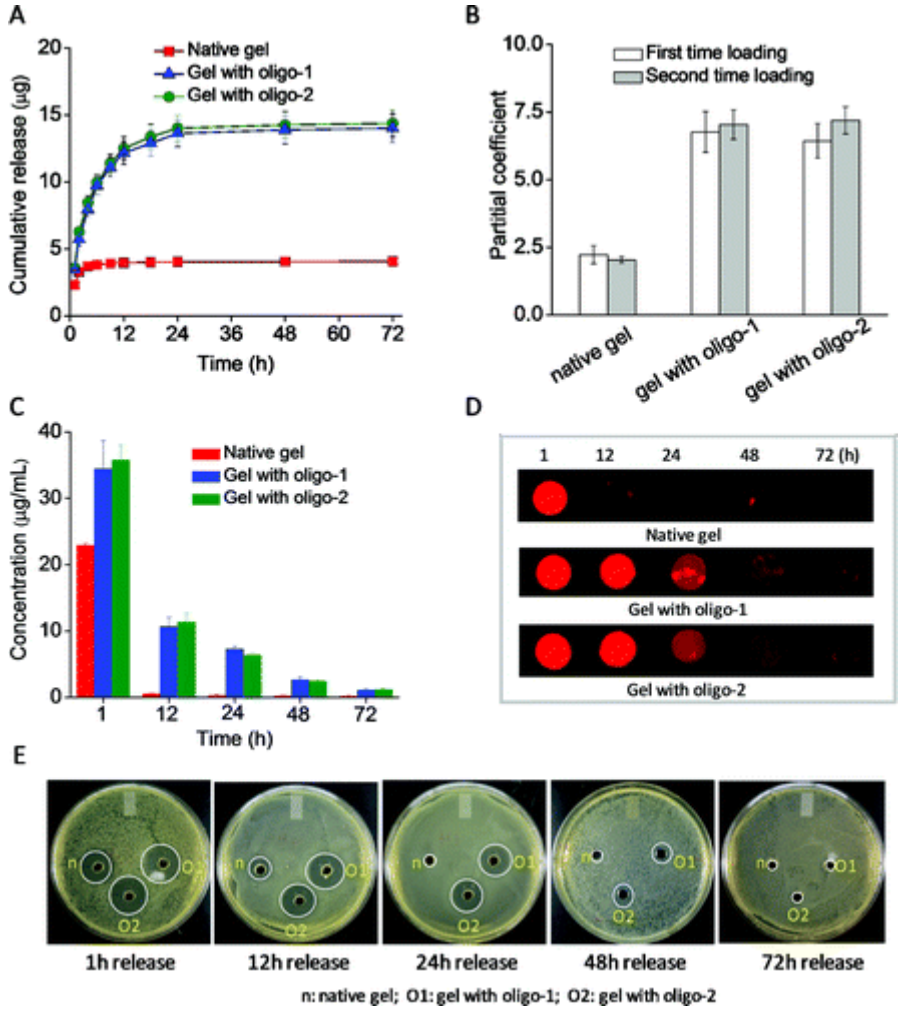

Figure A6. Examination of tetracycline reloading for bacterial inhibition. (A) Cumulative tetracycline release after tetracycline reloading. (B) Comparison of partition coefficients between the first and second time loading. (C) Concentrations of released tetracycline at representative time points. (D) Fluorescence images of hydrogels at different release time points. (E) Zones of bacterial inhibition in the hole-plate diffusion assay.

A.3. Discussions

The simplest method of preparing a hydrogel-based drug delivery system is to polymerize a drug-containing pregel solution in a one-step procedure. However, the gel electrophoresis analysis showed that free DNA oligonucleotides existed in the hydrogels after polymerization, although the majority of DNA oligonucleotides were successfully incorporated into the hydrogels (**Figure A1**). Free DNA oligonucleotides may neutralize drugs due to oligonucleotide–drug complexation during drug release. In addition, the polymerization procedure involves APS and TEMED that are toxic and need to be removed from the hydrogels. Thus, a two-step approach was used in this study to first synthesize the hydrogels and then load the drugs.

Drug loading is highly dependent on the partition coefficient and concentration gradient of drugs. The partition coefficient of a molecule in a hydrogel is mainly determined by steric, electrostatic, and chemical interactions (e.g., complexation).[141] The former two interactions are governed by the pores and ionizable groups of a hydrogel. The chemical interactions are governed by the formation of complexes of drugs and specific binding sites in the hydrogel. In general, native hydrogels do not have specific binding sites to form drug complexes. Therefore, to increase the partition coefficient of a solute, previous studies mainly focused on changing the pore sizes or ionizable groups of the hydrogels.[142–145] This study took a different approach to increase the partition coefficient by using DNA oligonucleotides as specific reaction sites within the hydrogels to form antibiotic–DNA complexes. The complexation decreases the concentration of free tetracycline in the hydrogel network and therefore allows more drugs to diffuse into the hydrogel due to the concentration gradient. The more oligonucleotides the hydrogel has, the more drugs that will diffuse into the hydrogel to form complexes. Therefore, the oligonucleotides act as a sink to absorb drugs into the hydrogel network.

On the basis of the total amount of released tetracycline, the calculated partition coefficient of tetracycline in the native hydrogel is ~2.2 (**Figure A2**). This result is consistent with the

published data showing that small molecules had an average partition coefficient ranging from 1.8 to 2.5 in unmodified hydrogels.[146] In comparison with the native hydrogel, tetracycline had higher partition coefficients in the DNA-functionalized hydrogels (**Figure A2**). For instance, the partition coefficient is higher than 7.5 when the oligo-1 concentration is 1 mM (**Figure A3**). Because the incorporation of the DNA oligonucleotides did not induce the significant changes of the hydrogel in swelling and shear moduli (**Figure A1**), it is likely that the overall physical properties (e.g., pore size) of the hydrogel did not change after oligo-1 incorporation. Therefore, the increase in the partition coefficient results from the role of the DNA oligonucleotides as a sink to sequester tetracycline in the hydrogels. Another important observation is that the partition coefficient exhibited a linear relationship to the oligo-1 concentration ranging from 0 to 1 mM but did not follow the same linear trend when the oligo-1 concentration was increased to more than 1 mM (**Figure A3**). Previous studies showed that oligonucleotide incorporation into hydrogels was less efficient with the increase in oligonucleotide concentration.[147] Therefore, future studies should focus on the optimization of polymerization conditions to improve oligonucleotide incorporation.

We also found that oligo-1 and oligo-2 exhibited no significant difference in enhancing tetracycline loading and controlling tetracycline release (**Figure A2**). The oligo-1 sequence was originally selected from a DNA library using a SELEX procedure for the purpose of binding to tetracycline specifically and strongly.[148] The oligo-2 sequence is a scrambled sequence of the oligo-1 and was used for comparison in this study. The little difference between oligo-1 and oligo-2 in loading and controlling the release of tetracycline indicates that tetracycline does not bind to oligo-1 specifically. It is more likely that the binding between oligo-1 and tetracycline results from nonspecific interactions as previous studies have shown that various small molecules can be nonspecifically intercalated into DNA or RNA molecules.[149,150] Although the procedure of selecting affinity oligonucleotides (i.e., nucleic acid aptamers) has been studied for more than 20

years, it is known that the selection of an aptamer with high binding affinity and specificity is not simple. Therefore, great effort has been made in improving the aptamer selection protocol for discovering high-affinity aptamers. The increase in binding affinity will have a profound effect on the release kinetics because the rate of drug release from a hydrogel is determined by the diffusion and dissociation of drugs from the reaction sites.[151] With a higher binding affinity, the dissociation constant will be lower, and the drug release rate will be slower. Meanwhile, it is important to note that the improvement of binding affinity will not increase the total amount of antibiotic loading because the efficiency of oligonucleotide-mediated drug loading is determined by reaction stoichiometry.

The effect of the tetracycline concentration on drug loading and release was also investigated. The partition coefficient of tetracycline in the DNA-functionalized hydrogel exhibited a bow-like trend (**Figure A4**). As previously mentioned, the partition coefficient of a molecule is directly affected by reaction sites (i.e., DNA oligonucleotides in this study) in a hydrogel. The oligonucleotide-based reaction sites will be gradually saturated as the concentration of tetracycline increases. Once the reaction sites are saturated, any further increase in drug concentration in the loading buffer will not significantly increase the drug loading. Because the partition coefficient is defined as the concentration of drugs in the hydrogel divided by that in the loading buffer, the calculated partition coefficient increased at the beginning and then gradually decreased with the increase in the tetracycline concentration (**Figure A4**).

Because the long-term goal of this study is to apply nucleic acid-functionalized hydrogels for antibiotic delivery in treating bacterial infections, in vitro antimicrobial experiments were pursued to examine the effectiveness of the hydrogels in bacterial inhibition. As expected, the DNA-functionalized hydrogels exhibited enhanced bacterial inhibition in comparison to the native hydrogel (**Figure A5**). We further performed an experiment to investigate the feasibility of refilling the hydrogels with fresh tetracycline after the release of initially loaded tetracycline. The refilled

hydrogels exhibited the same capabilities in loading tetracycline, controlling tetracycline release, and inhibiting bacterial growth (**Figure A6**). Refillable drug delivery systems may have broad implications for the treatment of human diseases. In particular, the development of refillable hydrogels may have a direct impact on the treatment of infectious eye diseases.[152,153] For instance, refillable nucleic-acid-functionalized hydrogels may be used to develop therapeutic contact lenses for treating eye infections. It is also important to note that stability is a critical issue when nucleic acids are used as antibiotic-binding effectors in a refillable drug delivery system. This potential problem can be solved by the use of chemically modified nucleic acid oligonucleotides against nuclease degradation.[154]

A.4. Conclusion

DNA-functionalized PEG hydrogels were investigated for loading and controlling the release of tetracycline. The experimental results have demonstrated that nucleic acid oligonucleotides can increase the partition coefficient of tetracycline between hydrogels and drug loading solutions. In addition, oligonucleotides can slow the release of tetracycline from hydrogels for enhanced bacterial inhibition. Oligonucleotide-functionalized hydrogels can also be refilled with fresh tetracycline and reproduce the functionality of controlling antibiotic release and inhibiting bacterial growth. Therefore, nucleic acid oligonucleotides are promising antibiotic-binding effectors for hydrogel functionalization and antibiotic delivery in treating bacterial infections.

Appendix B

Aptamer Hydrogel for Controlled Release of therapeutic DNA

B.1. Experimental Procedure

B.1.1. Materials

All oligonucleotides (Table B1) were purchased from Integrated DNA Technologies (Coralville, IA). Poly (ethylene glycol) diacrylate (PEGDA; Mn: ~6000 Da) and human thrombin were purchased from Sigma-Aldrich (St. Louis, MO). Ammonium persulfate (APS) and N,N,N′,N′-tetramethylenediamine (TEMED) were purchased from Fisher Scientific (Suwanee, GA). Human plasma was purchased from Innovative Research (Novi, MI).

Table B1 Sequences of oligonucleotides.

Name	Sequence (5'→3')
Apt	TGGTTGGTGTGGTTGG
IO_1	ACACACACACCCAACC
IO_2	ACACACACACCCAACCAC
IO_3	ACACACACACCCAACCACAC
S-IO_3	CATCGATTGGACTGCAGATC
TO	GTGTGGTTGGGTGTGTGTGT
S-TO	TACCGGGCCATTAACTGATG

Note: FAM, acrydite and biotin were added to the 5' end of the modified sequences.

B.1.2. Methods

B.1.2.1. Synthesis of IO-functionalized Hydrogels

PEG solution (20%) was sterilized by filtration through a 0.2 μm filter unit (Fisher Scientific, GA). Acrydite-modified IO sequences were added into the PEGDA solution for the synthesis of IO-functionalized hydrogels in a cylindrical mold in the presence of APS (1% w/v) and TEMED (1% w/v) via free radical polymerization. Hydrogels were allowed to cure at room temperature for 1 hour. Afterwards, hydrogels were thoroughly washed with the release medium that contained Tris acetate (20 mM, pH 7.5), NaCl (140 mM), KCl (5 mM), $MgCl_2$ (1 mM), $CaCl_2$ (1 mM). The washed hydrogels were dehydrated in a Labconco DNA concentrator (Kansas City, MO) for 2 hours. The dehydrated hydrogels were incubated overnight in 20 μL of aptamer solution for sufficient aptamer loading and hybridization with IO.

B.1.2.2. Gel Electrophoresis

Gel electrophoresis was used to qualitatively characterize the hybridization of DNA sequences. After the hybridization solutions were carefully loaded into the wells of a preformed polyacrylamide gel, electrophoresis was run at 120 V using a Bio-Rad Mini-PROTEAN tetra cell electrophoresis system for 45 minutes. The polyacrylamide gel was either imaged directly by the Maestro in vivo imaging system (company information) or stained with ethidium bromide and then imaged with the Bio-Rad GelDoc XR system (Hercules, CA).

B.1.2.3. Surface Plasmon Resonance (SPR)

The SPR spectroscopy was acquired by using SR7000DC (Reichert Analytical Instrument, Depew, NY).Biotinylated anti-thrombin aptamer (1 μM) was immobilized onto a streptavidin-coated sensor chip at a flow rate of 5 μL/min for 900s in the release medium that was also added

with Tween 20 (0.05 %). The association profile was generated by flowing the IO solution on the chip at 30 μL/min for 300 s and the dissociation profile was generated by flowing the release medium in the presence of 1 μM TO or S-TO at 30 μL/min for 300 s.

B.1.2.4. Quantification of Hydrogel Swelling

Water uptake was measured to determine the swelling of the hydrogels. In brief, the hydrogels were dehydrated by DNA concentrator. The dehydrated hydrogels were incubated in the release medium at 37 ℃ for 1 hour. After that, the hydrogel samples were taken out of the buffer, gently blotted with tissue paper, and weighed. The swelling of the hydrogels was calculated by the following equation: $swelling\ (\%) = [(W_s - W_i)/W_i] \times 100$, where W_s is the wet weight of the rehydrated hydrogel, and W_i is the initial weight of the dehydrated hydrogel. The hydrogels before and after swelling were also imaged using a digital camera (Nikon D60).

B.1.2.5. Melting Temperature Analysis

The melting temperature between the anti-thrombin aptamer and IO was calculated using "OligoAnalyzer 3.1" (http://www.idtdna.com/analyzer/applications/oligoanalyzer/). The calculation was performed with 2 μM oligo, 140 mM Na^+ and 1mM Mg^{2+}.

B.1.2.6. Aptamer Loading Examination

The anti-thrombin aptamer loading capacity was studied between dehydrated and non-dehydrated IO_3-functionalized hydrogels. 15 μL of FAM-aptamer solution was used to incubate with dehydrated and non-dehydrated hydrogels for overnight. Then 500 μL of fresh release medium was added to hydrogels for washing. After loading, the release medium was measured by Nanodrop 3300 to calculate the loading percentage. In addition, the 3D loading distribution was studied by imaging hydrogel cut in horizontal direction.

B.1.2.7. Aptamer Release

FAM-labeled anti-thrombin aptamer was used for the release tests. In the sustained release experiment, hydrogels were incubated in the release medium of 100 μL at 37 ℃ and at a shaking rate of 50 rpm. In the triggered release experiment, IO_3-functionalized hydrogels were used. The TO solution was added into the release medium at day 3. The molar ratio of TO to IO was 10:1. After 1 day triggering, the release medium was collected and replenished with a fresh release medium. The amount of anti-thrombin aptamer in the release medium was quantified by the measurement of fluorescence intensity at an excitation wavelength of 495 nm and an emission wavelength of 520 nm (Nanodrop 3300, Thermo Scientific, DE). The hydrogels were also imaged with a Maestro *in vivo* imaging system (PerkinElmer, CA).

B.1.2.8. Thrombin Time

The thrombin time (also known as the thrombin clotting time) was used to determine the bioactivity of the released anti-thrombin aptamer. 50 μL of release medium was incubated for 2 min at 37 ℃ in 100 μL of fresh human plasma. 50 μL of thrombin containing 2 NIH U/mL in 25 mM $CaCl_2$ was then added into the human plasma solution. Clotting time was measured using coagulometer (QuikCoag 1004, BioMedica Diagnostics, Canada). This experiment was performed in triplicate.

B.2. Results

B.2.1. Synthesis of Aptamer Functionalized Hydrogel

The overall concept is shown in **Figure B1.A**. The hydrogel matrix is chemically functionalized with an immobilizing oligonucleotide (IO) whose sequence is complementary to one part of the aptamer. Through this hybridization-mediated molecular binding, the IO-functionalized hydrogels would be able to sequester aptamers and control their release. Moreover, as the interaction of the IO and the aptamer is governed by base pairing, a triggering oligonucleotide (TO) that forms a more stable helix with the IO would be able to compete against and release the aptamer. After the release, the aptamer is transformed from its intermolecular hybridization state to the original functional structure via intramolecular base pairing. Therefore, it is promising to apply nucleic acid hybridization to achieve the sequestration and controlled release of functional nucleic acid aptamers.

IO-functionalized hydrogels were synthesized via free radical polymerization (**Figure B2.A**).[155] The pregel solution contained acrydite-modified IO, PEG diacrylate (PEGDA), ammonium persulfate (APS), and N,N,N′,N′-tetramethylenediamine (TEMED). APS and TEMED were used to catalyze the polymerization of IO and PEGDA. Since IO had an acrydite group, it would be chemically incorporated into the cross-linked hydrogel during the free radical polymerization. To illustrate the success of IO incorporation, the hydrogels were first treated with a FAM-labelled complementary DNA and then thoroughly washed. The imaging analysis showed that the FAM-labelled complementary DNA existed in the IO-functionalized hydrogel after washing. In contrast, the FAM-labelled complementary DNA was not observed in the control hydrogels (**Figure B2.B**). Thus, these data showed that IO was successfully incorporated into the hydrogel matrix.

After the demonstration of IO incorporation, experiments were carried out to illustrate whether the IO-functionalized hydrogel can sequester and control the release of nucleic acid aptamers. The model aptamer used herein was a DNA aptamer that was originally selected against thrombin.[156] This aptamer was chosen because it has been well studied and used in various applications.[157–159] Before aptamer loading, the hydrogel was thoroughly washed and dehydrated in a DNA concentrator for 2 hours. After the dehydration, the hydrogel was incubated in an aptamer solution to sequester and load the aptamer. It was found that the swelling was fast and able to reach equilibrium within one hour. The dehydrated hydrogels absorbed a large amount of aqueous solutions (**Figure B1.B**) and the calculated swelling ratio of the dehydrated hydrogel in equilibrium was more than 500% (**Figure B2.B**). This large swelling ratio allowed the absorption of virtually the equal volume of the aptamer solution into the dehydrated hydrogel, which led to high-efficiency loading of the aptamers. Moreover, the aptamers exhibited a more uniform distribution in the dehydrated hydrogel than the non-dehydrated one.

There have been a variety of polymeric systems developed so far for controlled release applications. Most of them are synthesized with a one-step approach that involves both the preparation of polymeric systems and the loading of therapeutic agents.[160,161] However, the synthesis of polymeric systems often involves toxic molecules or organic solvent. Moreover, unreacted monomers and reaction byproducts may exist in the polymeric systems. These molecules need to be removed to avoid undesired in vivo side effects. Removing these molecules can be achieved via washing whereas washing will lead to the loss of loaded drugs. In contrast, the method used in this study does not have this issue as hydrogel synthesis and aptamer loading are decoupled. APS, TEMED, unreacted

monomers and crosslinkers were removed from the hydrogel through washing. The washed hydrogel was then dehydrated and rehydrated for loading aptamers. However, while the dehydrated hydrogels can absorb a large amount of solution for drug loading, hydrogels usually have high permeability that can lead to the low retention of loaded drugs (**Figure B1.C**). This issue is not problematic for IO-functionalized hydrogels since IO can sequester the aptamer and control its release.

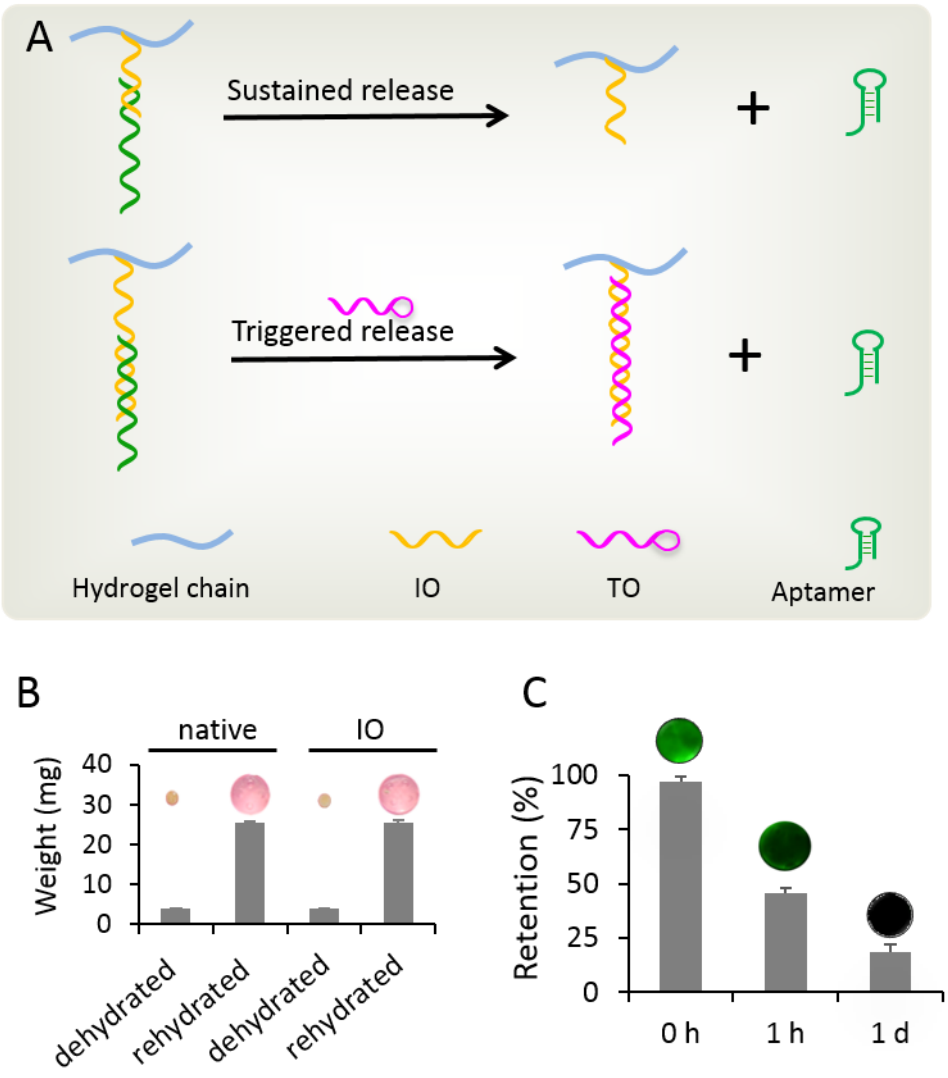

Figure B1. Synthesis of aptamer functionalized hydrogel. A) Schematic illustration of intermolecular hybridization-mediated release of aptamers. B) Solution sequestration of hydrogels after rehydration. C) Retention of aptamers in the native hydrogel. Aptamers were modified with FAM for detection.

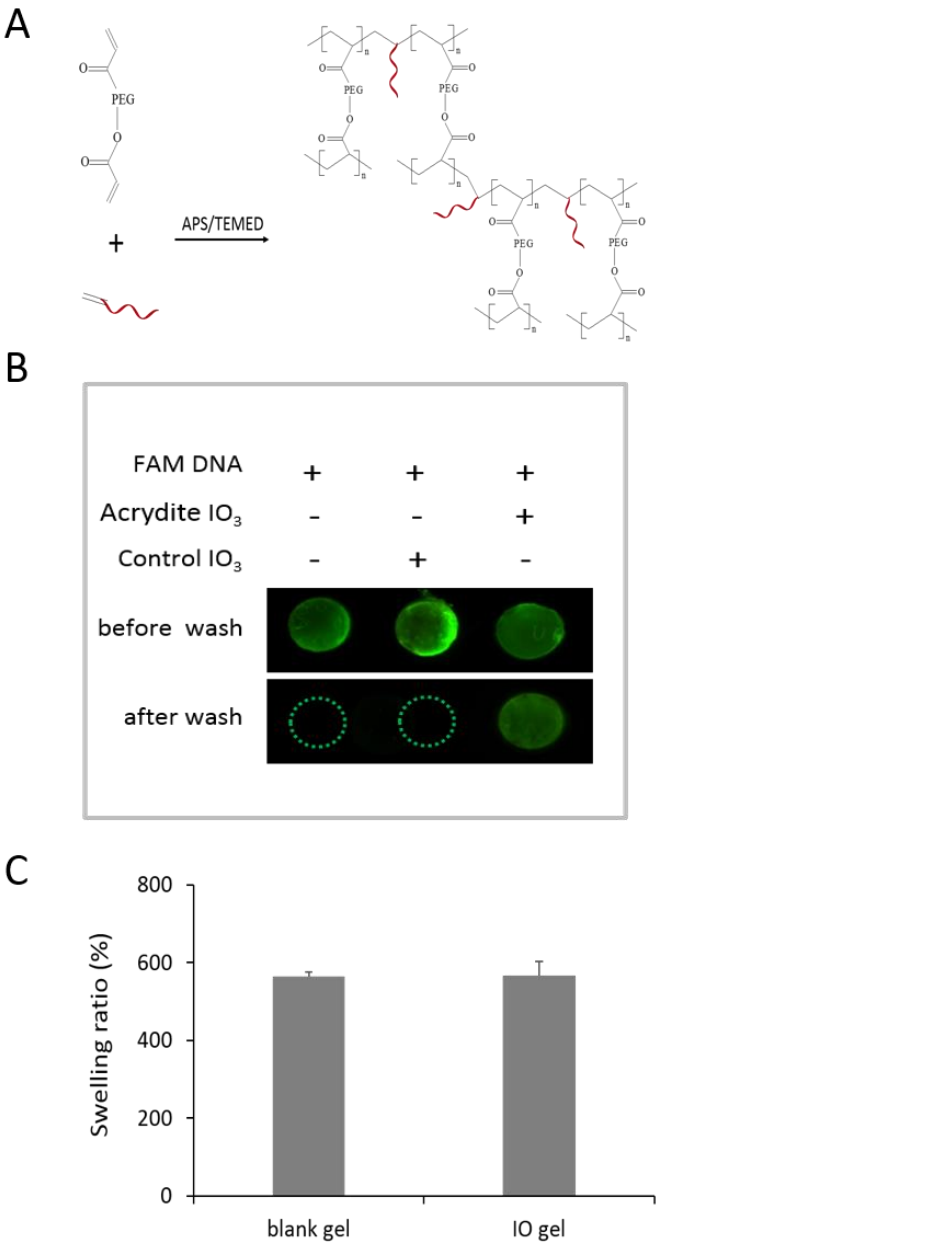

Figure B2. Synthesis of aptamer functionalized hydrogel. A) Schematic illustration of intermolecular hybridization-mediated release of aptamers. B) Solution sequestration of hydrogels after rehydration. C) Retention of aptamers in the native hydrogel. Aptamers were modified with FAM for detection.

B.2.2. Sustainable Therapeutic DNA Release

Three IO sequences (IO_1, IO_2, and IO_3) were used for the synthesis of IO-functionalized hydrogels to study the effect of IO on aptamer release. They formed 6, 8, and 10 base pairs with the anti-thrombin aptamer. The gel electrophoresis images show that these IO sequences were able to form double-stranded complexes with the aptamer. The melting temperature of these hybridized sequences increases with the hybridization length (Figure S3.A). As a higher melting temperature indicates higher strength of intermolecular hybridization, the capability of forming more stable hybridization with the aptamer would be $IO_3 > IO_2 > IO_1$.

After the demonstration of intermolecular hybridization between these three IOs and the aptamer, they were used to synthesize hydrogels for examining the effectiveness of DNA hybridization in controlling the sustained release of the aptamer. The scrambled IO_3 sequence was also used to functionalize the hydrogel as control. While the absorption of the solution into a dehydrated hydrogel can reach equilibrium within one hour, the dehydrated hydrogels were incubated in the aptamer solution overnight to allow for the sufficient hybridization between IO and the aptamer. The profiles of aptamer release from these hydrogels are shown in **Figure S3.B**. The initial 1 h burst release from the scrambled IO_3 functionalized hydrogel was 57.1%. By days 1 and 2, the cumulative aptamer release was 83.5% and 88.1%, respectively. In contrast to the hydrogel functionalized with the scrambled IO_3 sequence, the complementary IO-functionalized hydrogels exhibited promising sustained release profiles. During the first 1 h incubation in the release medium, the amounts of aptamers released from IO_3, IO_2 and IO_1 functionalized hydrogels were 10.5%, 11.8% and 14%, respectively. In comparison to the control hydrogel, the initial burst release was decreased by more than 40%. By day 1, the amounts of cumulative

aptamer release from IO_3, IO_2, and IO_1 functionalized hydrogels were 18.7%, 23.3%, and 32.7%, respectively. By day 15, the cumulative release was 33.9%, 57.4%, and 81.8%, respectively. These results show that the complementary IO-functionalized hydrogels allowed for the sustained release of the loaded aptamer. Moreover, the release rate of the aptamer could be facilely regulated by varying the hybridizing length of IO and the aptamer. The fluorescence imaging of the hydrogels was consistent with the measurement of the aptamer concentrations in the release medium (**Figure S3.C**).

While our results have for the first time demonstrated the application of reversible intermolecular hybridization for achieving the different sustained release kinetics of therapeutic oligonucleotides, one may argue that the similar release profiles can be achieved using a variety of biodegradable polymeric systems. For instance, poly(lactide-co-glycolide) (PLGA) copolymers have been widely studied to develop drug delivery systems to control the release of biologically potent drugs.[162] However, the IO-functionalized hydrogel is different from these degradation-driven release systems in two major aspects. First, the sustained release rate is regulated by the hybridizing length of IO and the aptamer. The way of controlling the release rate is simple. Moreover, in principle, by using the different hybridizing length, multiple aptamers can be incorporated into the same hydrogel functionalized with different IOs to achieve the different sustained release rates. In contrast, the biodegradation-driven release system will release them simultaneously without differentiation. Thus, IO-functionalized hydrogels has potential to advance the treatment of human diseases that need combinatorial delivery of multiple nucleic acid-based drugs. Second, previous studies including ours have demonstrated that DNA hybridization can be applied to trigger the release of protein drugs or even particles

from hydrogels.[163] Inspired by these previous studies, we further proposed to use a more competitive TO to hybridize with IO and to trigger the release of the aptamer. It is important to note that the current work is different from our previous one as the aptamer was used herein as a representative therapeutic oligonucleotide rather than an affinity site for sequestering protein drugs in hydrogels.

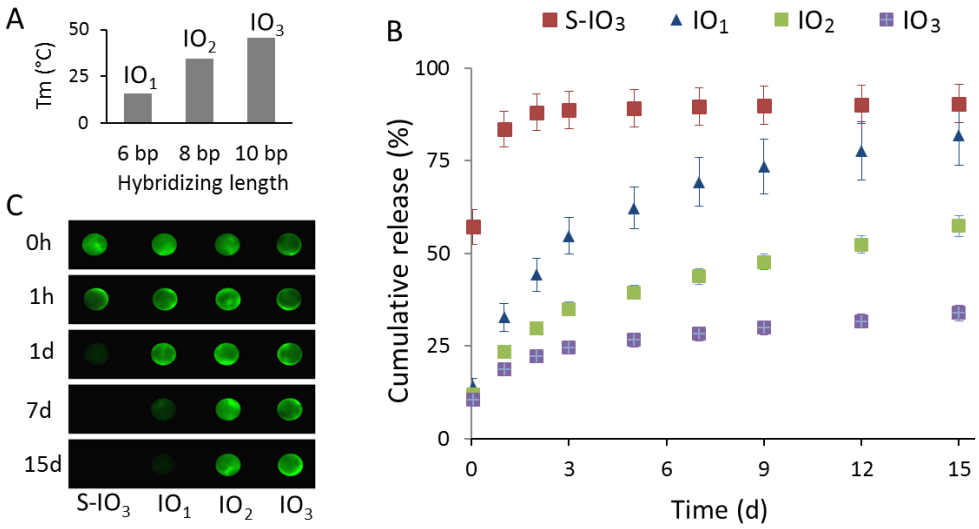

Figure B3. Sustained aptamer release from IO-functionalized hydrogels. A) Melting temperatures of three hybridized IOs of different length. B) Comparison of four hydrogels functionalized with different IOs in controlling aptamer release. S–IO_3 is the scrambled IO_3 sequence. C) Fluorescence images of the hydrogels at different time points. The dotted line was drawn for clear legibility.

B.2.3. Triggered Therapeutic DNA Release

Before illustrating TO-mediated active aptamer release from the hydrogel, we used gel electrophoresis and SPR to examine molecular competition. The gel electrophoresis images show that IO hybridized with the aptamer (Figure B4.A). More importantly, the IO-aptamer complex was dissociated in the presence of TO due to the formation of the new IO–TO complex (**Figure B4.A**). To confirm the gel electrophoresis analysis, we used SPR to determine the apparent dissociation rate constant. The result shows that the IO-aptamer dissociation rate constant was 1.08×10^{-3} s^{-1} in the absence of TO whereas it was 1.58×10^{-2} s^{-1} in the presence of TO. Thus, TO accelerated the dissociation rate by ~14 times (**Figure B4.B**). After the successful demonstration of TO in accelerating the IO-aptamer dissociation, we carried out another controlled release experiment in which TO was added into the system at day 3. The results showed that TO was able to trigger the release of the loaded aptamers (**Figure B4.C**) and the triggering effect was a function of the dose of TO. As our ultimate goal is to apply this aptamer release system to treat human disease, it is important to determine whether the released aptamers can recover its functional structure from its hybridization state after release. Thus, we used thrombin time to examine the bioactivity of the released anti-thrombin aptamers. The results show that the released anti-thrombin aptamers exhibited high bioactivity in inhibiting thrombin in the anti-coagulation assay (**Figure B4.D**).

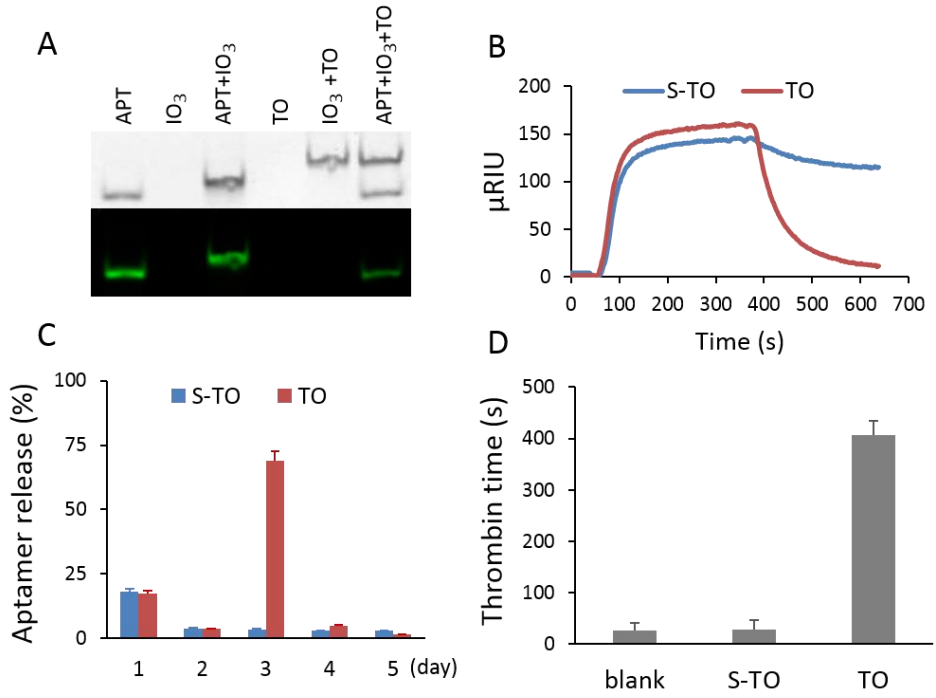

Figure B4. Triggered aptamer release from the IO_3-functoinalized hydrogel. A) Gel electrophoresis image of molecular hybridization. Top: ethidium bromide staining; bottom: fluorescence imaging. Apt was labeled with FAM. B) SPR analysis of TO-induced aptamer-IO dissociation. C) TO-triggered daily aptamer release from the hydrogel. TO was introduced into the release medium at day 3. D) Examination of aptamer bioactivity using a thrombin time assay.

B.3. Conclusion

We have successfully developed a programmable hydrogel that enables the sustained and triggered release of therapeutic nucleic acid aptamers via reversible DNA hybridization. The release kinetics can be regulated via the variation of hybridizing strength or the stimulation of triggering oligonucleotides. Importantly, the whole procedure of aptamer loading and release is operated under physiological conditions without the involvement of any toxic molecule or harsh condition. While nucleic acid aptamers were used as a testing model in this study, the same concept may be tuned and applied to the controlled release of other therapeutic oligonucleotides.

Reference

[1] Kanitakis J. Anatomy, histology and immunohistochemistry of normal human skin. Eur J Dermatol 2002;12:390–9.

[2] Butler J, Lewis R, Shier D. Hole's Human Anatomy & Physiology. McGraw-Hill Education 2012.

[3] Arens EA, Zhang H. The skin's role in human thermoregulation and comfort. Thermal and moisture transport in fribrous materials. 2006;1:560-602.

[4] Banks GJ. Legal and Ethical Safeguards: Protection of Society's Most Vulnerable Participants in a Commercialized Organ Tranplantation System. Am J Law Med 1995;45-110.

[5] Sen CK, Gordillo GM, Roy S, Kirsner R, Lambert L, Hunt TK, et al. Human skin wounds: a major and snowballing threat to public health and the economy. Wound Repair Regen 2009 ;17:763–71.

[6] Gottrup F. A specialized wound-healing center concept: importance of a multidisciplinary department structure and surgical treatment facilities in the treatment of chronic wounds. Am J Surg 2004;187:Suppl 38 – 43.

[7] Llames SG, Del Rio M, Larcher F, Garc á E, Garc á M, Escamez MJ, et al. Human plasma as a dermal scaffold for the generation of a completely autologous bioengineered skin. Transplantation 2004;77:350–5.

[8] Ismarul IN, Ishak Y, Ismail Z, Mohd Shalihuddin WM. Characterization of collagen/chitosan films for skin regenerating scaffold. Med J Malaysia 2004;59:Suppl 57–8.

[9] EAGLSTEIN WH, IRIONDO M, LASZLO K. A Composite Skin Substitute for Surgical Wounds. Dermatologic Surg 1995;21:839–43.

[10] Boyce ST, Christianson DJ, Hansbrough JF. Structure of a collagen-GAG dermal skin substitute optimized for cultured human epidermal keratinocytes. J Biomed Mater Res 1988;22:939–57.

[11] Fontana JD, De Souza AM, Fontana CK, Torriani IL, Moreschi JC, Gallotti BJ, et al. Acetobacter cellulose pellicle as a temporary skin substitute. Appl Biochem Biotechnol 1990;25:253–64.

[12] Zhong SP, Zhang YZ, Lim CT. Tissue scaffolds for skin wound healing and dermal reconstruction. Wiley Interdiscip Rev Nanomed Nanobiotechnol 2:510–25.

[13] Horch RE, Kopp J, Kneser U, Beier J, Bach AD. Tissue engineering of cultured skin substitutes. J Cell Mol Med 2005;9:592–608.

[14] Wainwright DJ. Use of an acellular allograft dermal matrix (AlloDerm) in the management of full-thickness burns. Burns 1995;21:243–8.

[15] Boyce ST, Goretsky MJ, Greenhalgh DG, Kagan RJ, Rieman MT, Warden GD. Comparative assessment of cultured skin substitutes and native skin autograft for treatment of full-thickness burns. Ann Surg 1995;222:743–52.

[16] Compton, CC, Hickerson W, Nadire K, William BS. Acceleration of Skin Regeneration From Cultured Epithelial Autografts by Transplantation to Homograft Dermis. Journal of Burn Care & Rehabilitation 1993;14:581-698.

[17] Metcalfe AD, Ferguson MWJ. Tissue engineering of replacement skin: the crossroads of biomaterials, wound healing, embryonic development, stem cells and regeneration. J R Soc Interface 2007;4:413–37.

[18] Jones I, Currie L, Martin R. A guide to biological skin substitutes. Br J Plast Surg 2002;55:185–93.

[19] MacNeil S. Progress and opportunities for tissue-engineered skin. Nature 2007;445:874–80.

[20] Lee KH. Tissue-engineered human living skin substitutes: development and clinical application. Yonsei Med J 2000;41:774–9.

[21] Mano JF, Silva GA, Azevedo HS, Malafaya PB, Sousa RA, Silva SS, et al. Natural origin biodegradable systems in tissue engineering and regenerative medicine: present status and some moving trends. J R Soc Interface 2007;4:999–1030.

[22] Shevchenko R V, James SL, James SE. A review of tissue-engineered skin bioconstructs available for skin reconstruction. J R Soc Interface 2010;7:229–58.

[23] Karabekmez FE, Duymaz A, Moran SL. Early clinical outcomes with the use of decellularized nerve allograft for repair of sensory defects within the hand. Hand (N Y) 2009;4:245–9.

[24] Martin ND, Schaner PJ, Tulenko TN, Shapiro IM, Dimatteo CA, Williams TK, et al. In vivo behavior of decellularized vein allograft. J Surg Res 2005;129:17–23.

[25] Sun TJ, Han YF, Chai JK, Yang HM. Transplantation of Microskin Autografts With Overlaid Selectively Decellularized Split-Thickness Porcine Skin in the Repair of Deep Burn Wounds. Journal of Burn Care & Research 2011;32:e67-73.

[26] Compton CC, Gill JM, Bradford DA, Regauer S, Gallico GG, O'Connor NE. Skin regenerated from cultured epithelial autografts on full-thickness burn wounds from 6 days to 5 years after grafting. A light, electron microscopic and immunohistochemical study. Lab Invest 1989;60:600–12.

[27] Boyce ST, Kagan RJ, Greenhalgh DG, Warner P, Yakuboff KP, Palmieri T, et al. Cultured skin substitutes reduce requirements for harvesting of skin autograft for closure of excised, full-thickness burns. J Trauma 2006;60:821–9.

[28] Alexander JW, MacMillan BG, Law E, Kittur DS. Treatment of severe burns with widely meshed skin autograft and meshed skin allograft overlay. J Trauma 1981;21:433–8.

[29] Elkins RC, Dawson PE, Goldstein S, Walsh SP, Black KS. Decellularized human valve allografts. Ann Thorac Surg 2001;71:S428–32.

[30] Datta N, Pham QP, Sharma U, Sikavitsas VI, Jansen JA, Mikos AG. In vitro generated extracellular matrix and fluid shear stress synergistically enhance 3D osteoblastic differentiation. Proc Natl Acad Sci U S A 2006;103:2488–93.

[31] Reing JE, Zhang L, Myers-Irvin J, Cordero KE, Freytes DO, Heber-Katz E, et al. Degradation products of extracellular matrix affect cell migration and proliferation. Tissue Eng Part A 2009;15:605–14.

[32] Hodde JP, Record RD, Tullius RS, Badylak SF. Retention of endothelial cell adherence to porcine-derived extracellular matrix after disinfection and sterilization. Tissue Eng 2002;8:225–34.

[33] Stern MM, Myers RL, Hammam N, Stern KA, Eberli D, Kritchevsky SB, et al. The influence of extracellular matrix derived from skeletal muscle tissue on the proliferation and differentiation of myogenic progenitor cells ex vivo. Biomaterials 2009;30:2393–9.

[34] Zhang Y, He Y, Bharadwaj S, Hammam N, Carnagey K, Myers R, et al. Tissue-specific extracellular matrix coatings for the promotion of cell proliferation and maintenance of cell phenotype. Biomaterials 2009;30:4021–8.

[35] Singelyn JM, Sundaramurthy P, Johnson TD, Schup-Magoffin PJ, Hu DP, Faulk DM, et al. Catheter-deliverable hydrogel derived from decellularized ventricular extracellular matrix increases endogenous cardiomyocytes and preserves cardiac function post-myocardial infarction. J Am Coll Cardiol 2012;59:751–63.

[36] Grauss R., Hazekamp M., van Vliet S, Gittenberger-de Groot A., DeRuiter M. Decellularization of rat aortic valve allografts reduces leaflet destruction and extracellular matrix remodeling. J Thorac Cardiovasc Surg 2003;126:2003–10.

[37] Lynch SE, Williams RC, Poison AM, Howell TH, Reddy MS, Zappa UE, et al. A combination of platelet-derived and insulin-like growth factors enhances periodontal regeneration. J Clin Periodontol 1989;16:545–8.

[38] Murakami S, Takayama S, Ikezawa K, Sltimabukuro Y, Kitamura M, Nozaki T, et al. Regeneration of periodontal tissues by basic fibroblast growth factor. J Periodontal Res 1999;34:425–30.

[39] Kawai K, Suzuki S, Tabata Y, Ikada Y, Nishimura Y. Accelerated tissue regeneration through incorporation of basic fibroblast growth factor-impregnated gelatin microspheres into artificial dermis. Biomaterials 2000;21:489–99.

[40] Kanematsu A, Yamamoto S, Noguchi T, Ozeki M, Tabata Y, Ogawa O. Bladder regeneration by bladder acellular matrix combined with sustained release of exogenous growth factor. J Urol 2003;170:1633–8.

[41] Lee KY, Peters MC, Anderson KW, Mooney DJ. Controlled growth factor release from synthetic extracellular matrices. Nature 2000;408:998–1000.

[42] Babensee JE, McIntire L V., Mikos AG. Growth Factor Delivery for Tissue Engineering. Pharm Res n.d.;17:497–504.

[43] Tabata Y. Protein release from gelatin matrices. Adv Drug Deliv Rev 1998;31:287–301.

[44] Lin C-C, Anseth KS. PEG hydrogels for the controlled release of biomolecules in regenerative medicine. Pharm Res 2009;26:631–43.

[45] Nimni ME. Polypeptide growth factors: targeted delivery systems. Biomaterials 1997;18:1201–25.

[46] Lee J-Y, Nam S-H, Im S-Y, Park Y-J, Lee Y-M, Seol Y-J, et al. Enhanced bone formation by controlled growth factor delivery from chitosan-based biomaterials. J Control Release 2002;78:187–97.

[47] Vasita R, Katti DS. Growth factor-delivery systems for tissue engineering: a materials perspective. Expert Rev Med Devices 2006;3:29–47.

[48] Rutkowski JM, Boardman KC, Swartz MA. Characterization of lymphangiogenesis in a model of adult skin regeneration. Am J Physiol Heart Circ Physiol 2006;291:H1402–10.

[49] Goldman J, Le TX, Skobe M, Swartz MA. Overexpression of VEGF-C causes transient lymphatic hyperplasia but not increased lymphangiogenesis in regenerating skin. Circ Res 2005;96:1193–9.

[50] Marchese C. Modulation of keratinocyte growth factor and its receptor in reepithelializing human skin. J Exp Med 1995;182:1369–76.

[51] Igarashi A, Nashiro K, Kikuchi K, Sato S, Ihn H, Fujimoto M, et al. Connective Tissue Growth Factor Gene Expression in Tissue Sections From Localized Scleroderma, Keloid, and Other Fibrotic Skin Disorders. J Invest Dermatol 1996;106:729–33.

[52] Enhancement of epidermal regeneration by biosynthetic epidermal growth factor. J Exp Med 1986;163:1319–24.

[53] Igarashi A, Okochi H, Bradham DM, Grotendorst GR. Regulation of connective tissue growth factor gene expression in human skin fibroblasts and during wound repair. Mol Biol Cell 1993;4:637–45.

[54] Yang Y, Xia T, Zhi W, Wei L, Weng J, Zhang C, et al. Promotion of skin regeneration in diabetic rats by electrospun core-sheath fibers loaded with basic fibroblast growth factor. Biomaterials 2011;32:4243–54.

[55] Furuya T, Hashimoto M, Koda M, Murata A, Okawa A, Dezawa M, et al. Treatment with basic fibroblast growth factor-incorporated gelatin hydrogel does not exacerbate mechanical allodynia after spinal cord contusion injury in rats. J Spinal Cord Med 2013;36:134–9.

[56] Lee HJ, Koh W-G. Hydrogel Micropattern-Incorporated Fibrous Scaffolds Capable of Sequential Growth Factor Delivery for Enhanced Osteogenesis of hMSCs. ACS Appl Mater Interfaces 2014;6:9338–48.

[57] Morimoto N, Yoshimura K, Niimi M, Ito T, Aya R, Fujitaka J, et al. Novel collagen/gelatin scaffold with sustained release of basic fibroblast growth factor: clinical trial for chronic skin ulcers. Tissue Eng Part A 2013;19:1931–40.

[58] Fujisato T. Effect of basic fibroblast growth factor on cartilage regeneration in chondrocyte-seeded collagen sponge scaffold. Biomaterials 1996;17:155–62.

[59] Wang X, Ding B, Li B. Biomimetic electrospun nanofibrous structures for tissue engineering. Mater Today 2013;16:229–41.

[60] Vyas K, Vasconez H. Wound Healing: Biologics, Skin Substitutes, Biomembranes and Scaffolds. Healthcare 2014;2:356–400.

[61] Stock UA, Vacanti JP. Tissue Engineering: Current State and Prospects. Annu Rev Med 2001;52:443-51.

[62] Hodde JP, Badylak SF, Brightman AO, Voytik-Harbin SL. Glycosaminoglycan content of small intestinal submucosa: a bioscaffold for tissue replacement. Tissue Eng 1996;2:209–17.

[63] Lindberg K, Badylak SF. Porcine small intestinal submucosa (SIS): a bioscaffold supporting in vitro primary human epidermal cell differentiation and synthesis of basement membrane proteins. Burns 2001;27:254–66.

[64] Bejjani GK, Zabramski J. Safety and efficacy of the porcine small intestinal submucosa dural substitute: results of a prospective multicenter study and literature review. J Neurosurg 2007;106:1028–33.

[65] Material from pig intestine is remedy for deep sores, incontinence. Purdue News 2000. http://www.purdue.edu/uns/html4ever/0002.Badylak.SIS.html.

[66] Crapo PM, Gilbert TW, Badylak SF. An overview of tissue and whole organ decellularization processes. Biomaterials 2011;32:3233–43.

[67] Cass AEG, Zhang Y. Nucleic acid aptamers: ideal reagents for point-of-care diagnostics? Faraday Discuss 2011;149:49–61.

[68] Andrée B, Bär A, Haverich A, Hilfiker A. Small intestinal submucosa segments as matrix for tissue engineering: review. Tissue Eng Part B Rev 2013;19:279–91.

[69] Kim MS, Hong KD, Shin HW, Kim SH, Kim SH, Lee MS, et al. Preparation of porcine small intestinal submucosa sponge and their application as a wound dressing in full-thickness skin defect of rat. Int J Biol Macromol 2005;36:54–60.

[70] Wilson GJ, Courtman DW, Klement P, Lee JM, Yeger H. Acellular matrix: a biomaterials approach for coronary artery bypass and heart valve replacement. Ann Thorac Surg 1995;60:S353–8.

[71] Courtman DW, Pereira CA, Kashef V, McComb D, Lee JM, Wilson GJ. Development of a pericardial acellular matrix biomaterial: biochemical and mechanical effects of cell extraction. J Biomed Mater Res 1994;28:655–66.

[72] Cartmell JS, Dunn MG. Effect of chemical treatments on tendon cellularity and mechanical properties. J Biomed Mater Res 2000;49:134–40.

[73] Crapo PM, Gilbert TW, Badylak SF. An overview of tissue and whole organ decellularization processes. Biomaterials 2011;32:3233–43.

[74] Arai S, Orton C. Solid-phase tissue electrophoresis enhances sodium dodecyl sulfate-based decellularization of xenogeneic bioscaffolds. FASEB J 2009;23: Suppl 817.

[75] Nonaka PN, Uriarte JJ, Campillo N, Melo E, Navajas D, Farré R, et al. Mechanical properties of mouse lungs along organ decellularization by sodium dodecyl sulfate. Respir Physiol Neurobiol 2014;200:1–5.

[76] Liao J, Joyce EM, Sacks MS. Effect of trypsin and Triton-X 100 for decellularization of porcine aortic heart valves. Biomaterials 2008;29:1065-74.

[77] Yu BT, Li WT, Song BQ, Wu YL. Comparative study of the Triton X-100-sodium deoxycholate method and detergent-enzymatic digestion method for decellularization of porcine aortic valves. Eur Rev Med Pharmacol Sci 2013;17:2179–84.

[78] Vavken P, Joshi S, Murray MM. TRITON-X is most effective among three decellularization agents for ACL tissue engineering. J Orthop Res 2009;27:1612–8.

[79] Wang H, Lin X-F, Wang L-R, Lin Y-Q, Wang J-T, Liu W-Y, et al. Decellularization technology in CNS tissue repair. Expert Rev Neurother 2015;15:493–500.

[80] Moore MA, Samsell B, Wallis G, Triplett S, Chen S, Jones AL, et al. Decellularization of human dermis using non-denaturing anionic detergent and endonuclease: a review. Cell Tissue Bank 2015;16:249–59.

[81] Parolari A, Songia P, Myasoedova V, Poggio P. Re: Development of a next-generation tissue valve using a glutaraldehyde-fixed porcine aortic valve treated with decellularization, α-galactosidase, space filler, organic solvent and detoxification. Eur J Cardiothorac Surg 2015;48:104-13.

[82] Da Palma RK, Campillo N, Uriarte JJ, Oliveira LVF, Navajas D, Farré R. Pressure- and flow-controlled media perfusion differently modify vascular mechanics in lung decellularization. J Mech Behav Biomed Mater 2015;49:69–79.

[83] Gillies AR, Smith LR, Lieber RL, Varghese S. Method for Decellularizing Skeletal Muscle Without Detergents or Proteolytic Enzymes 2011;17:383-9.

[84] Zhai W, Chang J, Lin K, Wang J, Zhao Q, Sun X. Crosslinking of decellularized porcine heart valve matrix by procyanidins. Biomaterials 2006;27:3684–90.

[85] Cebotari S, Tudorache I, Jaekel T, Hilfiker A, Dorfman S, Ternes W, et al. Detergent decellularization of heart valves for tissue engineering: toxicological effects of residual detergents on human endothelial cells. Artif Organs 2010;34:206–10.

[86] Gilbert TW, Freund JM, Badylak SF. Quantification of DNA in biologic scaffold materials. J Surg Res 2009;152:135–9.

[87] Weymann A, Radovits T, Schmack B, Korkmaz S, Li S, Chaimow N, et al. Total aortic arch replacement: superior ventriculo-arterial coupling with decellularized allografts compared with conventional prostheses. PLoS One 2014;9:e103588.

[88] Wu Q, Bao J, Zhou Y, Wang Y, Du Z, Shi Y, et al. Optimizing perfusion-decellularization methods of porcine livers for clinical-scale whole-organ bioengineering. Biomed Res Int 2015;2015:785474.

[89] Cukierman E, Pankov R, Stevens DR, Yamada KM. Taking cell-matrix adhesions to the third dimension. Science 2001;294:1708–12.

[90] Guan JL, Shalloway D. Regulation of focal adhesion-associated protein tyrosine kinase by both cellular adhesion and oncogenic transformation. Nature 1992;358:690–2.

[91] Temenoff JS, Mikos AG. Review: tissue engineering for regeneration of articular cartilage. Biomaterials 2000;21:431–40.

[92] Agrawal CM, Ray RB. Biodegradable polymeric scaffolds for musculoskeletal tissue engineering. J Biomed Mater Res 2001;55:141–50.

[93] Place ES, George JH, Williams CK, Stevens MM. Synthetic polymer scaffolds for tissue engineering. Chem Soc Rev 2009;38:1139–51.

[94] Hutmacher DW, Sittinger M, Risbud M V. Scaffold-based tissue engineering: rationale for computer-aided design and solid free-form fabrication systems. Trends Biotechnol 2004;22:354–62.

[95] Sahoo S, Ang LT, Goh JC-H, Toh S-L. Growth factor delivery through electrospun nanofibers in scaffolds for tissue engineering applications. J Biomed Mater Res A 2010;93:1539–50.

[96] Ma Z, Gao C, Gong Y, Shen J. Cartilage tissue engineering PLLA scaffold with surface immobilized collagen and basic fibroblast growth factor. Biomaterials 2005;26:1253–9.

[97] Hile DD, Amirpour ML, Akgerman A, Pishko M V. Active growth factor delivery from poly(d,l-lactide-co-glycolide) foams prepared in supercritical CO2. J Control Release 2000;66:177–85.

[98] Wang X, Wenk E, Zhang X, Meinel L, Vunjak-Novakovic G, Kaplan DL. Growth factor gradients via microsphere delivery in biopolymer scaffolds for osteochondral tissue engineering. J Control Release 2009;134:81–90.

[99] Perets A, Baruch Y, Weisbuch F, Shoshany G, Neufeld G, Cohen S. Enhancing the vascularization of three-dimensional porous alginate scaffolds by incorporating controlled release basic fibroblast growth factor microspheres. J Biomed Mater Res A 2003;65:489–97.

[100] Cho MI, Lin WL, Genco RJ. Platelet-derived growth factor-modulated guided tissue regenerative therapy. J Periodontol 1995;66:522–30.

[101] Hosseinkhani H, Hosseinkhani M, Khademhosseini A, Kobayashi H, Tabata Y. Enhanced angiogenesis through controlled release of basic fibroblast growth factor from peptide amphiphile for tissue regeneration. Biomaterials 2006;27:5836–44.

[102] Discher DE, Mooney DJ, Zandstra PW. Growth factors, matrices, and forces combine and control stem cells. Science 2009;324:1673–7.

[103] Kireeva M, MO F, Yang G, Lau L. Cyr61, a product of a growth factor-inducible immediate-early gene, promotes cell proliferation, migration, and adhesion. Mol Cell Biol 1996;16:1326–34.

[104] Karande TS, Ong JL, Agrawal CM. Diffusion in Musculoskeletal Tissue Engineering Scaffolds: Design Issues Related to Porosity, Permeability, Architecture, and Nutrient Mixing. Ann Biomed Eng 2004;32:1728–43.

[105] Kim K, Yu M, Zong X, Chiu J, Fang D, Seo Y-S, et al. Control of degradation rate and hydrophilicity in electrospun non-woven poly(d,l-lactide) nanofiber scaffolds for biomedical applications. Biomaterials 2003;24:4977–85.

[106] Holland TA, Bodde EWH, Cuijpers VMJI, Baggett LS, Tabata Y, Mikos AG, et al. Degradable hydrogel scaffolds for in vivo delivery of single and dual growth factors in cartilage repair. Osteoarthritis Cartilage 2007;15:187–97.

[107] Obara K, Ishihara M, Ishizuka T, Fujita M, Ozeki Y, Maehara T, et al. Photocrosslinkable chitosan hydrogel containing fibroblast growth factor-2 stimulates wound healing in healing-impaired db/db mice. Biomaterials 2003;24:3437–44.

[108] Annabi N, Nichol JW, Zhong X, Ji C, Koshy S, Khademhosseini A, et al. Controlling the porosity and microarchitecture of hydrogels for tissue engineering. Tissue Eng Part B Rev 2010;16:371–83.

[109] Tabata Y, Miyao M, Ozeki M, Ikada Y. Controlled release of vascular endothelial growth factor by use of collagen hydrogels. J Biomater Sci Polym Ed 2000;11:915–30.

[110] Hutson CB, Nichol JW, Aubin H, Bae H, Yamanlar S, Al-Haque S, et al. Synthesis and characterization of tunable poly(ethylene glycol): gelatin methacrylate composite hydrogels. Tissue Eng Part A 2011;17:1713–23.

[111] Lee KY, Nakagawa T, Okano T, Hori R, Ono K, Tabata Y, et al. Novel therapy for hearing loss: delivery of insulin-like growth factor 1 to the cochlea using gelatin hydrogel. Otol Neurotol 2007;28:976–81.

[112] Battig MR, Huang Y, Chen N, Wang Y. Aptamer-functionalized superporous hydrogels for sequestration and release of growth factors regulated via molecular recognition. Biomaterials 2014;35:8040–8.

[113] Trujillo CA, Nery AA, Alves JM, Martins AH, Ulrich H. Development of the anti-VEGF aptamer to a therapeutic agent for clinical ophthalmology. Clin Ophthalmol 2007;1:393–402.

[114] Ulrich H, Trujillo C, Nery A, Alves J, Majumder P, Resende R, et al. DNA and RNA Aptamers: From Tools for Basic Research Towards Therapeutic Applications. Comb Chem High Throughput Screen 2006;9:619–32.

[115] Thiel KW, Giangrande PH. Therapeutic applications of DNA and RNA aptamers. Oligonucleotides 2009;19:209–22.

[116] Lin CH, Patei DJ. Structural basis of DNA folding and recognition in an AMP-DNA aptamer complex: distinct architectures but common recognition motifs for DNA and RNA aptamers complexed to AMP. Chem Biol 1997;4:817–32.

[117] Potty ASR, Kourentzi K, Fang H, Jackson GW, Zhang X, Legge GB, et al. Biophysical characterization of DNA aptamer interactions with vascular endothelial growth factor. Biopolymers 2009;91:145–56.

[118] Wang D-L, Song Y-L, Zhu Z, Li X-L, Zou Y, Yang H-T, et al. Selection of DNA aptamers against epidermal growth factor receptor with high affinity and specificity. Biochem Biophys Res Commun 2014;453:681–5.

[119] Udenfriend S, Stein S, Böhlen P, Dairman W, Leimgruber W, Weigele M. Fluorescamine: a reagent for assay of amino acids, peptides, proteins, and primary amines in the picomole range. Science 1972;178:871–2.

[120] Li S, Chen N, Zhang Z, Wang Y. Endonuclease-responsive aptamer-functionalized hydrogel coating for sequential catch and release of cancer cells. Biomaterials 2013;34:460–9.

[121] Chen J, Park K. Synthesis and characterization of superporous hydrogel composites. J Control Release 2000;65:73–82.

[122] Ashikari-Hada S, Habuchi H, Kariya Y, Kimata K. Heparin regulates vascular endothelial growth factor165-dependent mitogenic activity, tube formation, and its receptor phosphorylation of human endothelial cells. Comparison of the effects of heparin and modified heparins. J Biol Chem 2005;280:31508–15.

[123] Nuttelman CR, Rice MA, Rydholm AE, Salinas CN, Shah DN, Anseth KS. Macromolecular Monomers for the Synthesis of Hydrogel Niches and Their Application in Cell Encapsulation and Tissue Engineering. Prog Polym Sci 2008;33:167–79.

[124] Zweier JL, Kuppusamy P, Lutty GA. Measurement of endothelial cell free radical generation: evidence for a central mechanism of free radical injury in postischemic tissues. Proc Natl Acad Sci 1988;85:4046–50.

[125] Geiger M, Li RH, Friess W. Collagen sponges for bone regeneration with rhBMP-2. Adv Drug Deliv Rev 2003;55:1613–29.

[126] Uludag H, Gao T, Porter TJ, Friess W, Wozney JM. Delivery systems for BMPs: factors contributing to protein retention at an application site. J Bone Joint Surg Am 2001;83-A Suppl:S128–35.

[127] Bouxsein ML, Turek TJ, Blake CA, D'Augusta D, Li X, Stevens M, et al. Recombinant human bone morphogenetic protein-2 accelerates healing in a rabbit ulnar osteotomy model. J Bone Joint Surg Am 2001;83-A:1219–30.

[128] Carragee EJ, Chu G, Rohatgi R, Hurwitz EL, Weiner BK, Yoon ST, et al. Cancer risk after use of recombinant bone morphogenetic protein-2 for spinal arthrodesis. J Bone Joint Surg Am 2013;95:1537–45.

[129] Fu K, Klibanov AM, Langer R. Protein stability in controlled-release systems. Nat Biotechnol 2000;18:24–5.

[130] Gu F, Neufeld R, Amsden B. Maintenance of vascular endothelial growth factor and potentially other therapeutic proteins bioactivity during a photo-initiated free radical cross-linking reaction forming biodegradable elastomers. Eur J Pharm Biopharm 2007;66:21–7.

[131] Ekaputra AK, Prestwich GD, Cool SM, Hutmacher DW. The three-dimensional vascularization of growth factor-releasing hybrid scaffold of poly (ε-caprolactone)/collagen fibers and hyaluronic acid hydrogel. Biomaterials 2011;32:8108–17.

[132] Lee K, Silva EA, Mooney DJ. Growth factor delivery-based tissue engineering: general approaches and a review of recent developments. J R Soc Interface 2011;8:153–70.

[133] Leslie-Barbick JE, Moon JJ, West JL. Covalently-Immobilized Vascular Endothelial Growth Factor Promotes Endothelial Cell Tubulogenesis in Poly(ethylene glycol) Diacrylate Hydrogels. J Biomater Sci Polym Ed 2009;20:1763-79.

[134] Ng EWM, Shima DT, Calias P, Cunningham ET, Guyer DR, Adamis AP. Pegaptanib, a targeted anti-VEGF aptamer for ocular vascular disease. Nat Rev Drug Discov 2006;5:123–32.

[135] Wu Z, Tang Y, Fang H, Su Z, Xu B, Lin Y, et al. Decellularized scaffolds containing hyaluronic acid and EGF for promoting the recovery of skin wounds. J Mater Sci Mater Med 2015;26:5322.

[136] Bannasch H, Stark GB, Knam F, Horch RE, Föhn M. Decellularized dermis in combination with cultivated keratinocytes in a short- and long-term animal experimental investigation. J Eur Acad Dermatol Venereol 2008;22:41–9.

[137] PLGA/gelatin hybrid nanofibrous scaffolds encapsulating EGF for skin regeneration. J Biomed Mater Res A 2015;103:2225-35.

[138] Collagen/chitosan based two-compartment and bi-functional dermal scaffolds for skin regeneration. Mater Sci Eng C Mater Biol Appl 2015;52:155-62.

[139] Stegemann JP, Kaszuba SN, Rowe SL. Review: advances in vascular tissue engineering using protein-based biomaterials. Tissue Eng 2007;13:2601–13.

[140] Simón-Yarza T, Formiga FR, Tamayo E, Pelacho B, Prosper F, Blanco-Prieto MJ. Vascular endothelial growth factor-delivery systems for cardiac repair: an overview. Theranostics 2012;2:541–52.

[141] Fatin-Rouge N, Milon A, Buffle J, Goulet RR, Tessier A. Diffusion and Partitioning of Solutes in Agarose Hydrogels: The Relative Influence of Electrostatic and Specific Interactions. J Phys Chem B 2003;107:12126–37.

[142] Giddings JC, Kucera E, Russell CP, Myers MN. Statistical theory for the equilibrium distribution of rigid molecules in inert porous networks. Exclusion chromatography. J Phys Chem 1968;72:4397–408.

[143] Doi M. Equilibrium partition coefficient of macromolecules between random porous network and bulk liquid. J Chem Soc Faraday Trans 2 1975;71:1720-1729.

[144] Pujar NS, Zydney AL. Electrostatic effects on protein partitioning in size-exclusion chromatography and membrane ultrafiltration. J Chromatogr A 1998;796:229–38.

[145] Yao Y, Lenhoff AM. Determination of pore size distributions of porous chromatographic adsorbents by inverse size-exclusion chromatography. J Chromatogr A 2004;1037:273–82.

[146] Merrill EW, Dennison KA, Sung C. Partitioning and diffusion of solutes in hydrogels of poly(ethylene oxide). Biomaterials 1993;14:1117–26.

[147] Venkatesh S, Wower J, Byrne ME. Nucleic acid therapeutic carriers with on-demand triggered release. Bioconjug Chem 2009;20:1773–82.

[148] Niazi JH, Lee SJ, Gu MB. Single-stranded DNA aptamers specific for antibiotics tetracyclines. Bioorg Med Chem 2008;16:7245–53.

[149] Reha D, Kabelác M, Ryjácek F, Sponer J, Sponer JE, Elstner M, et al. Intercalators. 1. Nature of stacking interactions between intercalators (ethidium, daunomycin, ellipticine, and 4',6-diaminide-2-phenylindole) and DNA base pairs. Ab initio quantum chemical, density functional theory, and empirical potential study. J Am Chem Soc 2002;124:3366–76.

[150] Lerman LS. Structural considerations in the interaction of DNA and acridines. J Mol Biol 1961;3:18–30.

[151] Fan T-H, Soontornworajit B, Karzar-Jeddi M, Zhang X, Wang Y. An aptamer-functionalized hydrogel for controlled protein release: A modeling study. Soft Matter 2011;7:9326.

[152] Lo R, Li P-Y, Saati S, Agrawal R, Humayun MS, Meng E. A refillable microfabricated drug delivery device for treatment of ocular diseases. Lab Chip 2008;8:1027–30.

[153] Choonara YE, Pillay V, Danckwerts MP, Carmichael TR, du Toit LC. A review of implantable intravitreal drug delivery technologies for the treatment of posterior segment eye diseases. J Pharm Sci 2010;99:2219–39.

[154] Burmeister PE, Lewis SD, Silva RF, Preiss JR, Horwitz LR, Pendergrast PS, et al. Direct in vitro selection of a 2'-O-methyl aptamer to VEGF. Chem Biol 2005;12:25–33.

[155] Zhang X, Soontornworajit B, Zhang Z, Chen N, Wang Y. Enhanced loading and controlled release of antibiotics using nucleic acids as an antibiotic-binding effector in hydrogels. Biomacromolecules 2012;13:2202–10.

[156] Bock LC, Griffin LC, Latham JA, Vermaas EH, Toole JJ. Selection of single-stranded DNA molecules that bind and inhibit human thrombin. Nature 1992;355:564–6.

[157] Oroval M, Climent E, Coll C, Eritja R, Avi ñó A, Marcos MD, et al. An aptamer-gated silica mesoporous material for thrombin detection. Chem Commun 2013;49:5480–2.

[158] Cho H, Baker BR, Wachsmann-Hogiu S, Pagba C V., Laurence TA, Lane SM, et al. Aptamer-Based SERRS Sensor for Thrombin Detection. Nano Lett 2008;8:4386–90.

[159] Heckel A, Mayer G. Light regulation of aptamer activity: an anti-thrombin aptamer with caged thymidine nucleobases. J Am Chem Soc 2005;127:822–3.

[160] Ho KY, Ord M, Dodou K. Effect of drug-polymer binary mixtures on the in-vitro release of ibuprofen from transdermal drug-in-adhesive layers. Drug Discov Ther 2008;2:277–81.

[161] Hofmann S, Foo CTWP, Rossetti F, Textor M, Vunjak-Novakovic G, Kaplan DL, et al. Silk fibroin as an organic polymer for controlled drug delivery. J Control Release 2006;111:219–27.

[162] Makadia HK, Siegel SJ. Poly Lactic-co-Glycolic Acid (PLGA) as Biodegradable Controlled Drug Delivery Carrier. Polymers (Basel) 2011;3:1377–97.

[163] El-Hamed F, Dave N, Liu J. Stimuli-responsive releasing of gold nanoparticles and liposomes from aptamer-functionalized hydrogels. Nanotechnology 2011;22:494011.

VITA

Xiaolong Zhang

Education

Ph.D. Bioengineering. December 2015
The Pennsylvania State University, University Park, PA.

M.S. Environmental Engineering. December 2010
University of Connecticut, Storrs, CT.

M.S. Biochemistry and Molecular Biology. June 2009
Tongji University, Shanghai, China.

B.A. Bioengineering June 2006
Northeast Agriculture University, Haerbin, China.

Peer-reviewed Publications

Zhang, XL, Battig, M, Chen, NC, Gaddes, ER, Duncan, KL, Wang, Y. Chimeric oligonucleotide-protein hydrogels as an extracellular matrix mimic for loading cells and growth factors. Biomaterials. (Submitted)

Li, SH, Chen, NC, Gaddes, ER, **Zhang, XL**, Dong, C, and Wang, Y. A Drosera-bioinspired hydrogel for catching and killing target cells. Scientific Reports. 2015. (Accepted)

Zhang, XL, Battig, M., and Wang, Y. Programmable hydrogels for the controlled release of therapeutic nucleic acid aptamers via reversible DNA hybridization. Chemical Communications. 2013. 49, 9600-9602.

Zhang, XL, Soontornworajit, B, Zhang, ZY, Chen, NC, Wang, Y. Enhanced loading and controlled release of antibiotics using nucleic acids as an antibiotic-binding effector in hydrogels, Biomacromolecules. 2012. 13, 2202-2210.

Fan, T, Soontornworajit, B, Karzar, M, **Zhang, XL**, Wang, Y. An aptamer-functionalized hydrogel for controlled protein release: A modeling study. Soft Matter. 2011. 7, 9326-9334.